INTEGRATION OF MASSIVE PLUG-IN HYBRID ELECTRIC VEHICLES INTO POWER DISTRIBUTION SYSTEMS: MODELING, OPTIMIZATION, AND IMPACT ANALYSIS

by

Jun Tan

A Dissertation Submitted in

Partial Fulfillment of the

Requirements for the Degree of

Doctor of Philosophy

in Engineering

at

The University of Wisconsin-Milwaukee

May 2017

ABSTRACT

INTEGRATION OF MASSIVE PLUG-IN HYBRID ELECTRIC VEHICLES INTO POWER DISTRIBUTION SYSTEMS: MODELING, OPTIMIZATION, AND IMPACT ANALYSIS

by

Jun Tan

The University of Wisconsin-Milwaukee, 2017
Under the Supervision of Professor Lingfeng Wang

With the development of vehicle-to-grid (V2G) technology, it is highly promising to use plug-in hybrid electric vehicles (PHEVs) as a new form of distributed energy resources. However, the uncertainties in the power market and the conflicts among different stakeholders make the integration of PHEVs a highly challenging task. Moreover, the integration of PHEVs may lead to negative effects on the power grid performance if the PHEV fleets are not properly managed.

This dissertation studies various aspects of the integration of PHEVs into power distribution systems, including the PHEV load demand modeling, smart charging algorithms, frequency regulation, reliability-differentiated service, charging navigation, and adequacy assessment of power distribution systems. This dissertation presents a comprehensive methodology for modeling the load demand of PHEVs. Based on this stochastic model of PHEV, a two-layer evolution strategy particle swarm optimization (ESPSO) algorithm is proposed to integrate PHEVs into a residential distribution grid. This dissertation also develops an innovative load frequency control system, and proposes a hierarchical game framework for PHEVs to optimize

their charging process and participate in frequency regulation simultaneously. The potential of using PHEVs to enable reliability-differentiated service in residential distribution grids has been investigated in this dissertation. Further, an integrated electric vehicle (EV) charging navigation framework has been proposed in this dissertation which takes into consideration the impacts from both the power system and transportation system. Finally, this dissertation proposes a comprehensive framework for adequacy evaluation of power distribution networks with PHEVs penetration.

This dissertation provides innovative, viable business models for enabling the integration of massive PHEVs into the power grid. It helps evolve the current power grid into a more reliable and efficient system.

To

my parents,

my parents in law,

my wife

and especially my son

TABLE OF CONTENTS

LIST OF FIGURES

LIST OF TABLES

LIST OF ABBREVIATIONS

ACE	Area Control Error
AER	All Electrical Range
AGC	Automatic Generation Control
ASAI	Average Service Availability Index
BESS	Battery Energy Storage System
CAIDI	Customer Average Interruption Duration Index
DG	Distributed Generation
DSM	Demand Side Management
ECPM	Energy Consumption Per Mile
EENS	Expected Energy Not Supply
ES	Evolution Strategy
ESPSO	Evolution Strategy Particle Swarm Optimization
EV	Electrical Vehicle
EVCS	Electric Vehicle Charging Station
EVNS	Electric Vehicle Navigation System
GA	Genetic Algorithm
HIDI	Household Interruption Duration Index
HIFI	Household Interruption Frequency Index
HIMI	Household Interruption Magnitude Index
ISO	Independent System Operator
LFC	Load Frequency Control
LMP	Locational Marginal Price

LOLP	Loss of Load Probability
LPMF	Load Profile Modeling Framework
MDP	Markov Decision Process
MPC	Model Predictive Control
MSR	Marginal Spinning Reserve
MTTR	Mean Time to Repair
NHTS	National Household Travel Survey
PHEV	Plug-in Hybrid Electric Vehicle
PIC	Potential Interruption Cost
PSO	Particle Swarm Optimization
PSOC	Power System Operation Center
SAIDI	System Average Interruption Duration Index
SAIFI	System Average Interruption Frequency Index
SOC	State of Charge
SSE	Sum of Squares due to Error
TSO	Transmission System Operator
TTF	Time to Failure
TTR	Time to Replace
V2B	Vehicle-to-Building
V2G	Vehicle-to-Grid
VPP	Virtual Power Plant
vTOU	Virtual Time-of-Use

ACKNOWLEDGEMENTS

First and foremost, I want to thank my advisor, Dr. Lingfeng Wang, for his continuous support of my Ph.D. study and research. Thanks for his professional advices and great effort to make my research productive. His enthusiasm in research motivates me to overcome the many challenges I encountered, especially during the tough times in my Ph.D. pursuit. It is really my honor to be his Ph.D. student.

I would like to express my tremendous thanks to Dr. David Yu, Dr. Chiu Law, Dr. Yue Liu, and Dr. Chao Zhu, for serving as my committee members. Thanks for their time, interest and insightful comments.

Thanks for the help from my fellow students Zhu, Rui, Yichi, Yingmeng, and Yunfan. Their encouragement and support means a lot to me.

Last but not least, I would like to thank my parents, my parents in law, my dear wife and son. Their love is the source of my strength. They bring beauty, happiness, and sweet memories to my life. I dedicate this dissertation to them.

1. Introduction

1.1 Motivations

With the development of vehicle-to-grid (V2G) technology as well as the growth of wind power generation, PHEVs are viewed as a vital technology to modern power systems as they may enable a higher penetration of renewable resources by providing extra energy storage capacity. With the V2G technology, PHEVs are able to serve as distributed energy resources by feeding power back to the grid when needed. Much research has investigated the benefits of integrating PHEVs into power systems, such as frequency regulation and vehicle-to-building (V2B) [1], [2].

The trend of developing the power grid towards a more sustainable and cleaner system makes the renewable resources such as wind and solar power a non-negligible and fast growing contributors to the overall generation portfolio. High penetration of wind power will inevitably reduce system inertia as the wind speed is difficult to be accurately predicted. Moreover, customers are encouraged by governments and regulatory authorities to sell excess power generated by distributed resources back to the utilities in the environment of smart grid. The dynamics of power grid nowadays are affected by more factors as the uncertainties increase on both generation and load sides. These uncertainties will increase the load prediction error which leads to an increase in active power imbalances. As a result, a large amount of regulation capacity is needed in the power system, and various generation units are participating in frequency regulation by contracting with the transmission system operator (TSO) [3].

Traditional generation units have very slow response time and limited ramp rate, thus their

performance in frequency regulation is not quite satisfactory. Basic load frequency control (LFC) systems and algorithms are studied in [4]-[7]. Much research has been conducted for developing Battery Energy Storage Systems (BESS) for frequency regulation [8]. However, due to the high cost of BESS, it is hard to use this technology widely. Fortunately, with the V2G technology in the future smart grid, PHEVs can serve as distributed resources and they are able to provide frequency regulation capacities to the power system through V2G aggregators. With the emerging smart grid technologies, aggregators are envisioned to be able to coordinate the charging process of PHEVs and provide frequency regulation service by contracting a regulation capacity with the TSO [9]. However, the uncertainty of the market prices for electricity and frequency regulation service coupled with the conflict of interests among PHEV owners and the power system make the V2G frequency regulation a very challenging problem. Thus, an effective business model is highly needed for PHEVs providing frequency regulation service in a competitive electricity market. Although the widespread deployment of PHEVs is promising to serve as distributed energy storage which could provide ancillary services for power systems, it may lead to negative effects on the power grid if the PHEV fleets are not well coordinated. High penetration of PHEV fleets in the distribution networks will increase the peak load demand, which will result in transformer overload, voltage deviation, transmission line losses increase and harmonic distortion. Thus, it is highly important to formulate the control of PHEVs and the bidding of frequency regulation capacity as an integrated problem in a competitive electricity market.

Due to the various characteristics of electrical loads and the different requirements of utility customers, it is inefficient to serve all customers at the same reliability level. And the customers should be given additional flexibility to opt for the service reliability that suits them. The

reliability-differentiated pricing can reduce the system cost by reducing the service reliability of those customers who have low requirements on reliability and make additional system income by providing highly reliable service to those customers with high reliability requirements. From this point of view, the reliability-differentiated service is promising to reduce the reserve equipment and peak load. The majority of existing research was focused on the generation and transmission level [10]-[14]. Its basic principle is to divide customers into different classes, and these classes are served with different reliability levels by providing additional generation and transmission reserve capacity or through the operation of power system. The possibility and difficulties of implementing reliability-differentiated services are discussed in [10], where an approach is proposed to differentiate electricity prices based on the customers' priority of service during power generation shortage. A reliability-differentiated pricing policy based on outage cost is proposed in [11] which is a combination of priority pricing and real-time pricing. A differentiated pricing scheme is proposed in [12] for spinning reserve capacity purchase from a societal welfare point of view. The reliability index of loss of load probability (LOLP) is used to generate differentiated nodal pricing in [13]. In [14] a method is proposed to differentiate the electricity price by allocating grid cost between customer groups with different reliability categories.

Although the reliability-differentiated pricing appears very beneficial to realizing flexible demand side management (DSM), several critical issues need to be addressed in its real-world implementation. In particular, it is hard to differentiate the delivering of electricity in terms of reliability due to the intrinsic limitations of current power system [15]. As a result, this research field has not received sufficient attention in the recent decades. Historically, the difficulties for implementing reliability-differentiated services primarily lie in the following two aspects. 1) The

common reliability indices were developed to evaluate the performance of the overall system, and they are not fully capable of indicating the service quality of a specific customer. 2) In the traditional power grid, the power system cannot be operated to deliver the actual reliability service stipulated by the customers.

However, with smart grid technologies and the emergence of PHEVs, it is possible to implement the reliability-differentiated service in the distribution power grid and evolve it into a more reliable and efficient system. With the development of V2G technology, the PHEVs are able to serve as distributed energy storage resources and participate in ancillary services such as frequency regulation and spinning reserve. With real-time monitoring and advanced sensing technologies in smart grid, the power supply conditions of the customers can be obtained by the power grid, so the frequency, duration and magnitude of outages for a specific customer is known to the power system. Smart grid is also able to solve the dilemma of the second problem by controlling the power supply to the customers and distributed resources. So when a power outage occurs, the smart grid will cut off the power supply to customers with lower subscription of reliability, and use distributed resources such as PHEVs as spinning reserve to provide power for those customers with higher subscription of reliability. More recently it is becoming more viable to implement reliability-differentiated services with wider deployment of smart grid technologies

With the increasing penetration of electric vehicles (EVs) and the development of charging infrastructure, the electric vehicle charging stations (EVCS's) are becoming a vital recharging source for EVs. Home charging at a house garage may be more convenient for the EV owners. For people living in urban areas with high population density, the accessibility of personal garages is limited and public charging stations are needed to recharge their EVs. Moreover,

EVCSs can offer lower charging prices for EVs compared with home charging, as power can be purchased at a lower rate from the wholesale power market [16]. Also, EVCSs are a much needed recharging infrastructure for long-distance travelers who may run out of their batteries before returning home. These merits make the EVCS a promising charging infrastructure. However, as the penetration level of EVs grows, the intermittent charging loads may place additional stress on the power system by overloading the distribution transformers and transmission lines. Thus, a charging navigation system is needed to provide a novel business model for the EVs and the EVCSs by considering the traffic flow and the competition between the EVCSs.

1.2 Dissertation Objectives

The primary research objective of this dissertation is to develop an integrated framework to study impact of PHEVs on the power distribution system and develop effective control methods to coordinate the charging process of PHEVs. The major contributions of this dissertation are concluded as follows:

- Build the stochastic model of PHEVs' load demand;
- Propose a new intelligent hybrid algorithm.
- Design an LFC system with PHEVs.
- Propose a viable business model for PHEVs to participate in frequency regulation in a competitive electricity market.
- Propose a reliability-differentiated framework to enable reliability-differentiated service in a residential distribution network. Thus, the customers can be served at different reliability levels.

- Developed a reliability-differentiated pricing mechanism which is able to improve the reliability of the residential distribution system as well as provide differentiated power prices to the customers according to their different requirements on reliability.
- Proposed an integrated charging navigation framework to link the power system with transportation system. Thus, an optimal charging navigation strategy can be achieved to benefit both the power system and transportation system.
- Developed a traffic flow simulation method for EVs considering the real-world usage data of EVs.
- Proposed a novel business model for EVCSs based on game theory. Thus, the competition between charging stations can be modeled.
- Proposes a comprehensive framework for adequacy evaluation of power distribution network with large-scale PHEV penetrations.

1.3 Organization of Dissertation

This dissertation is organized as follows. In Chapter 1, the major issues in integrating PHEVs into power distribution system and the research objectives are introduced. Chapter 2 proposes a load profile modeling framework (LPMF) for PHEVs, which takes both the characteristics of driving pattern and vehicle parameters into consideration. In Chapter 3, a two-Layer intelligent optimization algorithm has been proposed to integrate PHEVs into residential distribution grids. A hierarchical game framework has been proposed in Chapter 4 to coordinate the charging process of PHEVs and enable PHEVs to participate in frequency regulation at the same time. Chapter 5 proposes a framework for implementing reliability-differentiated services in a residential distribution with PHEVs. Chapter 6 proposes an integrated framework for real-

time EV navigation, which considers both the impact from the transportation system and power system. Chapter 7 systematically investigated the impact of large scale penetration of PHEVs on power distribution system adequacy. The conclusions and the future works are presented in Chapter 8.

2. Stochastic Modeling of PHEV Load Demand

2.1 Introduction

For the modeling of driving pattern, different assumptions are made by researchers to simplify the study. In [17] it is assumed that the PHEVs have pre-specified arrival time, which is 6 pm, 9 pm and 10 am. References [18]-[21] use probabilistic methodology to model the arrival time, departure time and daily mileage. Copula functions are used to study the correlation of arrival time, departure time and daily mileage in [22]. A method based on the Markov chain is proposed in [23], [24] to find the correlation. These studies have shown to be effective in modeling driving patterns, but further analysis of vehicle characteristics is still needed.

To date, few studies have been carried out considering both the stochastic nature of driving pattern and vehicle characteristics. This chapter hereby proposes a load profile modeling framework (LPMF) for PHEVs, which takes both the characteristics of driving pattern and vehicle parameters into consideration. Moreover, to analyze the relationship between the arrival time, departure time and daily mileage of PHEVs, the authors propose a Stochastic Fuzzy Model to synthetize the driving pattern.

2.2 Studying NHTS Data

National Household Travel Survey (NHTS) 2009 [25] is the most comprehensive transportation report in United States thus far. It contains 1048575 single trips and each trip has 150 attributes. As a person may have several trips in a day, all the trips in a day should be considered to generate the daily driving pattern of PHEVs. Here we define the departure time as the first trip start time, and arrival time as the finial trip end time. The daily mileage driven is defined as the sum of the trip mileages in a day. According to NHTS 2009, the percentage of

vehicle versus the departure time is shown in Fig. 2.1, and the percentage of vehicle versus the arrival time is shown in Fig. 2.2. It is assumed that the driving habits of people will not change in the near future, so the travel survey data are used to predict the driving pattern. The PDFs of the arrival time, departure time and daily mileage can be fitted from their observed data. The quality of the curve fits is evaluated through the goodness-of-fit statistic: the sum of squares due to error (SSE).

$$\mathrm{SSE} = \sum_{i=1}^{n} \omega_i \, (y_i - \hat{y}_i)^2 \tag{2.1}$$

where y_i is the observed data and $\hat{y}_i$ is the predicted value from the fit, ω_i is the weighting coefficient and set $\omega_i = 1$.

As shown in Fig. 2.1, the departure time of vehicles follows a normal distribution which can be expressed as follows:

$$F_{dep}(t) = \frac{1}{\sigma\sqrt{2\pi}} e^{-(t-\mu)^2/2\sigma^2}, 0 < t < 24 \tag{2.2}$$

where μ=9.97, $\sigma = 2.2$ and SSE=0.0034.

Also, the PDF of the arrival time of vehicles is a normal distribution and can be expressed as follows:

$$F_{arr}(t) = \frac{1}{\sigma\sqrt{2\pi}} e^{-(t-\mu)^2/2\sigma^2}, 0 < t < 24 \tag{2.3}$$

where μ=17.01, $\sigma = 3.2$ and SSE=0.0026.

According to NHTS, the distribution of daily mileage can be described by a lognormal distribution as shown in Fig. 2.3. The PDF of the daily vehicle travel distance can be expressed as follows:

$$F_d(d) = \frac{1}{d\sigma\sqrt{2\pi}} e^{-(lnd-\mu)^2/2\sigma^2}, d > 0 \tag{2.4}$$

where d is the travel distance, μ is the mean of lnd, and σ is the standard deviation of the lognormal distribution. In this case, μ=3.2, $\sigma = 0.9$ and SSE=0.0036

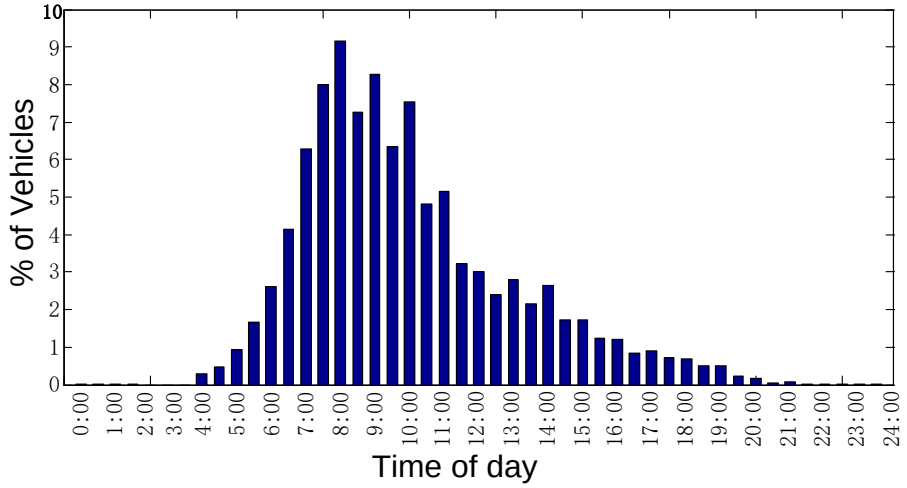

Figure 2. 1 Percentage of vehicles versus their departure time

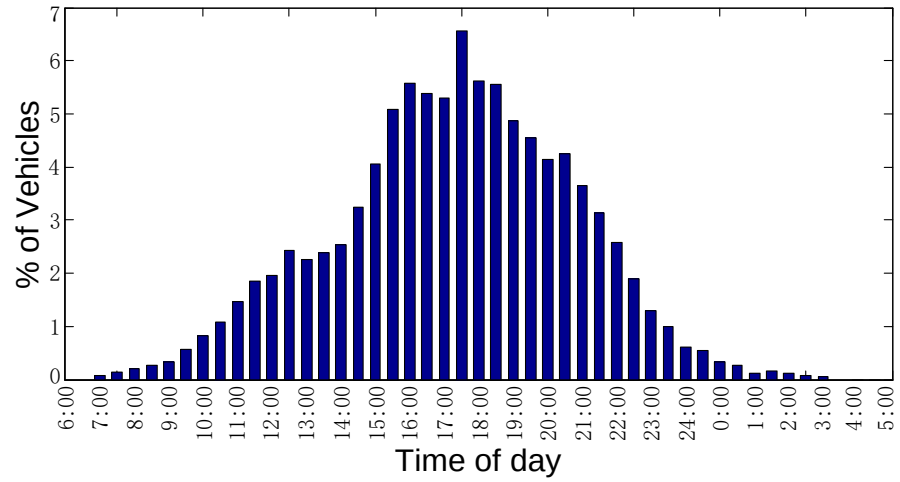

Figure 2. 2 Percentage of vehicles versus their arrival time.

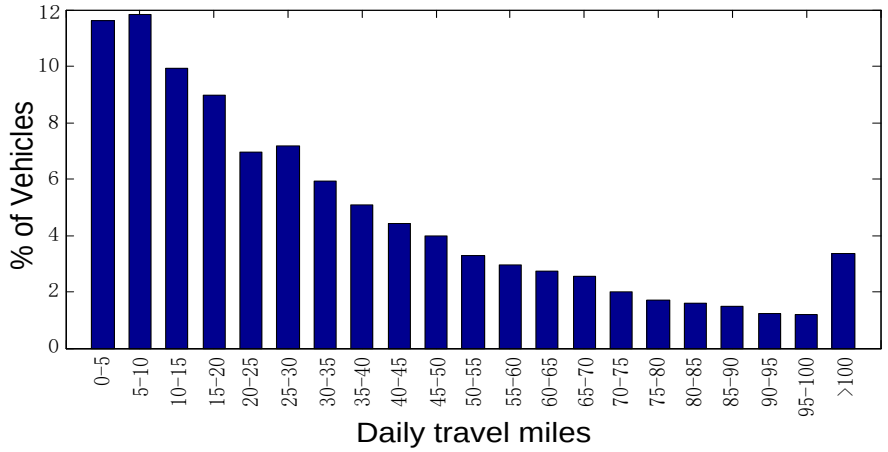

Figure 2. 3 Percentage of vehicles versus daily miles driven.

Fig. 2.4 is derived from the NHTS 2009 database. It describes the relationship between the arrival time and departure time of PHEVs. As shown in the figure, the PDF of departure time features a quite same shape in each time window of arrival time, which implies the two PDFs of departure time and arrival time are independent of each other. So the arrival time and departure time of a PHEV are two independent events. However, the daily mileage is correlated with the arrival time and departure time. It will cause inaccuracy if simply using the PDFs of arrival time, departure time and daily mileage to generate the driving pattern.

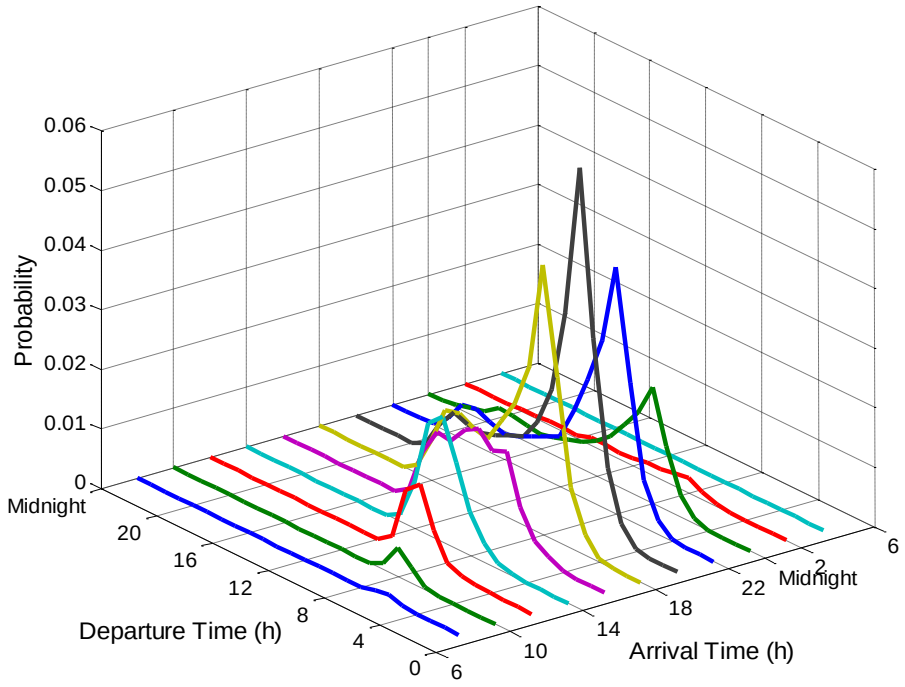

Figure 2. 4 PDF of departure time at different time windows of arrival time.

2.3 Stochastic Fuzzy Model of PHEV

By analyzing the travel data, it is found that the arrival time and departure time of a PHEV are two independent events; in other words, these two probability density functions do not have a dependent structure when they are combined to represent the activity of a PHEV. But when considering the data of daily mileage, it is a quite different case. The daily mileage is very

dependent on the arrival time and departure time [22]-[24]. For different combinations of arrival time and departure time, the probability density of the daily mileage may be different.

Here a fuzzy logic based stochastic model is proposed to generate driving patterns of PHEVs. As mentioned earlier, the major task of modeling the charging demand of PHEVs is to identify the time when PHEVs are plugged in and plugged out, coupled with the initial State of Charge (SOC) of the PHEVs. These three elements can be handled very well using the concept of fuzzy logic. As the control of PHEV charging is based on a sequence of time slots [17]-[24], [26]-[31] the plug-in and plug-out times are not necessary to be accurate values. Also, it is not necessary to know the accurate value of the SOC. The SOC can be classified into different stages, and it varies from one stage to another after charging during each time slot. Different stages of SOC can be converted into different ranges of the daily mileage. Fuzzy logic is used as a tool for pattern classification in this problem. The departure time, arrival time and daily mileage are divided into different ranges by membership functions, and their relationships are defined by fuzzy rules.

As shown in Fig. 2.5, symmetric 5-segment triangular membership functions are used as input and output variables. Fig. 2.5(a), (b) shows the input variables for the departure time and the arrival time, and their membership functions are defined as very early (VE), little early (LE), normal (N), little late (LL), and very late (VL). The output variable for daily mileage is shown in Fig. 2.5(c), and its membership functions are defined as small (S), small-medium (SM), medium (M), medium-large (ML), and large (L). The parameters of the maximum limit, the minimum limit and the mean value of each variable can be generated from its PDF, and these parameters shown in Fig. 2.5 are $\mathrm{Min}_{\mathrm{dep}} = 4,\ \mu_{\mathrm{dep}} = 9.97,\ \mathrm{Max}_{\mathrm{dep}} = 21,\ \mathrm{Min}_{\mathrm{arr}} = 7,\ \mu_{\mathrm{arr}} = 17.01,$ $\mathrm{Max}_{\mathrm{arr}} = 29, \mathrm{Min}_{\mathrm{d}} = 0, \mu_{\mathrm{d}} = 35.64, \mathrm{Max}_{\mathrm{d}} = 100.$

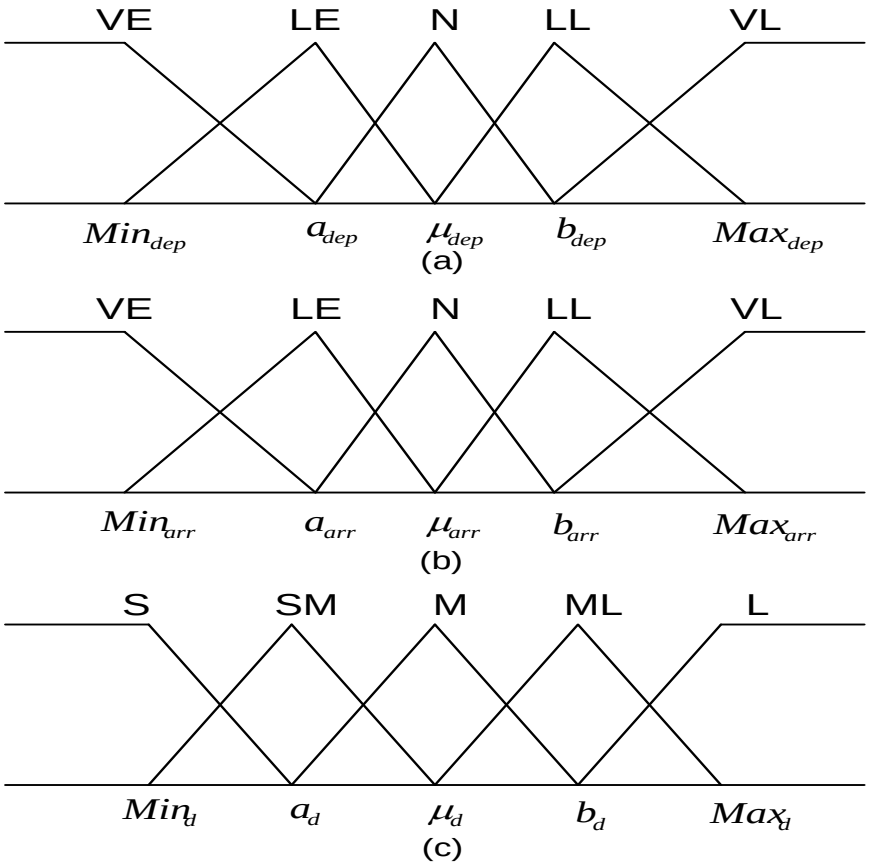

Figure 2. 5 Fuzzy membership functions. (a) Departure time pattern. (b) Arrival time pattern. (c) Daily travel mileage pattern.

In the proposed Stochastic Fuzzy Model, the mapping from input space to the output space is a probabilistic distribution over the fuzzy rules. To indicate this stochastic process, a probability matrix P is defined as follows:

$$P = \begin{bmatrix} p^{d}_{VE,VE} & p^{d}_{VE,LE} & p^{d}_{VE,N} & p^{d}_{VE,LL} & p^{d}_{VE,VL} \\ p^{d}_{LE,VE} & p^{d}_{LE,LE} & p^{d}_{LE,N} & p^{d}_{LE,LL} & p^{d}_{LE,VL} \\ p^{d}_{N,VE} & p^{d}_{N,LE} & p^{d}_{N,N} & p^{d}_{N,LL} & p^{d}_{N,VL} \\ p^{d}_{LL,VE} & p^{d}_{LL,LE} & p^{d}_{LL,N} & p^{d}_{LL,LL} & p^{d}_{LL,VL} \\ p^{d}_{VL,VE} & p^{d}_{VL,LE} & p^{d}_{VL,N} & p^{d}_{VL,LL} & p^{d}_{VL,VL} \end{bmatrix} \quad (2.5)$$

$$\forall\, d \epsilon [S, SM, M, ML, L]$$

where each entry of P is a row vector which is a probability distribution over the membership functions of daily mileage base on a combination of membership functions of arrival time and

departure time.

For instance, one entry of P is defined as follows:

$$p^{d}_{VE,LE} = [p^{S}_{VE,LE}, p^{SM}_{VE,LE}, p^{M}_{VE,LE}, p^{ML}_{VE,LE}, p^{L}_{VE,LE}] \quad (2.6)$$

where $p^{d}_{VE,LE}$ indicate the probability distribution vector over membership functions of daily mileage when arrival time is VE and departure time is LE. Its entries are the probabilities of choosing a certain membership function of daily mileage.

The proposed stochastic fuzzy rules can be expressed in the form of IF-THEN statements such as:

IF DT (departure time) is LE and AT (arrival time) is LL, **THEN** DM (daily mileage) is M with probability of $p^{M}_{LE,LL}$.

Once the parameters of membership functions as shown in Fig. 2.5 are chosen, the probability matrix P can be obtained by statistical method according to NHTS 2009. Then according to the stochastic fuzzy rules, the daily mileages can be generated. The quality of fitness of the generated daily mileages can be evaluated through SSE as defined in (2.1). To ensure that the Stochastic Fuzzy Model predicts the driving pattern correctly, the parameters of the membership functions should be appropriately chosen. Here a Particle Swarm Optimization (PSO) algorithm is used to find the optimal parameters of the membership functions.

PSO was developed based on the collective behaviors exhibited in bird flocking and fish schooling [32]. In PSO, a population of particles flies in a search space and every particle has its own location and velocity. The possible solution of a problem is mapped to a search space, and the location of each particle in the search space is a potential solution to the target problem. The fitness of each potential solution is evaluated by an objective function. The best position of the i_{th} particle is stored as $pBest_i$ (personal best position) and the best position of all the particles is

stored as gBest (global best position). These particles can learn from their own and others' experiences. The position and velocity of each particle are continuously adjusted according to (2.7)-(2.9). When the iterative procedure is finished, the best value position gBest can be used to optimize the objective function.

$$v_{id}^{k+1} = wv_{id}^{k} + C_1 \cdot rand_1 \cdot \left(pBest_i - x_{id}^{k}\right) + C_2 \cdot rand_2 \cdot \left(gBest - x_{id}^{k}\right) \tag{2.7}$$

$$x_{id}^{k+1} = x_{id}^{k} + v_{id}^{k+1} \tag{2.8}$$

$$w = w_{max} - k \cdot \frac{w_{max} - w_{min}}{k_{max}} \tag{2.9}$$

where v_{id} is the velocity of particle i at dimension d; x_{id} is the position of particle i along dimension d; w is the inertia weight; and k is the iteration number.

In this parameters-tuning problem, there are 6 parameters $a_{dep}, b_{dep}, a_{arr}, b_{arr}, a_d, b_d$ as shown in Fig. 2.5, which need to be optimized. Each parameter can be defined as a dimension of the search space, and the range of the specific parameter can be encoded as the coordinates in the specified dimension. The objective is to minimize the SSE of the generated daily mileages. Solving the problem is equivalent to finding the optimal location in the search space. After certain iterations the PSO algorithm converges as shown in Fig. 2.6. The global best value is SSE=0.0095 and the optimized parameters of the membership functions are shown in Table 2.1.

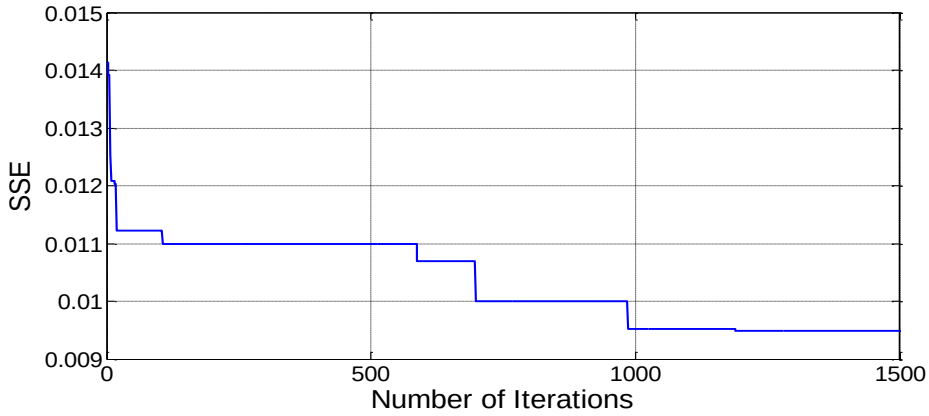

Figure 2. 6 Convergence curve of the PSO algorithm.

Table 2. 1 Optimal Values of Membership Function Parameters

a_{dep}	b_{dep}	a_{arr}	b_{arr}	a_d	b_d
9.13	13.27	11.93	19.22	13.68	87.74

Based on these the Stochastic Fuzzy Model is able to predict the driving pattern of PHEVs. The computational procedure of the driving pattern of PHEVs can be illustrated as follows:

Step 1: Generate the departure time and the arrival time for a specified number of PHEVs according to the PDFs (2.2) and (2.3).

Step 2: Map the crisp input values generated in Step 1 to linguistic values using the fuzzification method.

Step 3: Generate probability matrix P according to NHTS data and parameters in Table 2.1.

Step 4: Generate linguistic output values according to the stochastic fuzzy rules obtained from probability matrix P and convert them to crisp values.

Step 5: Output the value of driving distance together with its related departure time and arrival time for each PHEV.

2.4 Vehicle Type Analysis

PHEVs are classified by its all electrical range (AER) and the percentage of PHEV-x is shown is Table 2.2 [33]. For instance, PHEV-30 indicates it has an AER of 30 miles. Different types of PHEV-x have different energy consumption per mile (ECPM) and battery capacities, and they are shown in Table 2.3 [20]. Assume the four types of vehicles have equal percentage of distribution. To render this study closer to real world scenarios, the proposed PHEV LPMF will randomly select the AERs and vehicle types of PHEVs based on their percentage of distribution.

Table 2. 2 Percentage of PHEVs With Different AERs

	PHEV-30	PHEV-40	PHEV-60
Percentage	21%	59%	20%

Table 2. 3 Battery Capacity for Different Types of PHEV (kWh)

Vehicle Type	PHEV-30	PHEV-40	PHEV-60
Compact	7.8	10.4	15.6
Mid-size	9	12	18
Mid-size	11.4	15.2	22.8
Full-size SUV	13.8	18.4	27.6

2.5 Charging Level and Initial SOC

The charging level of PHEVs could be very different due to various charging facilities. For instance, in [17] it is assumed that the charging level is 4 kW based on a 230 V/4.6 kW outlet in Belgium. In [34] a charging level of 240 V/30A is used, and in [20] outlets of 120V/15 A and 240/50 A are considered. As this study is focused on residential level impact of PHEVs, the AC Level 1 (1.8 kW) and AC Level 2 (3.6 kW) are considered and the charging rate is randomly selected from these two charging levels with equal probability for each PHEV.

SOC is defined as the percentage of energy remaining in the battery. Minimum SOC is set to 20% to extend the battery life. PHEV can operate in charge-depleting mode, which implies all or part of its energy is provided by its battery. Here we define a factor λ as the percentage of mileage driven in all electrical mode. Assume the PHEV has an AER of d_R, and the energy consumption of the PHEV is proportional to the travel distance d. The initial SOC of a PHEV

with a daily travel distance d is:

$$SOC_{initial} = \begin{cases} \left(1 - \frac{\lambda \cdot d}{d_R}\right) \times 100\%, 0 < \lambda d < 0.8 d_R \\ 20\%, \lambda d \geq 0.8 d_R \end{cases} \quad (2.10)$$

The energy required to fulfill the battery is:

$$E_{req} = \frac{(1 - SOC_{initial}) \cdot C}{\eta} \quad (2.11)$$

where C is the battery capacity and η is the charging efficiency factor.

2.6 Obtaining PHEV Load Profile

The load profile of PHEVs is obtained from the proposed LPMF as shown in Fig. 2.7. First, the driving pattern is generated by the proposed Stochastic Fuzzy Model as mentioned in this section. Then the daily mileage is combined with vehicle parameters to generate the required energy according to (2.10) and (2.11). Finally, the load profile is obtained through the required energy and its driving pattern based on a charging algorithm.

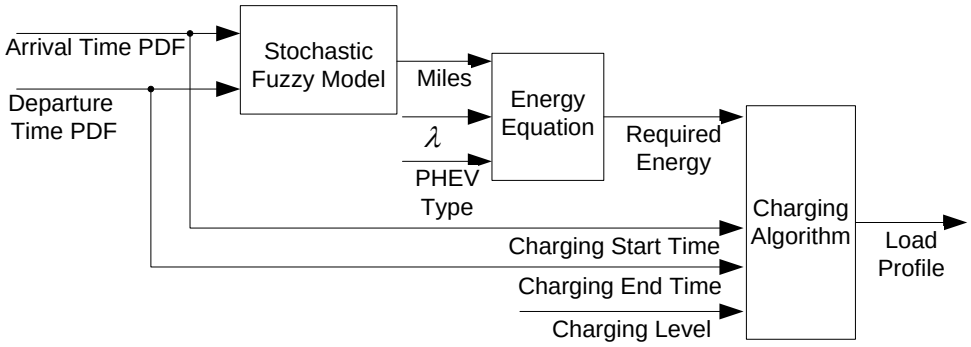

Figure 2. 7 The PHEV load profile modeling framework.

3. Two-Layer Intelligent Optimization for integration of PHEVs into Residential Distribution Grid

3.1 Introduction

The development of vehicle-to-grid (V2G) technology in the smart grid context is reshaping the traditional view of power grid. With the increasing penetration of intermittent generation units and loads, energy storage devices are highly needed in nowadays' power grid, and PHEVs may be a promising solution to this problem. V2G can benefit the power grid by shaving the peak load and providing ancillary services such as frequency regulation and spinning reserves. Although V2G is a promising technology, its real-world implementation demands an effective business model coupled with a more advanced battery technology. Some research has been conducted for reducing the impacts of PHEVs on power systems based on various optimization criteria and algorithms [26]-[28]. Also, some studies have been carried out in investigating the V2G benefits and feasibility [29]-[31]. However, little work has been done to combine these two technologies together for formulating an integrated problem.

Based on the proposed Stochastic Fuzzy Model of PHEV in Chapter 2, this chapter has developed a novel business model for PHEVs to provide frequency regulation service as well as participate in peak load shaving in a residential distribution grid. This chapter proposes a virtual time-of-use (vTOU) rate based on the load demand to encourage the PHEV owners to participate in peak load shaving by providing economic incentives. In this chapter, an aggregator is designed to coordinate the charging process of PHEVs in a residential distribution grid to achieve four goals by flattening the load demand, improving power quality, providing frequency regulation service, and minimizing the total cost. To solve the formulated problem, an evolution strategy

particle swarm optimization (ESPSO) algorithm is proposed which is achieved by hybridizing the evolution strategy (ES) and particle swarm optimization (PSO). The simulation results show that the ESPSO approach is a very effective algorithm in solving the target problem.

3.2 System Model

3.2.1 Battery Degradation Cost

Battery Degradation is one of the major challenges of V2G technology [35]. The extra battery degradation cost due to V2G activities can be expressed as follows [36]:

$$Cost_{bat} = \frac{c_b E_b + c_L}{L_C E_b DOD} E_{dis} \tag{3.1}$$

where c_b is the battery cost per kWh, c_L is the labor cost for battery replacement, E_b is the battery capacity, L_C is the battery life cycle at a determined depth of discharge, E_{dis} is the discharge energy by PHEVs, and DOD is the depth of discharging. In this study, c_b=\$300/kWh, c_L =\$240 and L_C=5000 at 80% discharge [35].

3.2.2 Smart Pricing Policy

In order to reduce peak load of the system, a vTOU rate policy is developed based on system load demand to regulate the charging process of PHEVs. The price is defined as follows:

$$r(t) = \beta_1 + \beta_2 \cdot \alpha^{\frac{P_{sys}^t - P_{avg}}{P_{avg}}} \tag{3.2}$$

where β_1, β_2, α are price parameters, $P_{sys}^t$is the load demand of the system at time slot t and P_{avg} is the average load demand of the system. In the studied system, we set β_1=\$0.1/kWh, β_2=0.2 \$/kWh and α=10.

This virtual dynamic electricity market price is sensitive to the load demand, and it

increases very quickly with the increase of load demand especially at peak load time.

3.2.3 Frequency Regulation

V2G technology enables PHEVs to provide frequency regulation service for the power system. The PHEVs are contracted with TSO through aggregators, and TSO provides economic incentives for PHEVs participating in the regulation service. When a PHEV provides the regulation service, the net energy exchange tends to be zero over a long time [35]. Thus, the PHEVs are paid by the power capacity provided for frequency regulation. In this study, PHEVs are utilized to provide regulation service when they are in idle state.

3.3 Mathematical Modeling of PHEVs

The charging time horizon for a day can be represented as a vector $\mathbf{T} = [1,\cdots,t,\cdots,T]$ which includes T equal time slots. The PHEVs also can be described as a vector $\mathbf{N} = [1,\cdots,d,\cdots,N]$. For the d_{th} PHEV, the plug-in time $t_{in,d}$, plug-out time $t_{out,d}$ and required charging energy $E_{req,d}$ can be generated by the procedure described in Fig. 2.7. In this study, we use boldface letters to denote vectors.

As demonstrated in [27], it is more cost effective to let PHEVs charge at the rated charging power so that more revenues can be earned by providing frequency regulation service. Thus, PHEVs can be controlled at three states: charging, discharging and idle. The charging strategy can be expressed as a vector k as follows:

$$\mathbf{k_d} = \left[k_d^{t_{in,d}},\cdots,k_d^t,\cdots,k_d^{t_{out,d}}\right], \forall\ d \epsilon \mathbf{N} \tag{3.3}$$

where $k_d^t = 1$ means the d_{th} PHEV is in charging state at time slot t, $k_d^t = -1$ implies the d_{th} PHEV is in discharging state at time slot t and $k_d^t = 0$ indicates the PHEV is in idle state at time

slot t.

The required energy constraint is described in (3.4):

$$E_{req,d} = \sum_{t=t_{in,d}}^{t_{out,d}} k_d^t \cdot P_{rate}^d, \forall\, d \epsilon \mathbf{N} \tag{3.4}$$

where P_{rate}^d is the rated charging power of the d_{th} PHEV.

It is assume that only the PHEVs in idle state can respond to the frequency regulation service call. We defined three vectors $\mathbf{C} = [C_1 \cdots, C_d, \cdots, C_N]$, $\mathbf{D} = [D_1 \cdots, D_d, \cdots, D_N]$ and $\mathbf{I} = [I_1 \cdots, I_d, \cdots, I_N]$ to indicate the charging, discharging and idle state of PHEVs at each time slot as shown in (3.5)-(3.10).

$$C_d = \left[C_d^{t_{in,d}}, \cdots, C_d^t, \cdots, C_d^{t_{out,d}}\right], \forall\, d \epsilon \mathbf{N} \tag{3.5}$$

$$C_d^t = \begin{cases} 1, & \text{if } k_d^t = 1 \\ 0, & \text{otherwise} \end{cases}, \ \forall\, t \epsilon \mathbf{T}; \forall\, d \epsilon \mathbf{N} \tag{3.6}$$

$$D_d = \left[D_d^{t_{in,d}}, \cdots, D_d^t, \cdots, D_d^{t_{out,d}}\right], \forall\, d \epsilon \mathbf{N} \tag{3.7}$$

$$D_d^t = \begin{cases} 1, & \text{if } k_d^t = -1 \\ 0, & \text{otherwise} \end{cases}, \ \forall\, t \epsilon \mathbf{T}; \forall\, d \epsilon \mathbf{N} \tag{3.8}$$

$$I_d = \left[I_d^{t_{in,d}}, \cdots, I_d^t, \cdots, I_d^{t_{out,d}}\right], \forall\, d \epsilon \mathbf{N} \tag{3.9}$$

$$I_d^t = \begin{cases} 1, & \text{if } k_d^t = 0 \\ 0, & \text{otherwise} \end{cases}, \ \forall\, t \epsilon \mathbf{T}; \forall\, d \epsilon \mathbf{N} \tag{3.10}$$

where d means the d_{th} PHEV and t indicate the t_{th} time slot.

Thus, the frequency regulation capacity of the system can be calculated as (3.11):

$$P_{Reg}^t = \sum_{d=1}^{N} I_d^t \cdot P_{rate}^d, \forall\, t \epsilon \mathbf{T} \tag{3.11}$$

The total charging power of PHEVs is illustrated as (3.12) and the average load demand of the system is represented in (3.13):

$$P_{EV}^t = \sum_{d=1}^{N} k_d^t \cdot P_{rate}^d, \forall\, t \epsilon \mathbf{T} \tag{3.12}$$

$$P_{avg} = \frac{1}{T}\sum_{t=1}^{T}(P_{Base}^{t} + P_{EV}^{t}) \tag{3.13}$$

where $P_{Base}^{t}$is the non-PHEV load of the system.

The total discharging energy provided by PHEVs is:

$$E_{dis} = \sum_{d=1}^{N}\sum_{t=t_{in,d}}^{t_{out,d}} D_{d}^{t} \cdot P_{rate}^{d} \tag{3.14}$$

So a feasible control strategy of PHEVs can be described as follows:

$$\mathbf{K} = \{\mathbf{k_d}|\text{s.t. (3.4)}\},\forall\ d\in\mathbf{N} \tag{3.15}$$

The objective function is designed to minimize the total cost of the system consisting of three parts: the charging cost, the battery cost due to V2G, and the profit earned by providing frequency regulation service.

The charging cost accounts for both the cost for charging and the revenue earned by discharging as shown below:

$$Cost_{chg} = \sum_{t=1}^{T} P_{EV}^{t} \cdot r(t) \tag{3.16}$$

The battery cost is defined as (3.1), and the revenue earned by regulation service is as follows:

$$Earn_{reg} = \sum_{t=1}^{T} P_{Reg}^{t} \cdot reg(t) \tag{3.17}$$

where $reg(t)$ is the regulation service price at time slot t. The total cost should be:

$$Cost = Cost_{chg} + Cost_{bat} - Earn_{reg} \tag{3.18}$$

So the objective function can be represented as follows:

$$\min\{Cost|\text{s.t. (3.15)}\} \tag{3.19}$$

3.4 The Two-Layer Intelligent Optimization Algorithm

3.4.1 Dominant Solution Matrix

The feasible solutions for the formulated problem constitute a very large search space. To simplify the problem, it is crucial to find dominant solutions from the feasible solutions. As frequent switching between charging and discharging modes will greatly expedite the degradation progress of batteries [27], the charging and discharging time slots should be wisely arranged to avoid PHEV's frequent switching between different control states.

The charging sequence of PHEVs can be classified into different patterns based on various V2G strategies. We defined a strategy vector $\boldsymbol{s}$ to indicate the V2G strategy of each PHEV as follows:

$$\boldsymbol{s} = [s_1, \cdots, s_d, \cdots, s_N] \tag{3.20}$$

where s_d is the possible V2G strategy of the d_{th}PHEV.

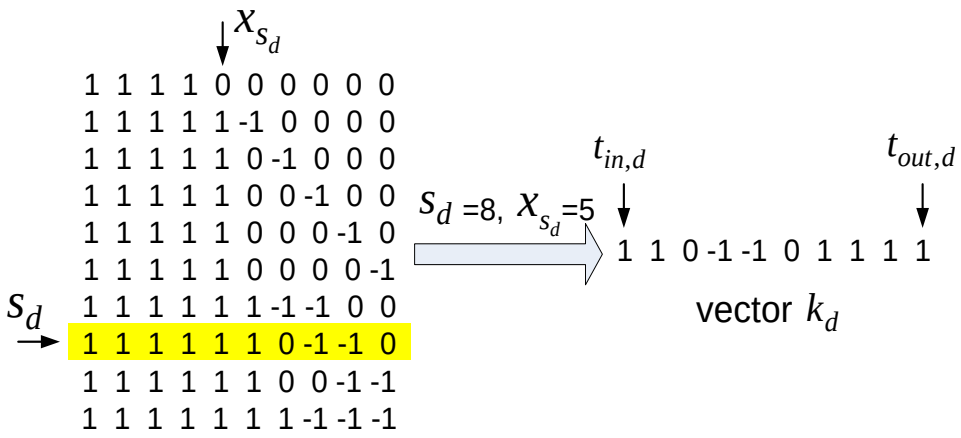

Figure 3. 1 The principle of dominant solution matrix.

Based on the above two principles, the dominant solution matrix of the d_{th} PHEV DS_d is shown in Fig. 3.1. The dominant charging sequence can be generated from this matrix by selecting different V2G strategies s_d and the sequence starting point x_{s_d}. As shown in Fig. 3.1, the row of this matrix indicates different possible V2G strategy patterns. Once a sequence pattern is selected, the possible charging solutions of this specific PHEV can be obtained by shifting the sequence. For instance, as shown in Fig. 3.1 the V2G strategy $s_d = 8$ and the sequence starting

point $x_{s_d} = 5$, so the 8th row is selected and the sequence is started from the 5th column of this row.

For all the PHEVs, the dominant solution matrix is represented as follows:

$$\boldsymbol{DS} = [DS_1 \cdots DS_d \cdots DS_N], \forall\, d\epsilon \boldsymbol{N} \tag{3.21}$$

3.4.2 Evolution Strategy Particle Swarm Optimization

In this section, an evolution strategy particle swarm optimization algorithm (ESPSO) is designed to solve the formulated problem. ESPSO is essentially a two-layer intelligent space search algorithm. In the upper layer, an evolution strategy is used to find an optimal V2G strategy; and based on this V2G strategy, a PSO algorithm is proposed to find the optimal charging sequence in the lower layer. The existing methods such as PSO or genetic algorithm (GA) are not able to effectively solve the three states charging process of PHEVs, as they usually suffer from the curse of dimensionality due to the huge search space. The proposed ESPSO approach solves this complex problem by dividing it into two layers, which drastically narrows the search space.

In this algorithm, the dominant solution matrix **DS** is mapped to a search space. Each PHEV is viewed as a dimension in the search space, and the sequence starting point x_{s_d} is the coordinate in this specific dimension. The V2G strategy is evolved based on (3.22), (3.23). Then both the original and evolved particles keep updating their flying trajectories according to (3.24)-(3.26).

$$es_{id}^{k} = s_{id}^{k} + w \cdot N(0, \sigma_d) \tag{3.22}$$

$$s_{id}^{k+1} = \begin{cases} es_{id}^{k}, & if\ Cost_i < pBest_i \\ s_{id}^{k}, & otherwise \end{cases} \tag{3.23}$$

$$v_{is_{id}^{k+1}}^{k+1} = wv_{is_{id}^{k}}^{k} + C_1 \cdot rand_1 \cdot \left(pBest_i - x_{is_{id}^{k}}^{k}\right) + C_2 \cdot rand_2 \cdot \left(gBest - x_{is_{id}^{k}}^{k}\right) \quad (3.24)$$

$$x_{is_{id}^{k+1}}^{k+1} = x_{is_{id}^{k}}^{k} + v_{is_{id}^{k+1}}^{k+1} \quad (3.25)$$

$$w = w_{max} - k \cdot \frac{w_{max} - w_{min}}{k_{max}} \quad (3.26)$$

where s_{id}^{k} is the original V2G strategy of particle, $es_{id}^{k}$is the evolved V2G strategy, $v_{is_{id}^{k}}^{k}$ is the velocity of the particle, $x_{is_{id}^{k}}^{k}$ is the position of particle, w is the inertia weight, k is the iteration number, i is the particle number, and d is the dimension number.

The computational procedure of the ESPSO algorithm can be elaborated as follows:

- Step 1: Initialize all the particles in the search space. Particle positions and velocities are set randomly to be within the feasible search space.
- Step 2: Evolve the particles according to (3.22).
- Step 3: Evaluate the fitness of each original particle and its corresponding evolved particle with respect to the objective function.
- Step 4: Compute the fitness value of each original particle; and if it is a better solution for this particle, then store its position as a $pBest$ position for this specific particle.
- Step 5: Compute the fitness value of each evolved particle; and if it is better than the current $pBest$ value, then update the corresponding original particle with the evolved particle and store its position as a new $pBest$ position for this specific particle; otherwise, keep the original particle unchanged.
- Step 6: Check the fitness value of each particle. If it is the best solution for all particles, then store the particle's position as $gBest$ position.
- Step 7: Update the position and velocity of each particle according to (3.24)-(3.26).
- Step 8: If $v_{is_{id}^{k}}^{k} > V_{max}$, then $v_{is_{id}^{k}}^{k} = V_{max}$; If $v_{is_{id}^{k}}^{k} < V_{min}$, then $v_{is_{id}^{k}}^{k} = V_{min}$; If

$x^k_{is^k_{id}} > X_{max}$, then $x^k_{is^k_{id}} = X_{max}$; If $x^k_{is^k_{id}} < X_{min}$, then $x^k_{is^k_{id}} = X_{min}$.

- Step 9: If the stopping criterion is satisfied, then go to Step 10; otherwise, go to Step 2.
- Step 10: Output the optimal solution.

3.5 Case Studies

The residential distribution grid studied here is based on the topology of an IEEE 34-node test feeder [37] as shown in Fig. 3.2. In the test system, load point 1 is connected to the grid, and there are 198 houses randomly allocated at other 33 load points. The non-PHEV load profile of a house in winter is scaled from [38]. It is assumed that each house has two vehicles, and the penetration level of the PHEVs is defined as the ratio between the numbers of PHEVs and all vehicles. The power flow is based on a backward-forward sweep method [39].

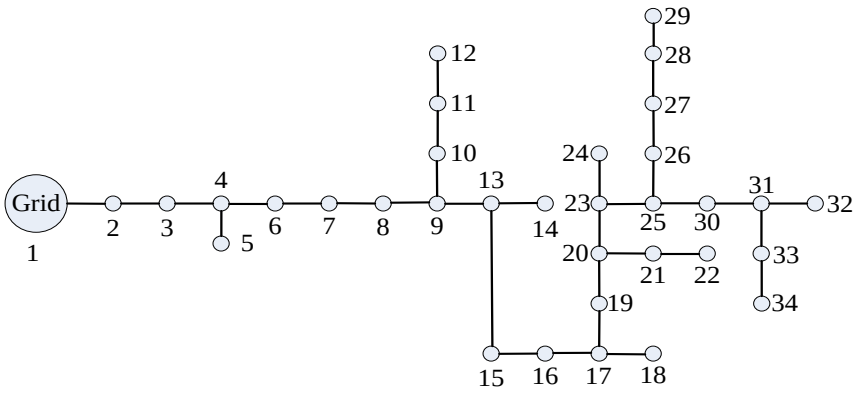

Figure 3. 2 The topology of the studied residential distribution grid.

The simulation is carried out in a residential distribution grid based on different PHEV modeling methods. The charging process of PHEVs based on uncontrolled charging, PSO based smart charging and the proposed ESPSO approach respectively. The total load demand of the system is compared based on three different cases.

- Case 1: The load demand of PHEVs is modelled by the proposed Stochastic Fuzzy

Model and LPMF.

- Case 2: The PHEV model only takes the driving patterns into consideration, without considering the vehicle parameters.
- Case 3: The PHEV model only takes the vehicle parameters into consideration, without considering the driven pattern.

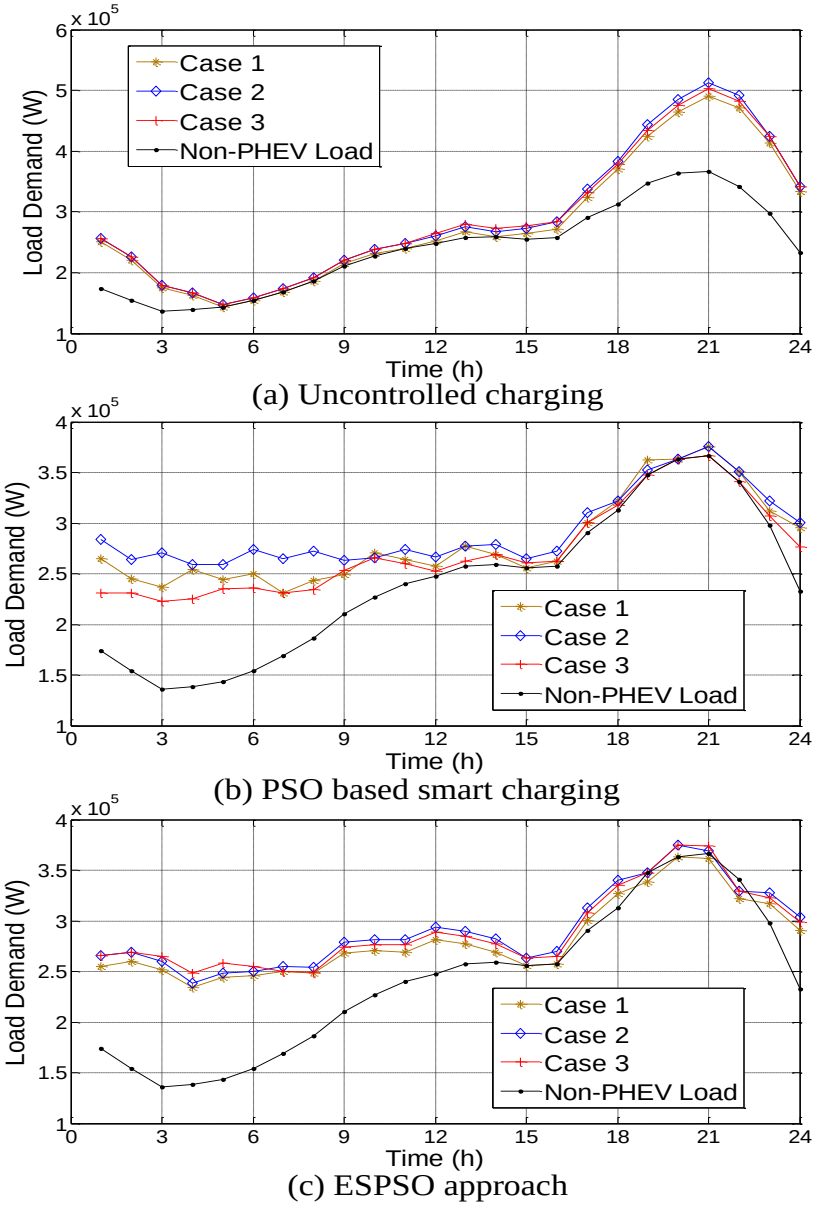

Figure 3. 3 Load demand curves of the tested system with different PHEV modeling methods and control strategies.

The simulation results are shown in Fig. 3.3. The load demands of the three cases are quite different as can be seen from the figure. According to the load demand curves for Case 2 and Case 3, it can be concluded that inaccurate modeling of driving pattern will bring error to the load profile prediction of PHEVs. The proposed Stochastic Fuzzy Model and LPMF result in more accurate predictions.

In this section, various simulations are carried out to demonstrate the effectiveness of the proposed ESPSO approach. Two control strategies, uncontrolled charging and PSO algorithm based smart charging are used as benchmarking control strategies. The simulations are carried out based on these three control strategies at different PHEV penetration levels of 10%, 20%, 50% and 100%.

Fig. 3.4 shows the final battery SOCs and battery SOC variance profiles with ESPSO approach at 10% PHEV penetration level. It is clear that the proposed ESPSO approach is effective in charging the PHEVs into desired SOCs. The vTOU rate for different control strategies is shown in Fig. 3.5. It is clear that the vTOU rate is increasing very quickly with peak load. So the PHEVs will automatically avoid charging at peak load hours of high electricity rates. The proposed ESPSO approach is able to optimally allocate available V2G capacity for both peak load shaving and frequency regulation to achieve the maximum profit. Fig. 3.6 shows the percentage of V2G capacity used for peak load shaving at different PHEV penetration levels. As shown in the figure, ESPSO approach allocates less V2G capacity for peak load shaving at higher penetration level. This is because at the high PHEV penetration level, the load demand can be flatten by just shifting the charging load to valley hours, and it is more profitable to use more V2G capacity for frequency regulation. Fig. 3.7 shows the load demand of the system based on the three control strategies. The proposed ESPSO approach reduces the peak load, and

the load demand curve becomes more flattened. Fig. 3.8 shows voltage curves of the load point 34 of the tested system with different control strategies. As shown in the figure, the proposed algorithm can reduce the voltage deviation effectively.

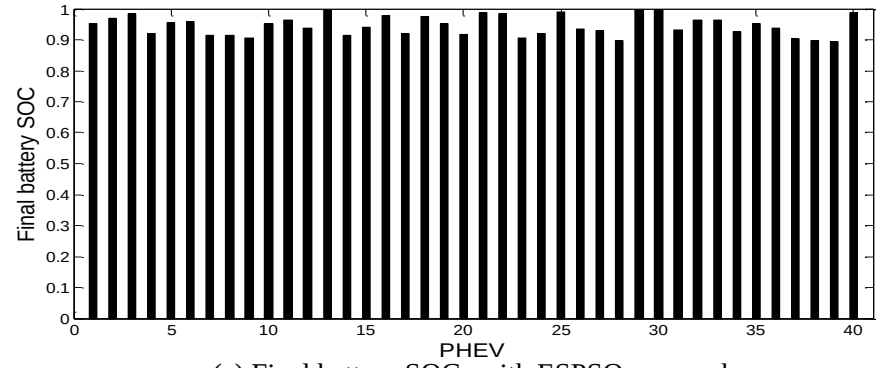

(a) Final battery SOCs with ESPSO approach

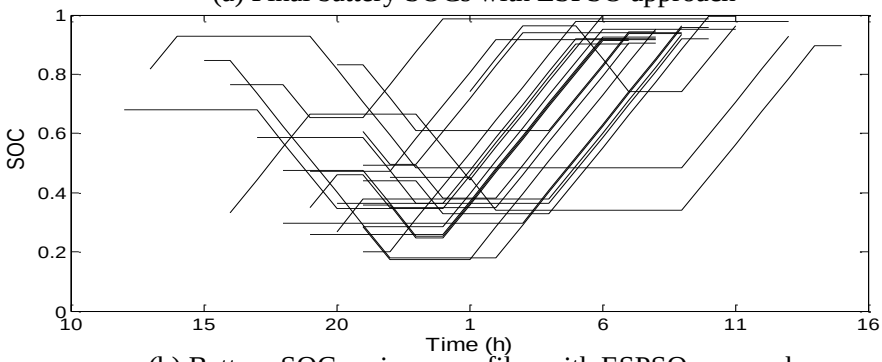

(b) Battery SOC variance profiles with ESPSO approach

Figure 3. 4 Final battery SOCs and battery SOC variance profiles with ESPSO approach at 10% PHEV penetration level.

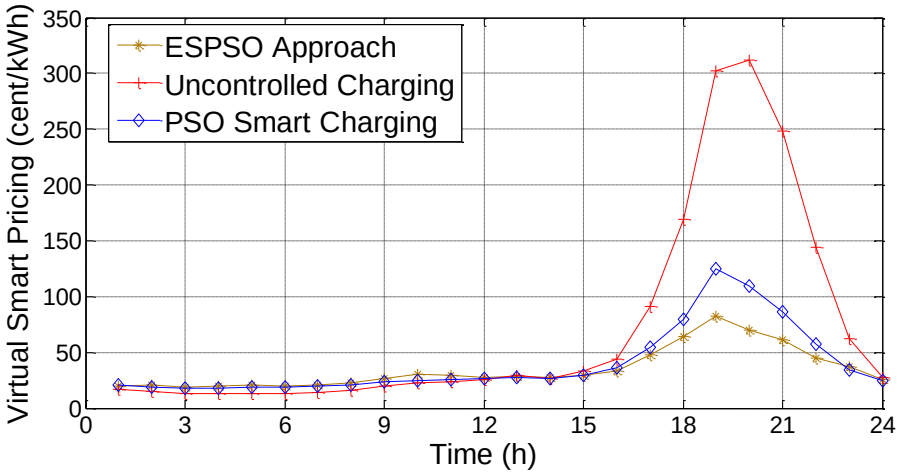

Figure 3. 5 Virtual time-of-use rate for different control strategies at 20% PHEV penetration level.

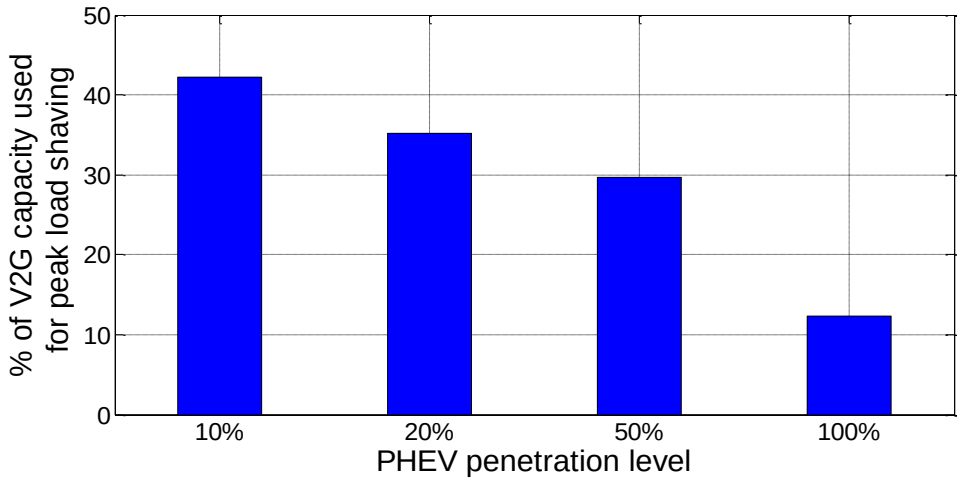

Figure 3. 6 Percentage of V2G capacity used for peak load shaving.

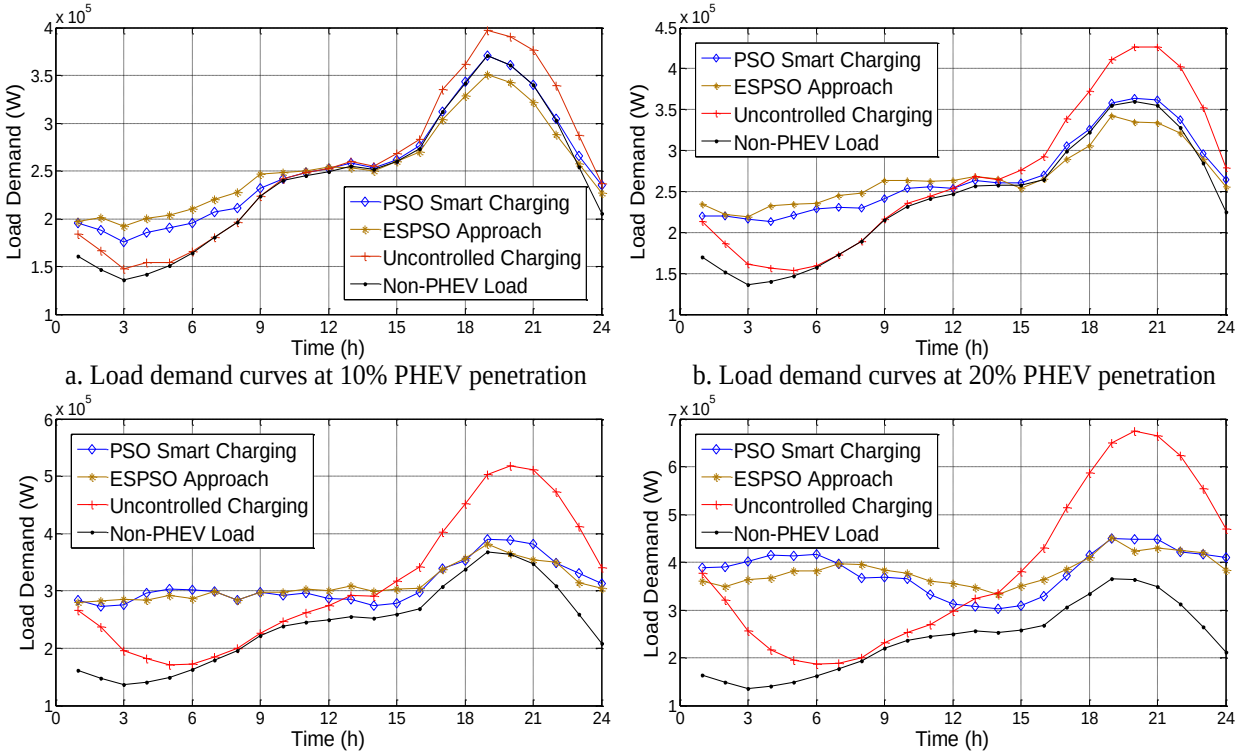

a. Load demand curves at 10% PHEV penetration

b. Load demand curves at 20% PHEV penetration

c. Load demand curves at 50% PHEV penetration

d. Load demand curves at 100% PHEV penetration

Figure 3. 7 Load demand curves of the studied system for different charging algorithms at different PHEV penetration levels.

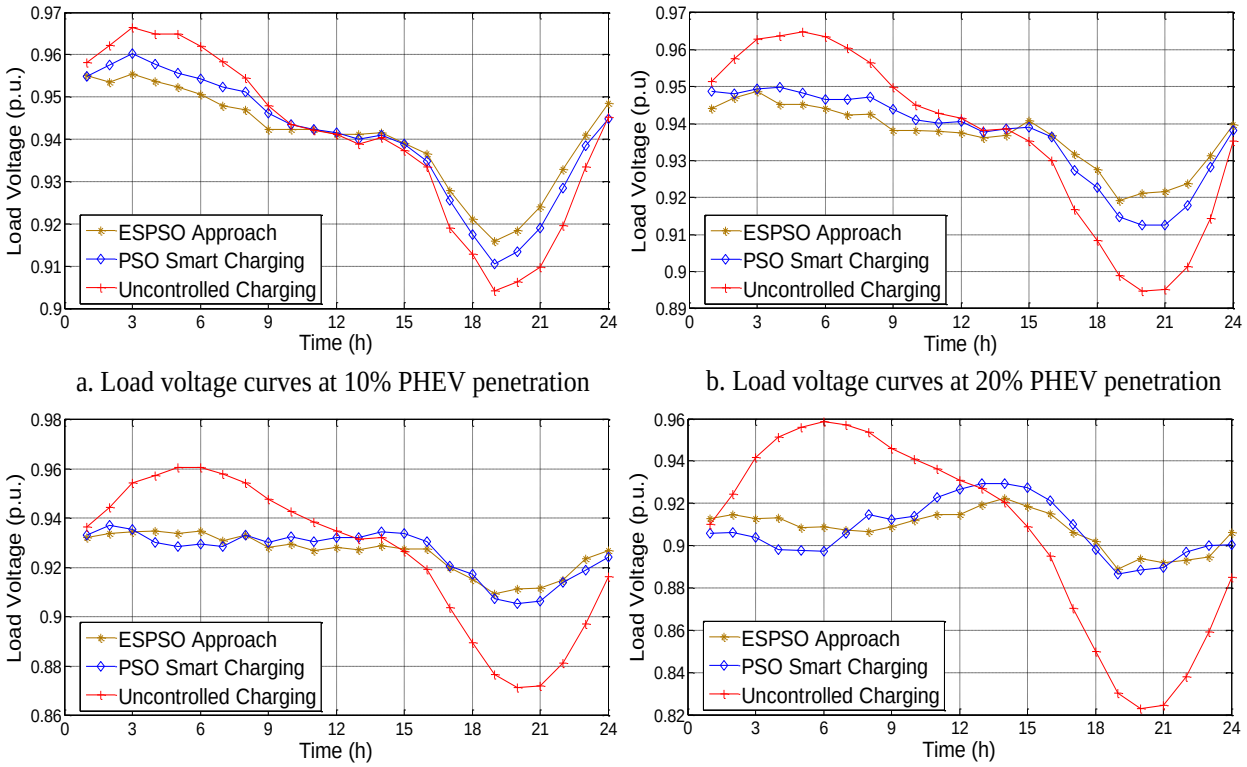

a. Load voltage curves at 10% PHEV penetration

b. Load voltage curves at 20% PHEV penetration

c. Load voltage curves at 50% PHEV penetration

d. Load voltage curves at 100% PHEV penetration

Figure 3. 8 Voltage curves of node 34 for different charging algorithms at different PHEV penetration levels.

Table 3.1 gives the total cost of the system with different control strategies. While incurring additional battery cost and somewhat reducing frequency regulation earnings, the proposed ESPSO approach results in the lowest charging cost by feeding power back to the grid at peak load hours. It turns out that the ESPSO approach is able to achieve the lowest total cost.

Table 3. 1 Cost of Different Control Strategies for 20% PHEV Penetration Level

	Charging Cost ($)	Battery Cost due to V2G ($)	Regulation Earnings ($)	Total Cost ($)
Uncontrolled Charging	884.85	N/A	61.34	823.51
PSO Smart Charging	157.84	N/A	61.34	96.50
ESPSO Approach	113.61	16.49	40.41	89.69

Table 3.2 gives the peak load of the system with different control strategies and penetration level. It shows that the ESPSO approach can effectively reduce the peak load. So for a fixed transformer power capacity in a residential distribution system, the proposed ESPSO approach can integrate more PHEVs into the system without overloading the transformer.

Table 3. 2 Peak Load of Different Control Strategies at Different PHEV Penetration Level (kW)

	10%	20%	50%	100%
Uncontrolled Charging	395	432	524	686
PSO Smart Charging	372	372	394	452
ESPSO Approach	351	355	381	446

4. A Game-theoretic Framework for Vehicle-to-Grid Frequency Regulation

4.1 Introduction

Various frameworks and algorithms have been proposed to apply V2G in frequency regulation [40]-[49]. In [40], the possibility for PHEVs to serve as primary frequency response unit is studied. PHEVs are used as supplementary LFC devices in [41]-[43]. Reference [44] applies particle swarm optimization and robust control to optimize the battery state of charge (SOC) of PHEVs during frequency regulation. Model predictive control (MPC) has been used by [45] to coordinate the control of PHEVs and wind turbine blade pitch angle to reduce the frequency fluctuation. Fuzzy control has been used to deal with the uncertainties of insolation and load variations in frequency regulation by [46]. The bidding of ancillary services has been studied in [47]-[49]. Reference [47] adopts fuzzy optimization to predict uncertainties of the electricity market. Reference [48] models the charging process of an EV as a Markov decision process (MDP) with uncertain electricity market prices. Differential game has been used by [49] to model the competitions between different control areas in a competitive ancillary service market. Smart charging algorithms are also studied by researchers to alleviate the impacts of PHEVs on power systems [26], [28]. However, few studies have taken both the frequency regulation and negative effects of PHEVs into consideration.

To date, little research has been performed to formulate the control of PHEVs and the bidding of frequency regulation capacity as an integrated problem in a competitive electricity market. This chapter designs an LFC system with PHEVs and proposes a hierarchical game framework for PHEVs to optimize their charging process and participate in frequency regulation

simultaneously. In the proposed game framework, a non-cooperative game is proposed to guide the frequency regulation capacity bids of aggregators in the upper level and a Markov game is adopted at the lower level to coordinate the charging of PHEVs based on the regulation price from the upper level game. The games at the two levels cooperate with one another, and will finally evolve to an optimal state where the performance for both the frequency regulation and the charging process are optimized.

4.2 LFC System with PHEVs

Generally speaking, frequency control in power systems consists of primary frequency control, secondary frequency control and tertiary frequency control [42]. Secondary control is also known as LFC, which is contracted by TSO. In a synchronous area of power system, the frequency fluctuation is caused by imbalance of active power generation and consumption. Although there are various excellent load prediction methods available, the imbalance always exists due to the prediction error coupled with short-term load and wind power variations. The TSO dispatches Automatic Generation Control (AGC) signals to the generation units to regulate frequency in the system based on Area Control Error (ACE). ACE should be driven to zero for maintaining the balance of active power. Equation (4.1) depicts the calculation of ACE [42]:

$$ACE = B\Delta f + \Delta P_{tie} \tag{4.1}$$

The difference of the actual tie-line power and the scheduled tie-line power which can be expressed as follows:

$$\Delta P_{tie} = \sum\left(P_{tie,act} - P_{tie,sch}\right) \tag{4.2}$$

Usually LFC is provided by thermal power plants. For a controlled area of the power system, it is connected with other areas through tie lines. The imbalance of active power in the area can be compensated for by the power from other areas through tie lines. However, due to the limited

transmission capacity of tie lines, usually the imbalance can only be partially compensated for through the tie lines. The power plants will have to make continuous adjustments to keep the active power balanced. When the control system in these power plants detects the frequency deviation in the area, it will adjust the mechanical power input of generators to drive the frequency back to the normal value.

We obtain the proposed LFC model by adding PHEV aggregators into a generalized LFC model [50], [51] as shown in Fig. 4.1. Fig. 4.1 shows the block diagram of a control area with n conventional generator units and J PHEV aggregators. The communication delay of the control system for the aggregators are model by a first order transfer function with time constant T_{EV}.

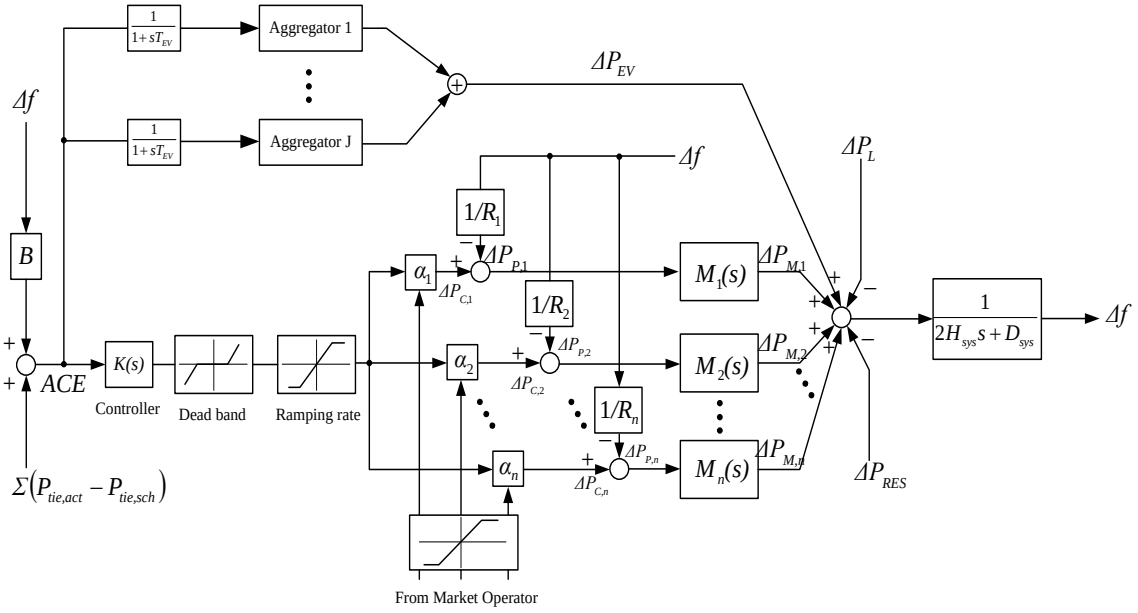

Figure 4. 1 LFC model with PHEV aggregators.

The dynamic relationship between the active power imbalance and frequency deviation is described in (4.3)-(4.5).

$$\Delta f(s) = \frac{1}{2H_{sys}s + D_{sys}} \left(\sum_{i=1}^{n} \Delta P_{M,i}(s) + \Delta P_{EV}(s) - \Delta P_{RES}(s) - \Delta P_L(s) \right) \tag{4.3}$$

$$\Delta P_{M,i}(s) = M_i(s) \cdot \left(\Delta P_{C,i}(s) - \Delta P_{P,i}(s) \right) \tag{4.4}$$

$$\Delta P_{P,i}(s) = \frac{\Delta f(s)}{R_i} \tag{4.5}$$

Ramping rates of the generating units are affected by many factors such as generating unit type and capacity. The ramping rates of the conventional generating units are quite small compared with EVs. The fossil-fired steam turbine units can respond to AGC signals at 3% per minute for a 30% excursion. Nuclear plants typically can respond at 3% per minute for about 10 minutes within their regulation range. Hydro units have better response capabilities which can be regulated over their entire operating range within a minute [52]. However, EVs can cycle over their output range within a second. Thus, EVs are valuable resources for frequency regulation.

The PHEV control system is shown in Fig. 4.2. In the diagram, every transformer is connected to a residential distribution network, and PHEVs are connected to each residential distribution network. PHEVs are contracted with aggregators in each distribution network. Based on the contract with PHEV owners, the aggregator builds another contract with TSO. After the contract is established, the aggregator performs its own algorithm as long as it can respond to the frequency regulation signal from the TSO. That is, the aggregator can control the PHEVs in its residential distribution network to flatten the load demand of the system in the lower layer, and it can respond to the signal from TSO to participate in the frequency regulation in the upper layer. The aggregators can act as players in the electricity market who aim at maximizing their own profits. For example, the aggregators can request PHEVs to charge when the electricity price is low, and contract a higher regulation capacity with TSO when the regulation price is high. The aggregators can act as both sellers and customers in the electricity market. When a PHEV provides the regulation service, the net energy exchange tends to be zero over a long time period and the cost related with the net energy exchange can be ignored compared with the profits obtained from providing frequency regulation [35]. Thus, when a PHEV participates in

frequency regulation, its state of charge (SOC) will not be affected too much over time. This is why regulation suppliers should be paid based on their regulation capacity rather than the net energy output.

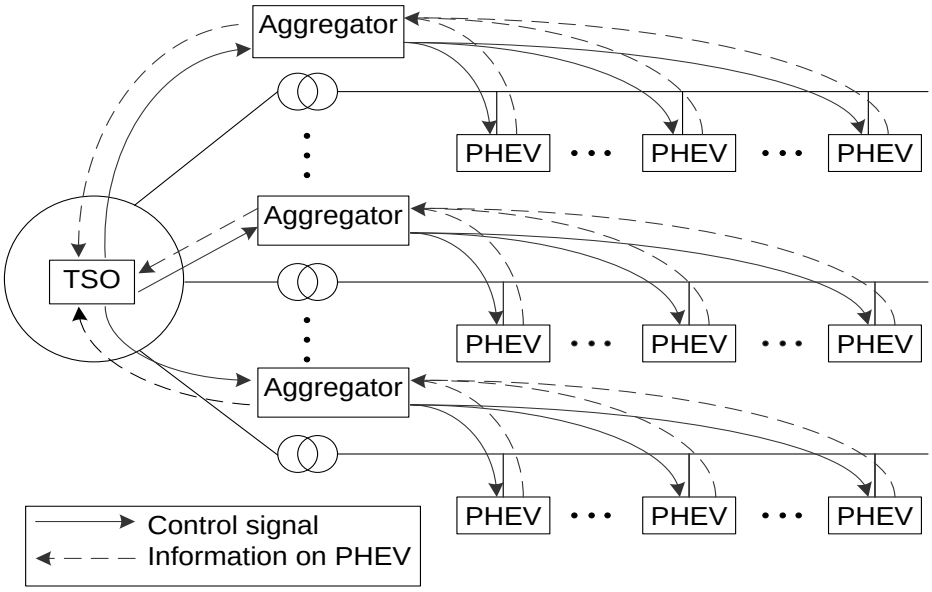

Figure 4. 2 Information flow of the LFC system with PHEVs.

4.3 Hierarchical Game Formulation

4.3.1 System Architecture

It is noteworthy that most existing game theory based studies only consider the competition on one side, i.e., either the competition between aggregators in bidding frequency regulation capacity or the competition between the PHEVs in maximizing their personal profits. The proposed hierarchical game framework carries out optimization on both sides, and the frequency regulation capacity bids are associated with the control process of PHEVs in this holistic framework. The architecture of the proposed hierarchical game is shown in Fig. 4.3. At the upper level, the aggregators use the current available regulation capacities of their PHEVs to bid for

frequency regulation prices through a non-cooperative game. Then the Markov game at the lower level will coordinate the charging process of PHEVs and update the available regulation capacity of PHEVs to enable the aggregator to bid a more favorable regulation price. A more favorable regulation price will help the Markov game evolve to a better control strategy which in turn facilitates the aggregator in bidding for an even higher regulation price. The games in the two levels will keep evolving and finally reach an optimal point where the performances for both sides are optimized.

Let $\boldsymbol{Ag} = \{1, 2, \dots, j, \dots, J\}$ denote the set of aggregators in a control area and the set of PHEVs under the control of aggregator j is expressed as $\boldsymbol{E_j} = \{1, 2, \dots, i_j, \dots, I_j\}, j \in \boldsymbol{Ag}$. In the competitive electricity market, the energy price and ancillary service prices are updated every hour. Thus, the system is optimized on an hourly basis and the planning time horizon is expressed as $\boldsymbol{D} = \{1, 2, \dots, h, \dots, H\}$.

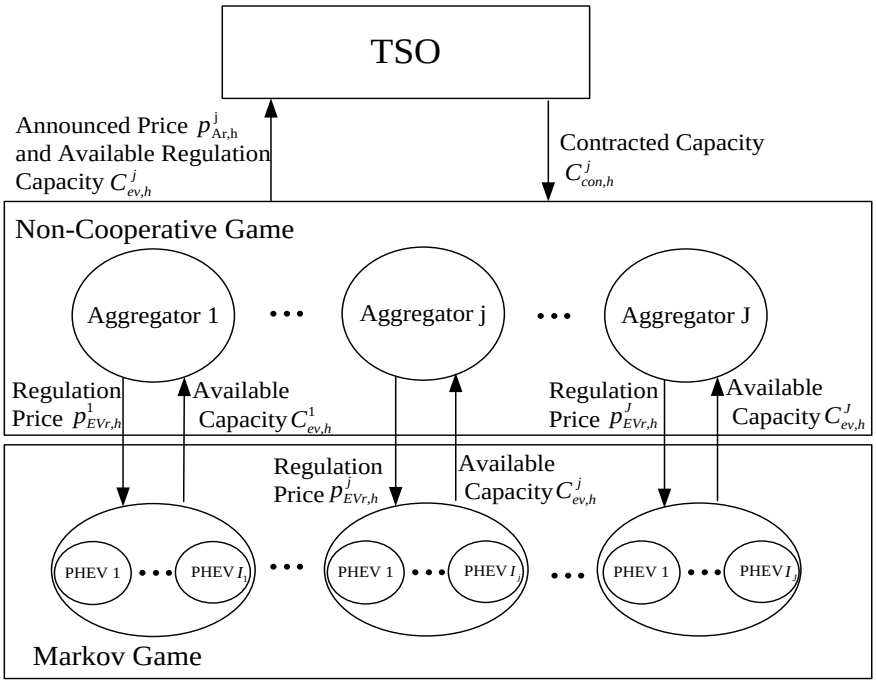

Figure 4. 3 Architecture of the proposed hierarchical game.

4.3.2 Markov Game among PHEVs

In this subsection, we formulate the interaction among multiple PHEVs as a Markov game. Markov game [53] extends MDP to the multi-agent case. Each player in a Markov game can be modeled as an MDP. We assume that once a PHEV is plugged in the power grid, it will provide the aggregator with the information on the plug-in time $h_{in,i}$, the estimated plug-out time $h_{out,i}$ and the required time to charge its battery to the desired SOC $SOC_{r,\pi}(h)$. We also assume that the PHEV owners agree not to unplug the PHEVs before their scheduled plug-out time, or else they will face financial penalty.

Theorem 4.1: In the proposed model, it is more cost effective to let PHEVs charge at the rated charging power.

Proof: see the Appendix.

Thus, PHEVs are controlled at three states: charging, discharging and idle. Then, we can define the charging process of a PHEV as a T-stage MDP Γ_{T_i} ($T_i = h_{out,i} - h_{in,i}$).

The state space of the MDP is naturally defined by the PHEV's current state as:

$$S_h := \{SOC_{r,\pi}(h), T_r(h), p_{e,h}, p^j_{EVr,h}\} \tag{4.6}$$

where $SOC_{r,\pi}(t)$ is the required time to charge its battery to the desired SOC at time step h under action strategy π, $T_r(h)$ is the remaining plug-in time at time step h, $p_{e,h}$ is the real time electricity price and $p^j_{EVr,h}$ is the real time frequency regulation price for PHEVs controlled by aggregator j.

We defined the action space of a PHEV as $\boldsymbol{A} = \{1, 0, -1\}$. Let $a_{s_h} \in A^{s_h}$ denote the action of a PHEV at state s_h and A^{s_h} is the action space of state s_h. $a_{s_h} = 1,0,-1$ denotes actions of charging, idle and discharging respectively. To ensure that the PHEVs are charged to the desired

SOC at the time of departure, the action space is defined as follows:

$$A^{S_h} := \begin{cases} \{1\}, & if\ T_r(h) \le SOC_{r,\pi}(h) \\ \{1,0\}, & if\ SOC_{r,\pi}(h) < T_r(h) \le SOC_{r,\pi}(h)+2 \\ \{1,0,-1\}, & if\ T_r(h) \ge SOC_{r,\pi}(h)+2 \end{cases} \tag{4.7}$$

The dynamics of the states is defined as follows:

$$SOC_{r,\pi}(h+1) = \begin{cases} SOC_{r,\pi}(h)-1, if\ a_{s_h}=1 \\ SOC_{r,\pi}(h), \quad if\ a_{s_h}=0 \\ SOC_{r,\pi}(h)+1, if\ a_{s_h}=-1 \end{cases} \tag{4.8}$$

$$T_r(h+1) = T_r(h) - 1 \tag{4.9}$$

In order to reduce peak load of the residential distribution network where the PHEV aggregator is located, a real time electricity price policy is developed based on system load demand to regulate the charging process of PHEVs. The price is defined as follows:

$$p_{e,h} = \alpha_e \cdot P_h^{sys} \tag{4.10}$$

where α_e is a price parameter, and P_h^{sys} is the load demand of the system at time slot h.

The load demand of the system P_h^{sys} is the total load of the residential distribution system which consists of both the base load and PHEV load. It can be expressed as follows:

$$P_h^{sys} = P_{base,h} + \sum_{i=1}^{I_j} P_{i,h}^{EV} \tag{4.11}$$

where $P_{base,h}$ is the base load of the system at time slot h, $P_{i,h}^{EV}$ is the charging power of the i_{th} PHEV at time slot h.

The frequency regulation price $p_{EVr,h}^{j}$ is provided by the upper level non-cooperative game of aggregators, and it will keep fixed during the iterations of the Markov game.

Considering the battery degradation cost [31] due to V2G activities, the immediate reward is defined as:

$$r_h(s_h, a_{s_h}) = \begin{cases} \left(p_{e,h} - \frac{c_b E_b + c_L}{L_C E_b DOD}\right) P_{rate}, if\ a_{s_h} = -1 \\ \left(p^j_{EVr,h} - \frac{c_b E_b + c_L}{L_C E_b DOD}\right) P_{rate}, if\ a_{s_h} = 0 \\ -p_{e,h} P_{rate}, \qquad if\ a_{s_h} = 1 \end{cases} \tag{4.12}$$

where P_{rate} is the rated charging power.

For a given policy $\pi_i = \left(a_{s_0}, a_{s_1}, a_{s_2}, \cdots, a_{s_{T-1}}\right), \forall a_{s_h} \in A^{s_h}$, the total reward over the T stages is:

$$U^{\pi}_{i,s_0} \coloneqq \sum_{h=0}^{T-1} \mathbb{E}_{s,\pi}[r_h] \tag{4.13}$$

To coordinate the set of I_J ($I_J = \{1, 2, \ldots, i_j, \ldots, I_j\}$) PHEVs controlled by aggregator j, we defined a Markov game $\mathbb{G}_{\mathrm{m}}$ as:

- Players: The set of all I_j PHEVs.
- Strategies: For each PHEV, choose an action strategy π_i.
- Payoffs: PHEV i receives payment $U_i(\pi_i, \pi_{-i})$ as shown in (4.13).

We adopt Nash equilibrium as the solution for the proposed Markov game. Nash equilibrium is the most important concept in game theory, which is a static stable strategy vector that no player has any incentive to unilaterally change its strategy from it. The definition of Nash equilibrium can be described as follows:

Definition 4.1: For the proposed Markov game $\mathbb{G}_{\mathrm{m}} = \{\mathrm{I_j}, \{\pi_{\mathrm{i}}\}_{\mathrm{i}\in \mathrm{I_j}}, \{\mathrm{U}^{\pi}_{\mathrm{i},s_0}\}_{\mathrm{i}\in \mathrm{I_j}}\}$, a strategy tuple $\Psi = \{\pi^*_{\mathrm{i}}\}_{\mathrm{i}\in \mathrm{I_j}}$ constitutes a Nash equilibrium when no player can improve its utility by unilaterally deviating from its current strategy. It can be expressed as a set of inequalities [54]:

$$U^{\pi}_{i,s_0}(\pi^*_i, \pi^*_{-i}) \geq U^{\pi}_{i,s_0}(\pi_i, \pi^*_{-i}),\ \forall i \in \boldsymbol{E_j} \tag{4.14}$$

We can find the approximate Nash equilibrium (4.15) by using the best response strategy [55]:

$$U^{\pi}_{i,s_0}(\pi^*_i, \pi^*_{-i}) \geq U^{\pi}_{i,s_0}(\pi_i, \pi^*_{-i}) - \varepsilon_1,\ \forall i \in \boldsymbol{E_j} \tag{4.15}$$

where ε_1 is a small positive constant which is set as $\varepsilon_1 = 0.05$.

Ultimately, the best response strategy is an iterative algorithm in which the players take turns to make decisions in a sequential manner. While having the knowledge of other players' strategies π_{-i}, the best response strategy π_i' for the player *i* is:

$$\pi_i' = argmax_{\pi_i}\{U_{i,s_0}^{\pi}(\pi_i, \pi_{-i})\},\ \forall i \in \boldsymbol{E_j} \tag{4.16}$$

The best response strategy for a player π_i' can be obtained by applying the backward recursion algorithm [56], which is elaborated as follows:

1) Set $V_{-1}(s) = 0$.

$$a_{s_T} = argmax_{A^{s_T}}\{r_T(s_T, a_{s_T}) + \sum_{s_{T-1}} p_T(s_{T-1}|s_T, a_{s_T})V_{-1}(s_{T-1})\} \tag{4.17}$$

$$V_0(s_T) \coloneqq r_T(s_T, a_{s_T}) = max_{A^{s_T}}\{r_T(s_T, a_{s_T}) + 0\} \tag{4.18}$$

2) For each time step n ($n = 0,1,2,\cdots,T-1$), the current best action strategy $\pi = (a_{s_0}, a_{s_1}, a_{s_2}, \cdots, a_{s_{T-1}})$ can be found by:

$$a_{s_{T-n}} = argmax_{A^{s_{T-n}}}\{r_{T-n}(s_{T-n}, a_{s_{T-n}}) + \sum_{s_{T-n-1}} p_{T-n}(s_{T-n-1}|s_{T-n}, a_{s_{T-n}})V_{n-1}(s_{T-n-1})\} \tag{4.19}$$

$$V_n(s_{T-n}) = r(s_{T-n}, a_s^{T-n}) + \sum_{s_{T-n-1}} p_{T-n}(s_{T-n-1}|s_{T-n}, a_{s_{T-n}})V_{n-1}(s_{T-n-1}) \tag{4.20}$$

where $p_T(s'|s, a_s)$ is the transition probability from state s to state s' with action a_s.

3) Output the best response strategy $\pi_i' = (a_{s_0}, a_{s_1}, a_{s_2}, \cdots, a_{s_{T-1}})$.

Once the Markov game reaches its equilibrium, the strategies of PHEVs are obtained and the frequency regulation capacity is calculated as follows:

1) Define a vector $\boldsymbol{I} = [\boldsymbol{I_1} \cdots, \boldsymbol{I_i}, \cdots, \boldsymbol{I_{I_j}}]$ to indicate idle states of PHEVs at each time slot as shown below:

$$\boldsymbol{I_i} = \left[I_i^{h_{in,i}}, \cdots, I_i^h, \cdots, I_i^{h_{out,i}}\right], \forall\ i \epsilon \boldsymbol{E_j} \tag{4.21}$$

where

$$I_i^h = \begin{cases} 1, & if PHEV\ i\ is\ in\ idle\ state \\ 0, & otherwise \end{cases}, \forall\ h \epsilon \boldsymbol{D}; \forall\ i \epsilon \boldsymbol{E_j} \tag{4.22}$$

2) Calculate the frequency regulation capacity as follows:

$$C_{ev,h}^j = \sum_{i=1}^{\boldsymbol{I_j}} I_i^h \cdot P_{rate}, \forall\ h \epsilon \boldsymbol{D} \tag{4.23}$$

The proposed best response algorithm is summarized in Algorithm 4.1 as follows:

Algorithm 4.1 Best response algorithm for Markov game

1: Input random initial strategies for all players and send the strategy information to the aggregator;

2: repeat

3: for i=1,…, I_J do

4: 1) The aggregator selects a PHEV i and provides the PHEV with the current strategies of other PHEVs π_{-i};

5: 2) The PHEV finds its current best response strategy π_i' based on (4.16). Then the player provides the aggregator with its current best response strategy π_i';

6: 3) The aggregator moves to the next player;

7: end for

8: until the approximate Nash equilibrium (4.15) is reached.

9: Calculate the frequency regulation capacity $C_{ev,h}^j$ at each time step and send it to the aggregator for frequency regulation capacity bids;

10: Output control strategies and stop.

4.3.3 Non-Cooperative Game of Aggregators

The aggregators bid with each other to sell regulation capacity to the TSO. They aim at selling the regulation capacity at a higher price to maximize their own welfare. Thus, we can formulate the competition of aggregators as a non-cooperative game as follows:

- Players: The set of all J aggregators.
- Strategies: For each aggregator, choose frequency regulation price $p_{Ar,h}^{j}$ at any time slot.
- Payoffs: The aggregator j receives payment $U_{A,h}^{j}\left(p_{Ar,h}^{j}, p_{Ar,h}^{-j}\right)$ as shown in (4.24).

The utility function of an aggregator can be expressed as follows:

$$U_{A,h}^{j} = \begin{cases} p_{Ar,h}^{j} C_{con,h}^{j} - \beta\left(C_{con,h}^{j} - C_{ev,h}^{j}\right)^{2}, r_{h}^{j} \le 1 \\ p_{Ar,h}^{j} C_{con,h}^{j}, \qquad\qquad\qquad\quad r_{h}^{j} > 1 \end{cases} \tag{4.24}$$

where $C_{ev,h}^{j}$ is the regulation capacity provided by PHEVs, $C_{con,h}^{j}$ is the regulation capacity contracted with TSO, $p_{Ar,h}^{j}$is the frequency regulation price bids by the aggregator and β is the parameter of the penalty function.

The capacity-to-contract ratio is defined in (4.25). It indicates how attractive the aggregator's price would be:

$$r_{h}^{j} = C_{ev,h}^{j} / C_{con,h}^{j} \tag{4.25}$$

After the bidding process, the aggregator will provide a frequency regulation price for PHEVs by:

$$p_{EVr,h}^{j} = \frac{U_{A,h}^{j}}{C_{ev,h}^{j}} = \begin{cases} \dfrac{p_{Ar,h}^{j} C_{con,h}^{j} - \beta\left(C_{con,h}^{j} - C_{ev,h}^{j}\right)^{2}}{C_{ev,h}^{j}}, & r_{h}^{j} \le 1 \\ \dfrac{p_{Ar,h}^{j} C_{con,h}^{j}}{C_{ev,h}^{j}}, & r_{h}^{j} > 1 \end{cases} \tag{4.26}$$

The strategy of TSO is to contract regulation capacities with PHEV aggregators. In a

competitive frequency regulation market, the TSO may assign regulation capacities to aggregators at each controlled time slot based on the frequency regulation prices provided by aggregators. Assume the total regulation capacity contracted with all the J aggregators in a control area is x_h, the contracted regulation capacity of the aggregator j at time h can be expressed as:

$$C_{con,h}^{j} = y_h^j x_h, \forall j \in \boldsymbol{Ag}, \forall h \in \boldsymbol{D} \tag{4.27}$$

where y_h^j is the percentage of regulation capacity contracted with aggregator j at time step h, $0 \le y_h^j \le 1$ and $\sum_{j=1}^{J} y_h^j = 1$.

Thus, we can denote the strategy of TSO as:

$$Y_h = [y_h^1, y_h^2, \dots, y_h^j, \dots, y_h^J], \forall j \in \boldsymbol{Ag}, \forall h \in \boldsymbol{D} \tag{4.28}$$

The welfare for TSO buying frequency regulation capacity from the aggregator j can be described as:

$$U_{TSO,h}^{j} = \begin{cases} R_j C_{con,h}^{j} - \alpha\left(C_{con,h}^{j} - C_{ev,h}^{j}\right)^2 - p_{Ar,h}^{j} C_{con,h}^{j}, & r_h^j \le 1 \\ R_j C_{con,h}^{j} - p_{Ar,h}^{j} C_{con,h}^{j}, & r_h^j > 1 \end{cases} \tag{4.29}$$

where R_j is a positive parameter for the welfare of the TSO in buying frequency regulation capacity from the aggregator j, α, γ and β are positive parameters for frequency regulation performance penalty, $\alpha = \gamma - \beta, \beta < \gamma, R_j > p_{Ar,h}^{j}$.

Based on the concept of replicator dynamics in evolutionary games [57], we propose a strategy dynamics to guide the strategy evolution of the TSO as follows:

$$\frac{\partial y_h^j}{\partial t} = \delta y_h^j \left(U_{TSO,h}^{j} / C_{con,h}^{j} - \bar{U}_{TSO,h}\right), \forall j \in \boldsymbol{Ag}, \forall h \in \boldsymbol{D} \tag{4.30}$$

where δ is the learning rate and $\bar{U}_{TSO,h}$ is the average utility per unit contracted regulation capacity of the TSO as shown below:

$$\bar{U}_{TSO,h} = \sum_{j=1}^{J} y_h^j \, U_{TSO,h}^j / C_{con,h}^j \tag{4.31}$$

The optimal strategy $Y_h^* = [y_h^{1*}, y_h^{2*}, \dots, y_h^{j*}, \dots, y_h^{J*}]$ of the TSO can be obtained when the strategy evolves to a stable state described as follows:

$$\frac{\partial y_h^j}{\partial t} = 0, \forall j \in \boldsymbol{Ag} \tag{4.32}$$

As the system is controlled at discrete time slots, the continuous strategy dynamics is approximated using a discrete strategy dynamics as follows:

$$y_h^j(n+1) = y_h^j(n) + \delta y_h^j(n) \left(U_{TSO,h}^j(n) / C_{con,h}^j(n) - \bar{U}_{TSO,h}(n) \right) \tag{4.33}$$

The stopping criterion for the strategy dynamics is:

$$\left| U_{TSO,h}^j(n) / C_{con,h}^j(n) - \bar{U}_{TSO,h}(n) \right| < \varepsilon_2 \tag{4.34}$$

where ε_2 is a small positive constant which is set as $\varepsilon_2 = 2.0$.

Algorithm 4.2 The iterative algorithm for the TSO

1: Input the frequency regulation price $p_{Ar,h}^j$ and the available capacity $C_{ev,h}^j$ provided by aggregators;

2: n=1;

3: repeat

4: for j=1,…, J do

5: Calculate the utility of $U_{TSO,h}^j(n)$ by (4.29);

6: end for

7: Calculate the average utility $\bar{U}_{TSO,h}(n)$ by (4.31);

8: for j=1,…, J do

9: Update the strategy according to (4.33)

10: end for

11: n=n+1.

12: until (4.34) is satisfied.

13: Calculate the contracted capacities $C_{con,h}^{j}$ and contract with aggregators.

14: Output control strategies and stop.

It is assumed that TSO knows the dynamic range of the regulation capacity of all the aggregators in a control area, thus it can assign a reasonable amount of regulation capacity x_h among aggregators and leave the rest regulation capacity demand to other generation units. This assumption guarantees that the contracted regulation capacities for aggregators will converge to the optimal point which maximizes the utility of TSO. Thus, during the convergence process of the non-cooperative game, we can assume that the TSO will contract a power capacity with the aggregator which will maximize the utility of the TSO as shown in (4.35). This assumption will not influence the convergence of the game as the game will finally converge to a point where the utility of TSO is maximized.

$$C_{con,h}^{j*} = argmax_{C_{con,h}^{j}}\left(U_{TSO,h}^{j}\right) = C_{ev,h}^{j} + \frac{R_j - p_{Ar,h}^{j}}{2\alpha} \tag{4.35}$$

Substituting $C_{ev,h}^{j} = C_{con,h}^{j} - \frac{R_j - p_{Ar,h}^{j}}{2\alpha}$ into (4.24), we can get

$$U_{A,h}^{j} = p_{Ar,h}^{j} C_{con,h}^{j} - \frac{\beta}{4\alpha^2}(R_j - p_{Ar,h}^{j})^2, r_h^j \le 1 \tag{4.36}$$

$$\frac{dU_{A,h}^{j}}{dp_{Ar,h}^{j}} = C_{con,h}^{j} + p_{Ar,h}^{j}\frac{dC_{con,h}^{j}}{dp_{Ar,h}^{j}} + \frac{\beta}{2\alpha^2}(R_j - p_{Ar,h}^{j}), r_h^j \le 1 \tag{4.37}$$

Apply $dU_{A,h}^{j}/dp_{Ar,h}^{j} = 0$, we can obtain $C_{con,h}^{j} = \frac{(\alpha+\beta)p_{Ar,h}^{j} - \beta R_j}{2\alpha^2}$ and $r_h^{j*} = \frac{C_{ev,h}^{j}}{C_{con,h}^{j}} = \frac{(2\alpha+\beta)p_{Ar,h}^{j} - (\alpha+\beta)R_j}{(\alpha+\beta)p_{Ar,h}^{j} - \beta R_j}$. Thus, we can obtain the following expression:

$$\frac{dU_{A,h}^{j}}{dp_{Ar,h}^{j}}\begin{cases}<0, & r_h^j > r_h^{j*}\\ >0, & r_h^j < r_h^{j*}\end{cases} \tag{4.38}$$

According to (4.38), aggregator j will increase the regulation price when $r_h^j < r_h^{j*}$ and will decrease the regulation price when $r_h^j > r_h^{j*}$. Thus, we can design an iterative algorithm to find the Nash equilibrium as follows:

$$p_{Ar,h}^{j}(m+1) = p_{Ar,h}^{j}(m) + \sigma(r_h^{j*} - r_h^j(m)) \tag{4.39}$$

where σ is the learning rate.

The algorithm stops when (4.40) is satisfied:

$$\left| r_h^j(m) - r_h^{j*} \right| < \varepsilon_3 \tag{4.40}$$

where ε_3 is a small positive constant which is set as $\varepsilon_3 = 0.01$.

After the Nash equilibrium for the non-cooperative game is reached, the frequency regulation price for PHEVs is updated according to (4.26). Then the Markov game will coordinate the changing process of PHEVs and update the available frequency regulation capacity $C_{ev,h}^{j}$ for aggregators. This iterative process will continue until (4.41) is satisfied.

$$\left| p_{EVr,h}^{j}(k+1) - p_{EVr,h}^{j}(k) \right| < \varepsilon_4 \tag{4.41}$$

where ε_4 is a small positive constant which is set as $\varepsilon_4 = 0.2$.

Algorithm 4.3 The iterative algorithm for the proposed hierarchical game.

1: Input random initial frequency regulation prices $p_{Ar,h}^{j}$ announced by aggregators;

2: k=1

3: repeat

4: Execute Algorithm 4.1;

5: Provide aggregators with available regulation capacity $C_{ev,h}^{j}$ at each time slot;

6: for h=1,…, H do

7: m=1;

8: repeat

9: for j=1,…, J do

10: 1) Aggregator j provides TSO with announced frequency regulation price $p_{Ar,h}^{j}$ and available regulation capacity $C_{ev,h}^{j}$;

11: 2) Calculate r_h^j according to (4.25);

12: 3) Update regulation price according to (4.39);

13: end for

14: Execute Algorithm 4.2;

15: TSO provides contracted regulation capacities $C_{con,h}^{j}$ to aggregators;

16: m=m+1;

17: until (4.40) is satisfied;

18: end for

19: Calculate frequency regulation price for PHEVs based on (4.26);

20: k=k+1;

21: until (4.41) is satisfied;

22: Output control strategies and stop.

4.4 Case Studies

Simulations are carried out to validate the proposed hierarchical game framework and the effectiveness of the proposed algorithms. As shown in Fig. 4.4, we adopt the well-known IEEE 39-bus test system to simulate the frequency control performance. The test system consists of 10 generators, 34 transmission lines, 12 transformers and 19 loads. The test system is divided into three control areas. The total generation includes 842 MW conventional power and 69 MW wind power. The total amounts of load in Area 1, Area 2 and Area 3 are 265.5, 233 and 125 MW, respectively. In the test system, we use G1 in Area 1, G9 in Area 2 and G4 in Area 3 as LFC units. The parameters for the generators, transformers, lines and loads of the test system are obtained from [58].

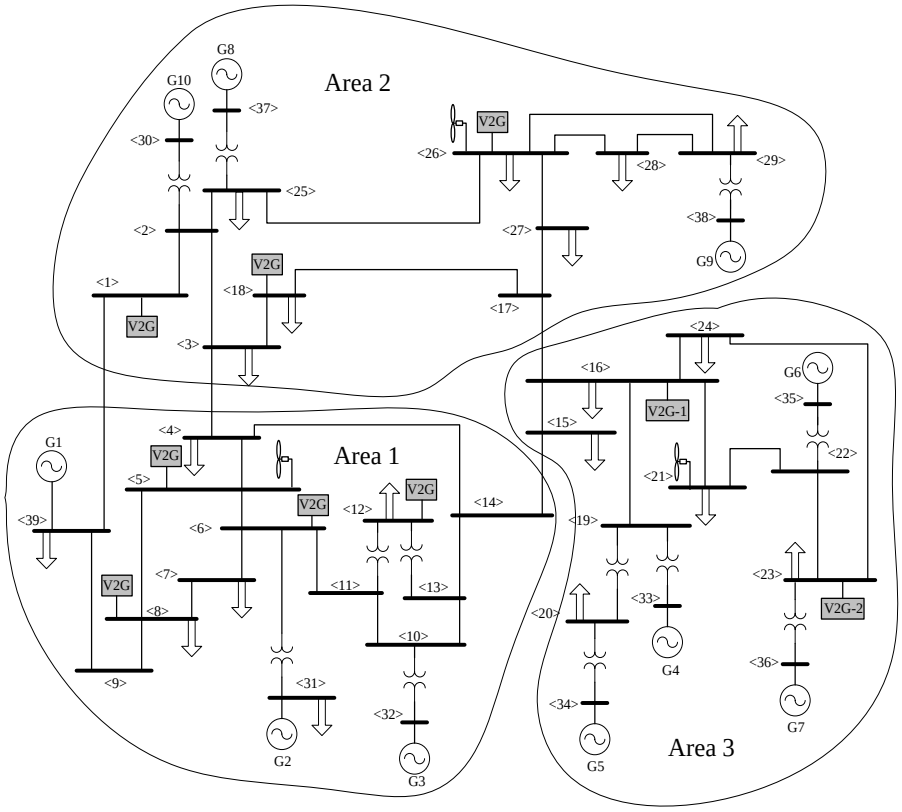

Figure 4. 4 Single line diagram of 39-bus test system.

In this simulation study, the test system is updated by four V2G residential distribution networks and one wind farm in Area 1, three V2G residential distribution networks and one wind

farm in Area 2, two V2G residential distribution networks and one wind farm in Area 3. As the three control areas are almost identical and have the same control system, we choose control area 3 as a demonstration of the performance of the proposed hierarchical game approach. There are two V2G residential distribution networks in the control area 3. Each V2G residential area has one PHEV aggregator to manage the PHEVs located in this residential area. Assume V2G residential area 1 and V2G residential area 2 has 1200 households and 2400 households respectively. Assume each house has two vehicles and the PHEV penetration level is 10%. Therefore, aggregator 1 controls 240 PHEVs and aggregator 2 serves 480 PHEVs. The non-PHEV load profile of a house in winter is scaled from [38]. In the simulation study, all the PHEVs are assumed to be the Chevrolet Volt with the battery capacity of 16 kWh. The charging level of PHEVs is set as AC Level 2 with 3.6 kW. The control time horizon is 24 hours. Uncontrolled charging and particle swarm optimization (PSO) based smart charging are used as the benchmarking control strategies. The driving pattern and the SOC of PHEVs are generated based on the model in Chapter 2.

Fig. 4.5 (a) shows the convergence process of the TSO's strategy with algorithm 4.2. It is clear that the strategy of TSO will evolve to a stable state after receiving the announced frequency regulation prices from the aggregators. The convergence process of the non-cooperative game is shown in Fig. 4.5 (b). The game converges after several iterations and the capacity-to-contract ratio reaches a stable state as described in (4.40).

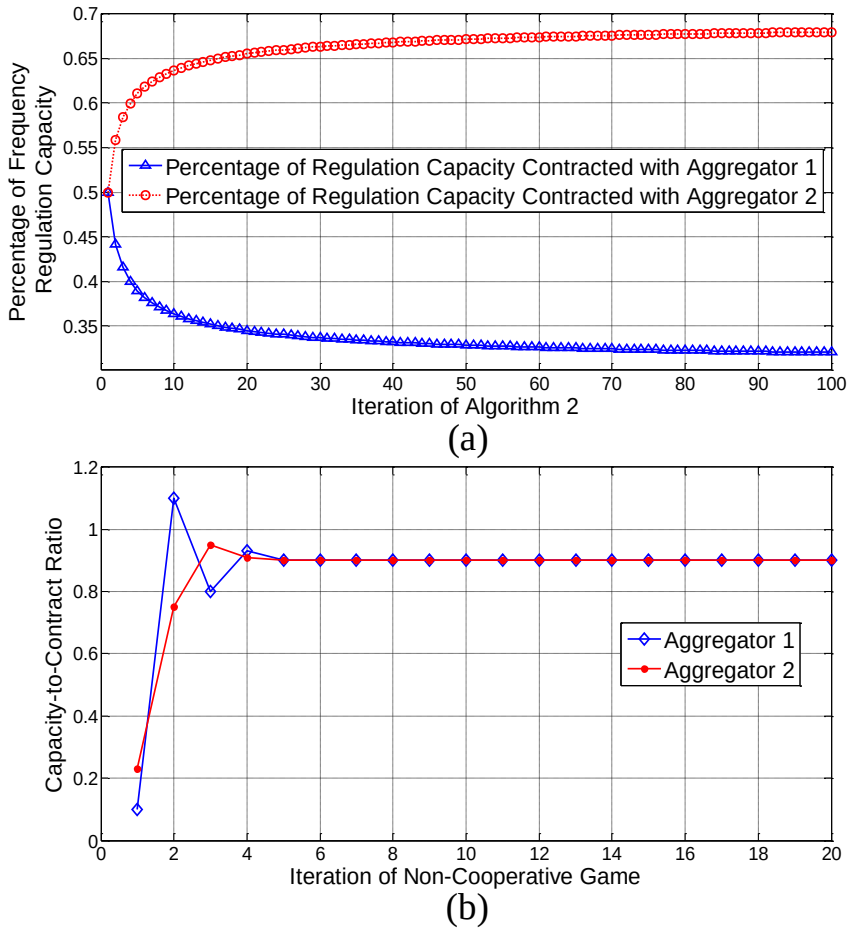

Figure 4. 5 The convergence process of the hierarchical game.

Fig. 4.6 shows the fluctuations of load demand and wind power in the test system. Simulations are carried out for four case studies. Case 1: system without PHEVs; Case 2: system with uncontrolled PHEVs; Case 3: PHEVs in the system with PSO smart charging; and Case 4: PHEVs in the system with the proposed hierarchical game approach. The RMS value of frequency deviation calculated by (4.42) is used as an index to illustrate the performance of the frequency regulation:

$$\Delta f_{RMS} = \sqrt{\frac{1}{N}\sum_{i=1}^{N} \Delta f_i^2} \tag{4.42}$$

where N is the number of samples and Δf is the frequency deviation.

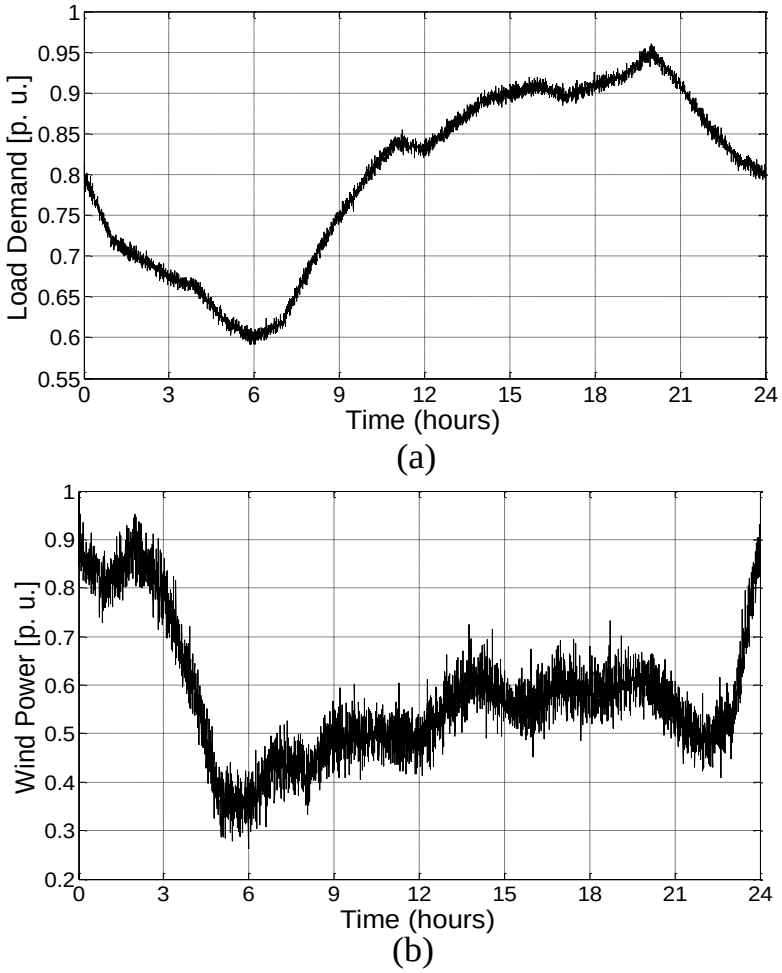

Figure 4. 6 (a) Daily load fluctuation in the control area; (b) Daily wind power fluctuation in the control area.

The simulation results are shown in Figs. 4.7-4.9. Fig. 4.7 shows the frequency fluctuation of the system in four case studies. As can be seen from Fig. 4.7(a), when there is no PHEV in the system, the frequency fluctuation is large. When there are PHEVs in the system, the frequency fluctuation is smaller and the proposed hierarchical game approach exhibits the best performance as shown in Fig. 4.7(b),(c),(d). Fig. 4.8 shows the RMS value of frequency deviation in every three hours. In the figure, Δf_{RMS} for Case 1 and Case 4 is about 0.028 Hz and 0.009 Hz respectively for the entire time span of 24 hours. For Case 2, Δf_{RMS} is quite the same as Case 4 except for the time period between 12 pm and 9 pm. In this time span, Case 2 shows an inferior performance which is also reflected in Fig. 4.7(b). The performance of Case 3 is better than Case

2 but is still inferior as compared with Case 4. This result can be explained by the availability of regulation capacity as shown in Fig. 4.9. In Case 2, the charging process of PHEVs is not controlled. PHEVs are charged immediately when they arrive home, so most PHEVs are in the charging state in the afternoon and evening which makes the regulation capacity quite small. In Case 3, the PSO based smart charging is able to shift some charging load to off-peak hours and increase the regulation capacity during the peak hours from 3 pm to 9 pm. Its performance is still inferior as compared with the proposed approach in Case 4 because it does not have an optimal regulation capacity bidding mechanism. As shown in Fig. 4.9, the regulation capacity decreases below 0.5 MW from 12 pm to 9 pm under uncontrolled charging. Therefore, the regulation capacity is not adequate in the time span between 12 pm and 9 pm in Case 2. Also, the regulation capacity is not adequate for Case 3 between 12 pm to 3 pm. When the hierarchical game approach is used, the charging sequences of PHEVs are optimally scheduled according to the regulation capacity bidding mechanism. With the hierarchical game approach, aggregators can attract more PHEVs to provide frequency regulation when the regulation capacity is inadequate by bidding higher regulation prices for the PHEVs. As shown in Fig. 4.9, the regulation capacity is larger than 0.5 MW for the entire time span in Case 4. It can be concluded that the proposed hierarchical game approach leads to the best performance in frequency regulation. The V2G power for frequency regulation of Case 4 is shown in Fig. 4.10.

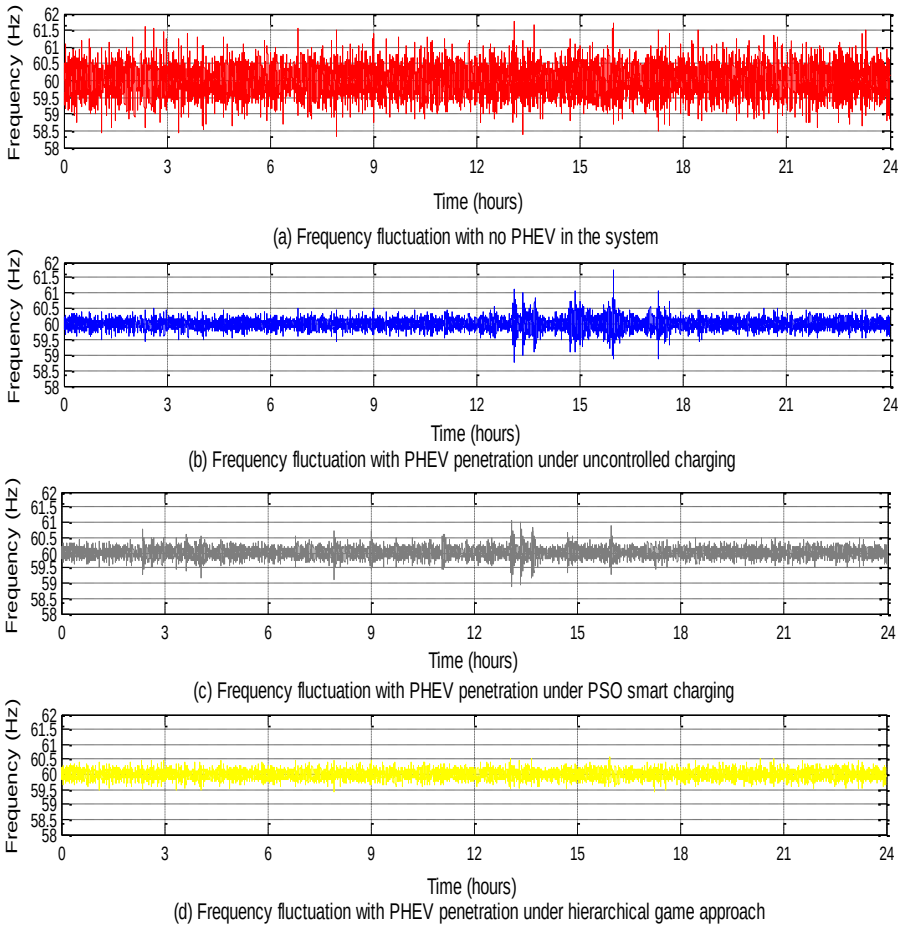

Figure 4. 7 Frequency fluctuation of the control area.

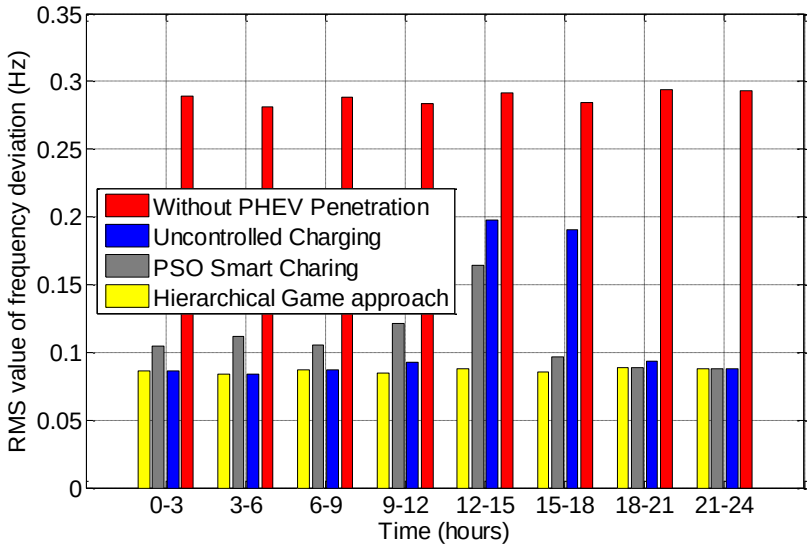

Figure 4. 8 RMS value of frequency deviation in every three hours.

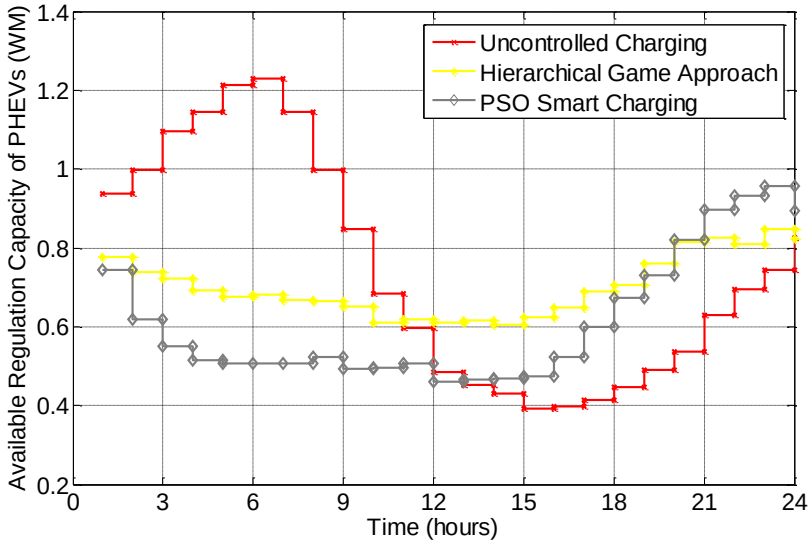

Figure 4. 9 Regulation capacity of PHEVs in the control area.

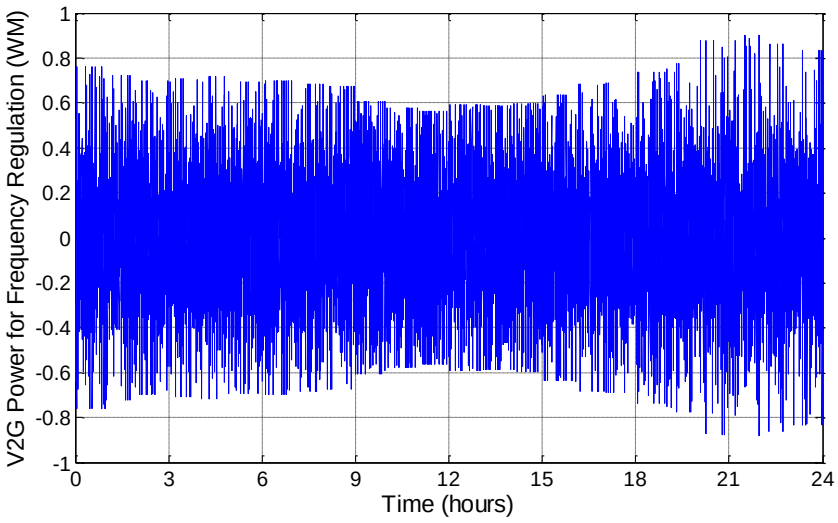

Figure 4. 10 V2G power of the aggregated PHEV for frequency regulation.

The load demand and the real-time electricity price of the residential area 1 in the control area are shown in Fig. 4.11 and Fig. 4.12, respectively. It can be seen that the proposed approach is able to flatten the load demand curve. Also, the proposed approach can lower the electricity price by reducing the peak load demand. Table 4.1 shows the cost of all PHEVs using different control strategies during a 24-hour time horizon. The proposed hierarchical game approach leads to a lower cost by charging at off-peak hours and bidding higher frequency regulation prices.

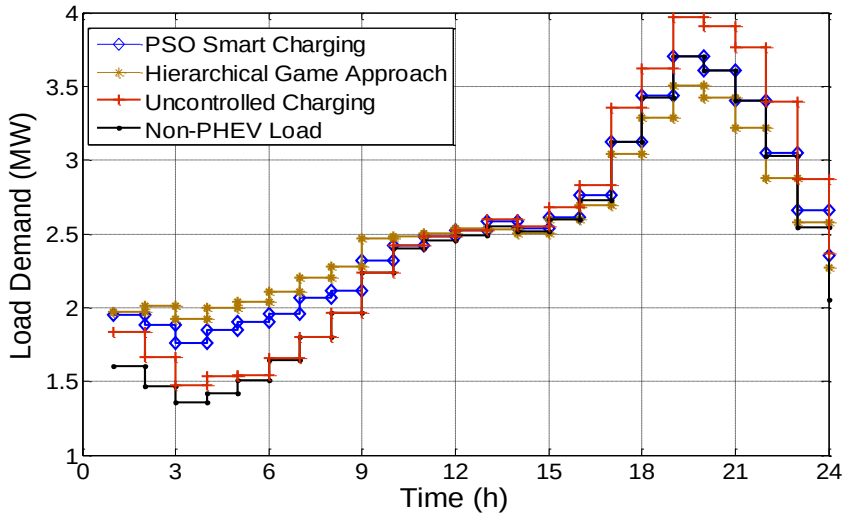

Figure 4. 11 Load demand of the residential area 1.

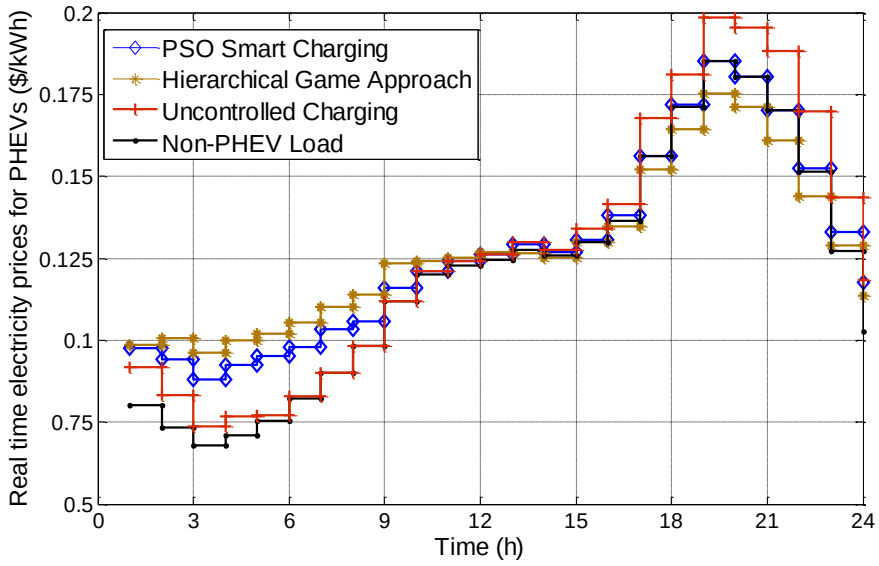

Figure 4. 12 Electricity price curves for PHEVs in residential area 1.

Table 4. 1 Costs of All the PHEVs in the Control Area

Criteria / Approaches	Charging Cost ($)	Regulation Earnings ($)	Total Cost ($)
Uncontrolled Charging	1178.34	154.25	1024.09
PSO Smart Charging	804.36	215.32	589.04
Hierarchical Game	655.43	241.56	413.87

5. Enabling Reliability-Differentiated Service in Residential Distribution Networks with PHEVs

5.1 Introduction

With the increasing deployment of PHEV fleets in the distribution system, their impact on the distribution system reliability cannot be neglected. The intermittent charging load of PHEVs may overload the transformers and transmission lines, which will increase the power system risk if it is not properly controlled. Various studies have been conducted on the optimal management of PHEVs [26]-[28], [59]-[66]. Among these methodologies, game-theoretic approaches [64]-[66] received much attention from researchers recently due to their capability in decentralized modeling and control. Instead of maximizing the total utility of the system, the game-theoretic approach ensures that the utility of each player is maximized. As a result, the game-theoretic approach based business model is more suitable for real-world implementations. This chapter proposed a hierarchical game approach to coordinate the charging process of PHEVs in a reliability-differentiated system. The proposed hierarchical game features a two-level structure. At the higher level, the management of V2G capacity of PHEVs is formulated as an evolutionary game [67]. Thus, each PHEV can find a balance of using the V2G capacity for peak load shaving and ancillary services when the evolutionary equilibrium is reached. At the lower level, a non-cooperative game is proposed to coordinate the charging process of PHEVs.

5.2 System Modeling

5.2.1 Reliability-Differentiated System Modeling

1) The framework for implementing reliability- differentiated service into residential distribution network

The structure of the proposed reliability-differentiated service is illustrated in Fig. 5.1. The household customers in a residential distribution grid are viewed as a class of customers subscribed to a certain level of reliability. In the wholesale market, the control center provides the information on the reliability level and total load demand of the residential area to the Independent System Operator (ISO), and this residential area is assigned with a locational marginal price (LMP) which can be derived according to reference [10]. This LMP will be further differentiated based on the different reliability requirements from the customers in the residential area. In the retail market, the households provide their desired priority indexes and load demand to the control center, and the control center will assign the reliability differentiated electricity prices to each household and provide a spinning reserve price for the distributed resources in this area.

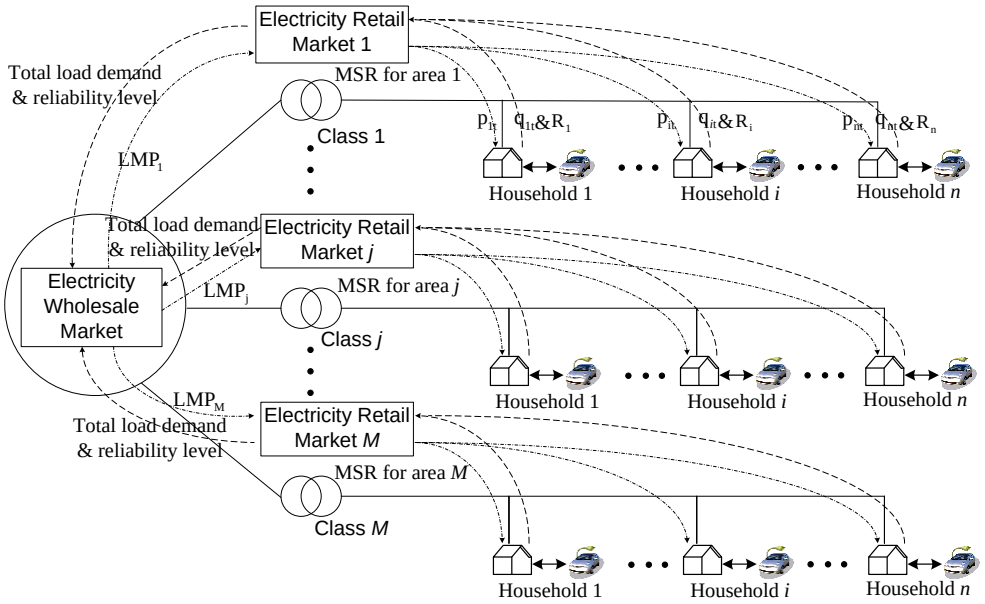

Figure 5. 1 Reliability-differentiated service framework.

In the proposed framework, households can subscribe to different reliability levels by selecting a value of priority index *R*. Households with higher values of *R* will have priority in continuing to be supplied by spinning reserves during a power outage. To evaluate the reliability service quality of households, this study develops multiple reliability indices at the household level. Three reliability indices for household are defined according to the interruption frequency, duration and magnitude, which are household interruption frequency index (HIFI), household interruption duration index (HIDI), and household interruption magnitude index (HIMI). HIFI indicates the average instances of interruption per year with the unit of interruptions/year. HIDI is the outage duration of the household suffered each year with the unit of hours/year. HIMI is the maximum interrupted power magnitude for each household with the unit of kW.

2) Reliability-differentiated pricing

The proposed reliability-differentiated pricing is designed based on the paid-for-performance mechanism [68], which implies the household with higher reliability request pays a higher electricity price. Also the proposed reliability-differentiated pricing is intended to encourage the customers to consume electricity wisely so as to enhance the system reliability by incorporating the risk of the residential distribution system into the pricing mechanism.

We formulate the operational reliability of the residential network by considering the real-time outage rate of the distribution transformer. According to reference [69], the transformer aging failure under various load conditions can be expressed as (5.1).

$$P_{af} = 1 - e^{\left(\frac{T_{LOI,total}}{Ce^{\frac{15000}{\theta_0+273}}}\right)^{\beta} - \left(\frac{T_{LOI,total}+\Delta t_e}{Ce^{\frac{15000}{\theta_0+273}}}\right)^{\beta}} \quad (5.1)$$

where $T_{LOI,total}$ is the loss of insulation life during a period, $\theta_0$is the reference temperature of transformer, C and β are constant values depending on the end-of-life failure of transformer.

Assuming the random failure probability is P_{rand}, the hybrid transformer failure probability model can be expressed as follows:

$$P_f = 1 - (1 - P_{rand}) \times (1 - P_{af}) \tag{5.2}$$

where P_{rand} is the transformer random failure rate, P_{af} is the transformer aging failure rate.

The mathematical model for calculating the current-dependent overload protection outage rate can be obtained through (5.3)-(5.5) [69]:

$$P_{pt}(I) = \begin{cases} P_{unreq}, & \text{if } I < I_{pe}(1-\varepsilon_I) \\ P_{req}\int_{I_{pe}(1-\varepsilon_I)}^{I} f(I_{pk})dI_{pk} + P_{unreq}\int_{I}^{I_{pe}(1+\varepsilon_I)} & \\ f(I_{pk})dI_{pk}, & \text{if } I_{pe}(1-\varepsilon_I) < I < I_{pe}(1+\varepsilon_I) \\ P_{req}, & \text{if } I > I_{pe}(1+\varepsilon_I) \end{cases} \tag{5.3}$$

$$f(I_{pk}) = \begin{cases} 0, & \text{if } I_{pk} < I_{pe}(1-\varepsilon_I) \text{ or } I_{pk} > I_{pe}(1+\varepsilon_I) \\ \dfrac{e^{\left(-(I_{pk}-I_{pe})^2/2\sigma^2\right)}}{\alpha_I\sigma\sqrt{2\pi}}, & \text{if} I_{pe}(1-\varepsilon_I) < I_{pk} < I_{pe}(1+\varepsilon_I) \end{cases} \tag{5.4}$$

$$\alpha_I = \phi\left(\frac{\varepsilon_I I_{pe}}{\sigma}\right) - \phi\left(\frac{-\varepsilon_I I_{pe}}{\sigma}\right) \tag{5.5}$$

where P_{pt} is the overload protection outage rate, P_{unreq} is the outage rate when the overload protection is not required, P_{req} is the outage rate when the overload protection is required, I_{pk} is the pick-up current for the protection relay, I_{pe} is the expectation value of I_{pk}, and ϕ is the cumulative distribution function of the standard normal distribution.

Then, the real-time transformer outage rate can be built by integrating the failure rate and overload protection rate as follows:

$$P_{trans}^t = 1 - (1 - P_f(t)) \times (1 - P_{pt}(I_t)) \tag{5.6}$$

We define the real-time potential interruption cost PIC_t as shown in (5.7), which is a scaled value of the expected loss of load.

$$PIC_t = \gamma P_{trans}^t (P_{sys}^t - P_{Anci}^t) \tag{5.7}$$

where P_{trans}^{t} is the real-time transformer outage rate,P_{sys}^{t} is the load demand of the system at time slot t , and P_{Anci}^{t} is the real-time ancillary service capacity.

The total cost of electricity can be expressed as follows:

$$\sum_{i=1}^{n} p_{i,t} q_{i,t} = q_{Tot,t} \cdot LMP_t + PIC_t, \quad \forall i \in N, \forall t \in T \tag{5.8}$$

where $p_{i,t}$ is the reliability-differentiated price for household *i,* $q_{i,t}$ is the load demand of household *i,* $q_{Tot,t}$ is the load demand of all households, and LMP_t is the real-time locational marginal price.

Considering the different priority indexes of households, the reliability-differentiated pricing for a residential distribution network with n household is described as follows:

$$p_{i,t} q_{i,t} = q_{i,t} LMP_t R_i + \sum_{\substack{j=1 \\ j \neq i}}^{n} q_{j,t} LMP_t \frac{1-R_j}{n-1} + \frac{q_{i,t}}{q_{Tot,t}} PIC_t, \ \forall i \in N, \forall t \in T \tag{5.9}$$

where R_i is the priority index for household *i.*

The reliability-differentiated pricing scheme for the households can be derived by solving (5.9). The household with a higher priority index will be assigned with a higher electricity price. When there is a shortage of generation capacity, those with lower priority indexes will be shed or cut off. When an interruption occurs in the distribution system (e.g., due to a transformer failure), part of the households under this transformer can still be supplied by distributed spinning reserves such as PHEVs. Similarly, only those with higher priority indexes can be continuously supplied. The marginal spinning reserve (MSR) price can be calculated as follows:

$$MSR_t = \frac{PIC_t}{P_{Anci}^{t}} \tag{5.10}$$

The proposed reliability-differentiated pricing model is shown in Fig. 5.2. As depicted in the figure, the reliability-differentiated prices for households are affected by their priority indexes, the LMP and the current potential interruption cost (PIC). PHEVs can affect the

reliability of the distribution system by its charging and discharging activities. As mentioned previously, the load demand will affect the failure rate of the transformer in the system, so the PHEVs' load demand profile will inevitably impact the current PIC. Then, the reliability-differentiated electricity price and marginal spinning reserve price are affected accordingly, and these changes in electricity price will in turn affect the optimal management of PHEVs. It is evident that achieving the optimal management of PHEVs demands a lower charging cost which is equivalent to having a lower PIC, and a lower PIC indicates a more reliable system. So it can be concluded that under the proposed reliability-differentiated pricing theory, achieving optimal management of the PHEVs is equivalent to optimizing the system reliability.

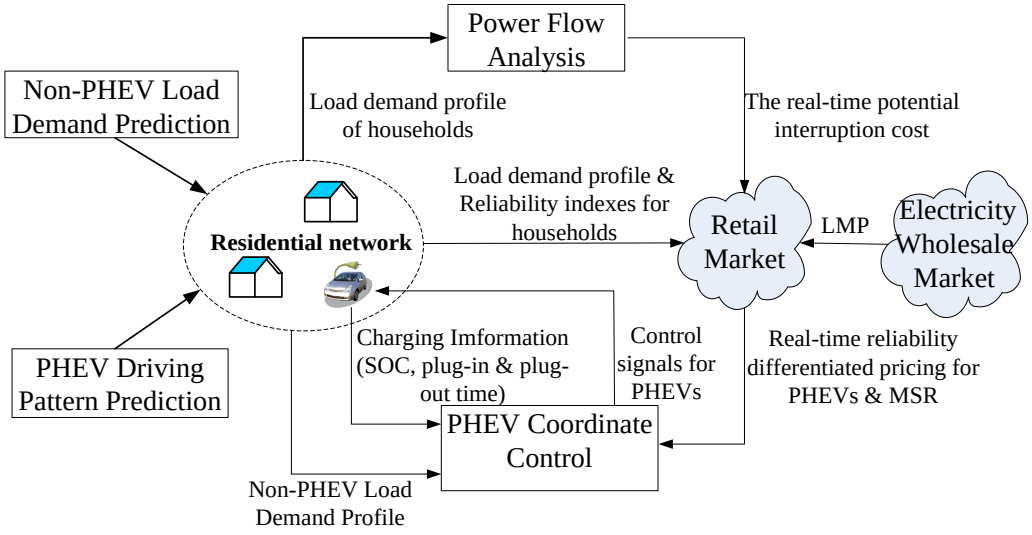

Figure 5. 2 The proposed reliability-differentiated pricing model.

5.2.2 Mathematical Modeling of PHEVs

1) Modeling the charging process of PHEVs

We use vectors $\mathbf{T} = [1,\cdots,t,\cdots,T]$ and $\mathbf{M} = [1,\cdots,d,\cdots,M]$ to indicate the charging time horizon and the numbering of PHEVs. In this study, vectors are denoted with boldface letters. The driving pattern and load demand of PHEVs are obtained from the results in Chapter 2. Then

we can generate the plug-in time $t_{in,d}$, plug-out time $t_{out,d}$ and the required energy $E_{req,d}$ of each PHEV in the system. It is more cost-effective to let PHEVs charge at the rated charging power so that more revenues can be earned by the V2G activities [27]. Thus, PHEVs can be controlled at three states: charging, discharging and idle. In this study, PHEVs are utilized to provide the ancillary services when they are in idle state.

V2G technology enables PHEVs to sell the energy back to the grid when needed. So PHEVs can use their V2G capacities to either perform peak load shaving or provide ancillary services (e.g., frequency regulation and spinning reserve) to the power system.

The V2G capacity of the d_{th} PHEV can be expressed as:

$$VCap_d = (t_{out,d} - t_{in,d})P_{rate}^d - E_{req,d}, \forall\, d \epsilon M \tag{5.11}$$

Then the total V2G capacity of all the PHEVs is:

$$VCap_{tot} = \sum_{d=1}^{M} VCap_d \tag{5.12}$$

The charging strategy can be expressed as a vector k:

$$\mathbf{k_d} = \left[k_d^{t_{in,d}}, \cdots, k_d^t, \cdots, k_d^{t_{out,d}}\right], \forall\, d \epsilon \mathbf{M} \tag{5.13}$$

where $k_d^t = 1$ means the d_{th} PHEV is in charging state at time slot t, $k_d^t = -1$ implies the d_{th} PHEV is in discharging state at time slot t, and $k_d^t = 0$ indicates the PHEV is in idle state at time slot t.

The required charging energy constraint is described in (5.14):

$$E_{req,d} = \sum_{t=t_{in,d}}^{t_{out,d}} k_d^t \cdot P_{rate}^d, \forall\, d \epsilon \mathbf{M} \tag{5.14}$$

The real-time state of charge (SOC) of a PHEV is indicated in (5.15):

$$SOC_d^{t_{x,d}} = SOC_d^{t_{in,d}} + \sum_{t=t_{in,d}}^{t_{x,d}} \frac{k_d^t \cdot P_{rate}^d}{Cap_d}, \forall\, d \epsilon \mathbf{M}, t_{x,d} \leq t_{out,d} \tag{5.15}$$

To protect battery from early degradation, the battery SOC should be bounded as follows:

$$\mathrm{SOC}_{\min,d} < \mathrm{SOC}_d^t < \mathrm{SOC}_{\max,d}, \forall\, d \epsilon \mathbf{M} \tag{5.16}$$

It is assumed that only the PHEVs in idle state can respond to the ancillary service calls. We defined three vectors $\mathbf{C} = [C_1 \cdots, C_d, \cdots, C_N]$, $\mathbf{D} = [D_1 \cdots, D_d, \cdots, D_N]$ and $\mathbf{I} = [I_1 \cdots, I_d, \cdots, I_N]$ to indicate the charging, discharging and idle states of PHEVs at each time slot as shown in (5.17)-(5.22).

$$C_d = \left[C_d^{t_{in,d}}, \cdots, C_d^t, \cdots, C_d^{t_{out,d}}\right], \forall\, d \epsilon \mathbf{M} \tag{5.17}$$

$$C_d^t = \begin{cases} 1, & \text{if } k_d^t = 1 \\ 0, & \text{otherwise} \end{cases}, \ \forall\, t \epsilon T; \forall\, d \epsilon \mathbf{M} \tag{5.18}$$

$$D_d = \left[D_d^{t_{in,d}}, \cdots, D_d^t, \cdots, D_d^{t_{out,d}}\right], \forall\, d \epsilon \mathbf{M} \tag{5.19}$$

$$D_d^t = \begin{cases} 1, & \text{if } k_d^t = -1 \\ 0, & \text{otherwise} \end{cases}, \ \forall\, t \epsilon \mathbf{T}; \forall\, d \epsilon \mathbf{M} \tag{5.20}$$

$$I_d = \left[I_d^{t_{in,d}}, \cdots, I_d^t, \cdots, I_d^{t_{out,d}}\right], \forall\, d \epsilon \mathbf{M} \tag{5.21}$$

$$I_d^t = \begin{cases} 1, & \text{if } k_d^t = 0 \\ 0, & \text{otherwise} \end{cases}, \ \forall\, t \epsilon \mathbf{T}; \forall\, d \epsilon \mathbf{M} \tag{5.22}$$

Thus, the V2G capacity used for ancillary services of the system at time slot t can be calculated as (5.23):

$$P_{\mathrm{Anci}}^t = \sum_{d=1}^{M} I_d^t \cdot P_{\mathrm{rate}}^d, \forall\, t \epsilon \mathbf{T} \tag{5.23}$$

where P_{rate}^d is the rated power for PHEV *d*.

The total charging power of PHEVs is illustrated as (5.24):

$$P_{\mathrm{EV}}^t = \sum_{d=1}^{M} C_d^t \cdot P_{\mathrm{rate}}^d, \forall\, t \epsilon \mathbf{T} \tag{5.24}$$

The total discharging energy provided by PHEVs is:

$$E_{\mathrm{dis}} = \sum_{d=1}^{M} \sum_{t=t_{in,d}}^{t_{out,d}} D_d^t \cdot P_{\mathrm{rate}}^d \tag{5.25}$$

So a feasible control strategy of PHEVs can be described as follows:

$$\mathbf{K} = \{\mathbf{k_d} | \text{s.t.} (5.14) - (5.16)\}, \forall\ \text{d} \epsilon \mathbf{M} \tag{5.26}$$

2) Dominant Solution Matrix

The feasible control strategy of PHEVs described in (5.26) involves a huge solution space. We can simplify the problem by finding the dominant solutions from the feasible solutions. To slow down the degradation progress of batteries, we should avoid frequent switching between charging and discharging modes [31]. Thus, we should wisely arrange the charging and discharging time slots to reduce the switching frequency between different control states. Based on the above principle, the dominant solution matrix of the d_{th} PHEV $\mathbf{DS_d}$ is shown in Fig. 5.3.

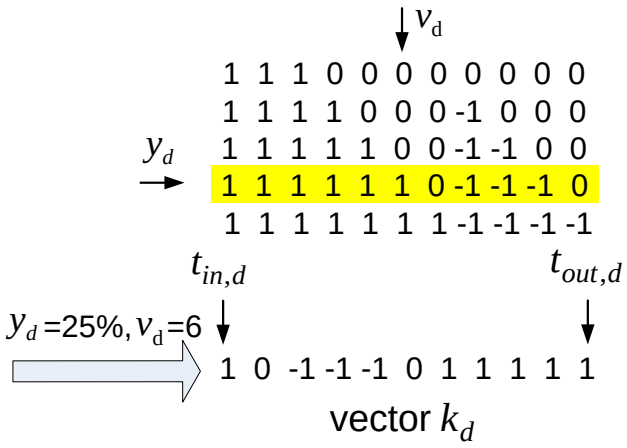

Figure 5. 3 Dominant solution matrix and percentage of V2G capacity.

The charging sequence of PHEVs can be classified into different patterns based on various V2G strategies. As the PHEVs can use their V2G capacity to either perform peak load shaving or provide ancillary services at each time slot, the V2G strategy is defined as the percentage of V2G capacity used for ancillary services as follows:

$$\text{y}_\text{d} = \frac{\Sigma_{\text{t=t}_{\text{in,d}}}^{\text{t}_{\text{out,d}}} \text{I}_\text{d}^\text{t} \cdot \text{P}_{\text{rate}}^\text{d}}{\text{VCap}_\text{d}},\ \forall\ \text{d} \epsilon \text{M} \tag{5.27}$$

As shown in Fig. 5.3, the dominant charging sequence for a PHEV can be generated from the dominate matrix $\mathbf{DS_d}$ by selecting different V2G strategies y_d and the sequence starting point

v_d. Once a V2G strategy is selected, the possible charging solution of this specific PHEV can be obtained by shifting the sequence. For instance, as shown in Fig. 5.3 the V2G strategy $y_d = 25\%$ and the sequence starting point $v_d = 6$.

The dominant solution matrices for all the PHEVs can be represented as follows:

$$\mathbf{DS} = [DS_1 \cdots DS_d \cdots DS_M], \forall\, \mathbf{d} \epsilon M \tag{5.28}$$

5.3 Hierarchical Game Formulation

The proposed hierarchical game framework consists of two levels of games. At the lower level, a non-cooperative game is formulated to coordinate the charging schedules of the PHEVs based on a specific V2G strategy. At the upper level, an evolutionary game is proposed to evolve the PHEVs' V2G strategies. During each evolving step of the evolutionary game, a new Nash equilibrium will be found in the non-cooperative game. Once the evolutionary equilibrium is reached, the games at the two levels will both reach their equilibriums. Then the solution to the formulated problem is found.

5.3.1 Non-cooperative Game Formulation

In this subsection, we formulate the charging scheduling process of multiple PHEVs through a non-cooperative PHEV interaction game $\mathbb{G}_1$ in the residential network as follows:

- Players: The set of all **M** PHEVs.
- Strategies: For each PHEV, choose an strategy vector $\mathbf{k_d}, \forall \mathbf{k_d} \in \mathbf{K}$.
- Payoffs: The d_{th} PHEV receives payment $U_d(k_d, k_{-d})$.

The payoff function of the d_{th} PHEV can be expressed as:

$$U_d(k_d, k_{-d}) = -\left(Cost^d_{Char} + Cost^d_{Bat} - Earn^d_{anci}\right) = -\sum_{t=t_{in,d}}^{t_{out,d}} C^t_d \cdot P^d_{rate} \cdot r_{d,t} -$$

$$\frac{c_b \cdot Cap_d + c_L}{L_C \cdot Cap_d \cdot DOD} \cdot \sum_{t=t_{in,d}}^{t_{out,d}} D^t_d \cdot P^d_{rate} + \sum_{t=t_{in,d}}^{t_{out,d}} I^t_d \cdot P^d_{rate} \cdot (reg_t + MSR_t) \quad (5.29)$$

where $Cost^d_{Char}$ is the charging cost of player *d,* $Cost^d_{Bat}$ is the cost of battery degradation of player *d,* $Earn^d_{anci}$ is the revenues earned by providing ancillary services of player *d,* reg_t is the real-time frequency regulation price.

We use Nash equilibrium as the solution of this game and it is defined as follows:

Definition 5.1: For the proposed non-cooperative game $\mathbb{G}_1 = \{M, \{k_d\}_{d\in M}, \{U_d\}_{d\in M}\}$, a strategy tuple $\Psi = \{k^*_d\}_{d\in M}$ constitutes a Nash equilibrium when no player can improve its utility by unilaterally deviating from its current strategy. It is formulated as a set of inequalities:

$$U_d(k^*_d, k^*_{-d}) \geq U_d(k_d, k^*_{-d}),\ \forall k_d \in \mathbf{K}, \forall d \in \mathbf{M} \quad (5.30)$$

To find the Nash equilibrium for the proposed game $\mathbb{G}_1$, we applied a dynamic best response strategy which is defined as follows:

Definition 5.2: For each player $d \in M$, while other players have a fixed strategy tuple k_{-d}, the best response strategy k'_d for the d_{th} player is:

$$k'_d = \text{argmax}_{k_d \in K}\{U_d(k_d,\ k_{-d})\}, \forall d \in \mathbf{M} \quad (5.31)$$

That is, the players will update their strategies in an iterative and sequential manner. For instance, for any player $d \in \mathbf{M}$, after receiving other players' strategies k_{-d} from the aggregator, the best response strategy k'_d is the one which gives the largest payoff to the player at the current state. Then other players will take turns to find their best response strategies. This iterative process continues until the Nash equilibrium is reached.

However, as the formulated utility function is discrete in strategies, the Nash Equilibrium may be lost due to the discretization of strategy variables [70]. To obtain a possibly missing

Nash equilibrium, we include a small positive parameter ε_1 in (5.30) to get an approximate Nash equilibrium as described in (5.32) [71]. As the approximate Nash equilibrium results in a similar performance and requires less computational time, it is used as the solution of the proposed non-cooperative game.

$$U_d(k_d^*, k_{-d}^*) \geq U_d(k_d, k_{-d}^*) - \varepsilon_1, \ \forall k_d \in K, \forall d \in M \tag{5.32}$$

Lemma 5.1: At least one Nash equilibrium exist in every game if the game has a finite number of players and action profiles [72].

Theorem 5.1: The proposed non-cooperative game will converge to the approximated Nash equilibrium (5.32).

Proof: see the Appendix.

The proposed best response algorithm is summarized in Algorithm 1 as follows:

Algorithm 5.1 The best response algorithm for the non-cooperative game

---

1: Input random initial strategies for all players and send the strategy information to the aggregator.

2: repeat

3: for d=1,…, M do

4: 1) The aggregator selects a player d and provides the player with the current strategies of other players k_{-d}

5: 2) The player finds its current best response strategy k_d' based on (5.31). Then the player provides the aggregator with its current best response strategy k_d'.

6: 3) The aggregator moves to the next player.

7: end for

8: until the approximate Nash equilibrium (5.32) is reached.

9: Output control strategies and stop.

5.3.2 Evolutionary Game Formulation

1) Formulation of an evolutionary game

In this subsection, we formulate the V2G activities of PHEVs as an evolutionary game. The evolutionary game extends the formulation of non-cooperative game by including the concepts of replicator dynamics and population [73]. In the context of evolutionary games, the population refers to a set of players with the same strategy and the replicator dynamics controls the reproduction speed of the population according to the payoff of the population's strategy [73]-[75].

For the proposed problem, the evolutionary game $\mathbb{G}_2$ can be naturally defined as follows:

- Players: The set of all M PHEVs.
- Strategy: The strategy of each player is a selection of a level of V2G capacity used for ancillary services and it can be denoted as $S = \{l_1, \dots, l_j, \dots, l_J\}$.
- Population: The set of players which have the same strategy l_j.
- Population share: Denote the number of players selecting strategy l_j as m_j, then $x_j = m_j/M$ is the population share.
- Payoffs: The d_{th} PHEV receives utility $\pi_d^{anci}(y_d, y_{-d})$ which is the per unit ancillary service revenue.

To simplify the problem, we define a continuous strategy state as $Y = [y_1, \dots, y_d, \dots, y_M]$ where the strategy for the d_{th} player y_d is defined as the percentage of V2G capacity used for ancillary services. Note that $y_d = \sum_{j=1}^{J} x_j l_j$, so the new strategy embodied the dynamics of the

population share. Instead of controlling the dynamic process of population share, the replicator dynamics now is used for guiding the evolving direction of the strategy state.

2) The evolution of strategy state and replicator dynamics

The revenue of the V2G activities for a PHEV can be expressed as the sum of earnings by offering ancillary services and performing peak load shaving as shown in (5.33):

$$\mathrm{Earn}_{\mathrm{V2G}}^{\mathrm{d}} = \mathrm{Earn}_{\mathrm{anci}}^{\mathrm{d}} + \mathrm{Earn}_{\mathrm{pls}}^{\mathrm{d}}, \ \ \forall \mathrm{d} \in \mathbf{M} \tag{5.33}$$

where $Earn_{anci}^{d}$ is the revenues earned by providing ancillary services of player *d,* $Earn_{pls}^{d}$ is the revenues earned by performing peak load shaving of player *d.*

Then the per unit ancillary service revenue for a PHEV is defined as follows:

$$\pi_{\mathrm{d}}^{\mathrm{anci}} = \frac{\mathrm{Earn}_{\mathrm{anci}}^{\mathrm{d}}}{\mathrm{y_d} \cdot \mathrm{VCap_d}}, \ \ \forall \mathrm{d} \in \mathbf{M} \tag{5.34}$$

where $\mathrm{Earn}_{\mathrm{anci}}^{\mathrm{d}} = \sum_{\mathrm{t=t_{in,d}}}^{\mathrm{t_{out,d}}} \mathrm{I}_{\mathrm{d}}^{\mathrm{t}} \cdot \mathrm{P}_{\mathrm{rate}}^{\mathrm{d}} \cdot (\mathrm{reg_t} + \mathrm{MSR_t})$.

The per unit V2G revenue for a PHEV is defined as:

$$\pi_{\mathrm{d}}^{\mathrm{V2G}} = \frac{\mathrm{Earn}_{\mathrm{V2G}}^{\mathrm{d}}}{\mathrm{VCap_d}}, \forall \mathrm{d} \in \mathbf{M} \tag{5.35}$$

The average per unit V2G revenue of all the players is as follows:

$$\overline{\pi}_{\mathrm{V2G}} = \frac{\sum_{\mathrm{d=1}}^{\mathrm{M}} \mathrm{Earn}_{\mathrm{V2G}}^{\mathrm{d}}}{\mathrm{VCap_{tot}}} \tag{5.36}$$

Theorem 5.2: $\mathrm{Earn}_{\mathrm{V2G}}^{\mathrm{d}}$ is a concave function of $\mathrm{y_d}$ and there exists a $\mathrm{y_d^*}$ for maximizing the value of $\pi_{\mathrm{d}}^{\mathrm{V2G}}$.

Proof: see the Appendix.

Accordingly, the replicator dynamics can be defined as follows:

$$\frac{\partial \mathrm{y_d}}{\partial \mathrm{t}} = \delta \mathrm{y_d}\left(\pi_{\mathrm{d}}^{\mathrm{anci}} - \overline{\pi}_{\mathrm{V2G}}\right), \forall \mathrm{d} \in \mathbf{M} \tag{5.37}$$

According to the proposed replicator dynamics (5.37), the percentage of V2G capacity used for ancillary services y_d will increase when the per unit ancillary service revenue for the PHEV π_d^{anci} is larger than the average per unit V2G revenue of all the PHEVs, and vice versa. This scenario coincides with our common sense of maximizing the profit.

3) Evolutionary equilibrium and the proposed iterative algorithm

The evolutionary equilibrium is the solution of evolutionary game which is a stable condition that the strategy state stops evolving. For the formulated problem, the evolutionary equilibrium is reached when the replicator dynamics (5.38) stops evolving. That is:

$$\frac{\partial y_d}{\partial t} = \dot{y}_d = 0, \forall d \in M \tag{5.38}$$

$$\pi_d^{anci} = \overline{\pi}_{V2G}, \forall d \in M \tag{5.39}$$

The evolutionary equilibrium is denoted by $Y^* = [y_1^*, y_2^*, \dots, y_d^*, \dots, y_M^*]$. The convergence of the proposed evolutionary game to the evolutionary equilibrium (5.38) can be proved by Lyapunov method [76].

Lemma 5.2: For a scalar function V of state x with continuous first order derivatives. If it satisfies the conditions:

- $V(x)$ is positive definite
- $\dot{V}(x)$ is negative definite
- $V(x) \to \infty$ when $\|x\| \to \infty$

then there exists a globally asymptotically stable equilibrium at the origin.

Theorem 5.3: The evolutionary game will converge to the evolutionary equilibrium (5.38).

Proof: see the Appendix.

We use a discrete replicator to approximate the time continuous replicator dynamics as follows:

$$y_d(h+1) = y_d(h) + \delta y_d(h)\left(\pi_d^{anci}(h) - \overline{\pi}_{V2G}(h)\right), \forall d \in M \quad (5.41)$$

The iterative algorithm for solving the proposed evolutionary game is summarized in Algorithm 5.2, and it converges when (5.42) is satisfied.

$$\left|\pi_d^{anci}(h) - \overline{\pi}_{V2G}(h)\right| < \varepsilon_2, \forall d \in M \quad (5.42)$$

Algorithm 5.2 The iterative algorithm for the evolutionary game

---

1: Input random initial V2G strategies for all players and send the strategy information to the aggregator.

2: h=1.

3: repeat

4: for d=1,…, M do

5: Calculate the per unit ancillary service revenue π_d^{anci} of player d according to (5.34).

6: end for

7: Calculate the average per unit V2G revenue $\overline{\pi}_{V2G}$ of all the players according to (5.36).

8: for d=1,…, M do

9: Update the percentage of using V2G capacity for ancillary services of player d according to (5.41).

10: end for

11: Execute Algorithm 5.1.

12: h=h+1.

13: until (5.42) is satisfied.

14: Output control strategies and stop.

5.4 Case Studies

5.4.1 Residential Distribution System Under Test

As shown in Fig. 5.4, the topology of the residential distribution system is determined based on an IEEE 34-node test feeder [37]. In the test system, load point 1 is connected to the grid through a distribution transformer and each of other load points has a house connected to each phase transformer for a total of 99 houses. The non-PHEV load profile of a house in winter is scaled from [38]. Assume each house has two vehicles. Then there is a total of 40 PHEVs in the test system for a 20% PHEV penetration level. The detailed procedures for reliability analysis can be found in our previous work [77]. The power flow analysis is performed based on a backward-forward sweep method [39]. To demonstrate the effectiveness of the proposed hierarchical game approach, uncontrolled charging and particle swarm optimization (PSO) algorithm [32] based smart charging are used as benchmarking control strategies.

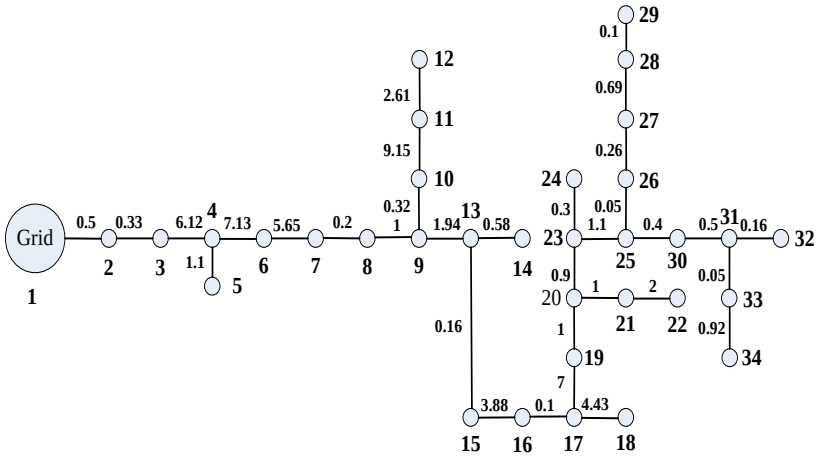

Figure 5. 4 The topology of the studied residential distribution grid.

5.4.2 Convergence and Effectiveness of the Hierarchical Game Approach

In this subsection, we will study the convergence behavior and the effectiveness of the proposed hierarchical game approach. Fig. 5.5 shows the convergence behavior of the non-cooperative game using Algorithm 5.1. As shown in the figure, the payoffs of all the players converge to a stable state after several iterations. The convergence behavior of the evolutionary game is shown in Fig. 5.6. In Fig. 5.6 (a), the per unit ancillary service revenue for each player converges to the average per unit V2G revenue for all the players as described in (5.39). In Fig. 5.6 (b), the per unit V2G revenue of each player converges to the average per unit V2G revenue of all the players, and the average per unit V2G revenue increases during the converging process until it reaches the maximum point. The results in Fig. 5.6 agree very well with the theoretical analysis in the previous Section. The effectiveness of the proposed hierarchical game approach for charging the PHEVs to the desired SOC is illustrated in Fig. 5.7. It shows that the final SOCs of PHEVs at the time when they are plugged out. As shown in the figure, all the PHEVs have been adequately charged at the end of the charging process.

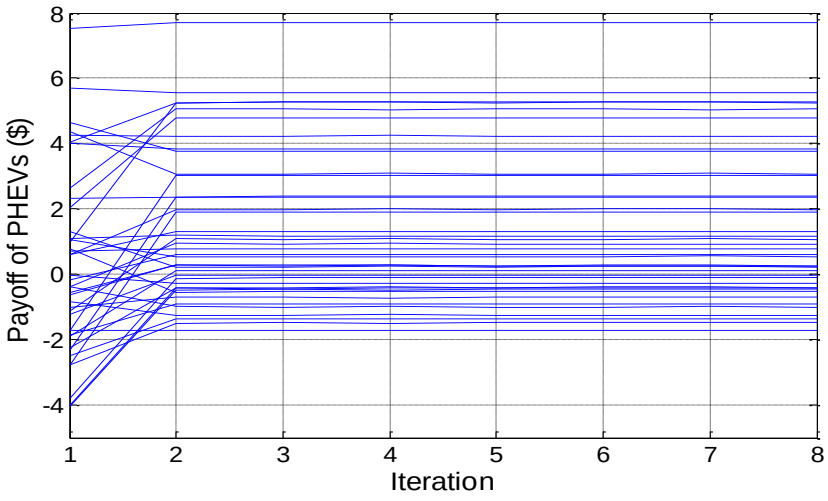

Figure 5. 5 Convergence curves of non-cooperative game using algorithm 5.1.

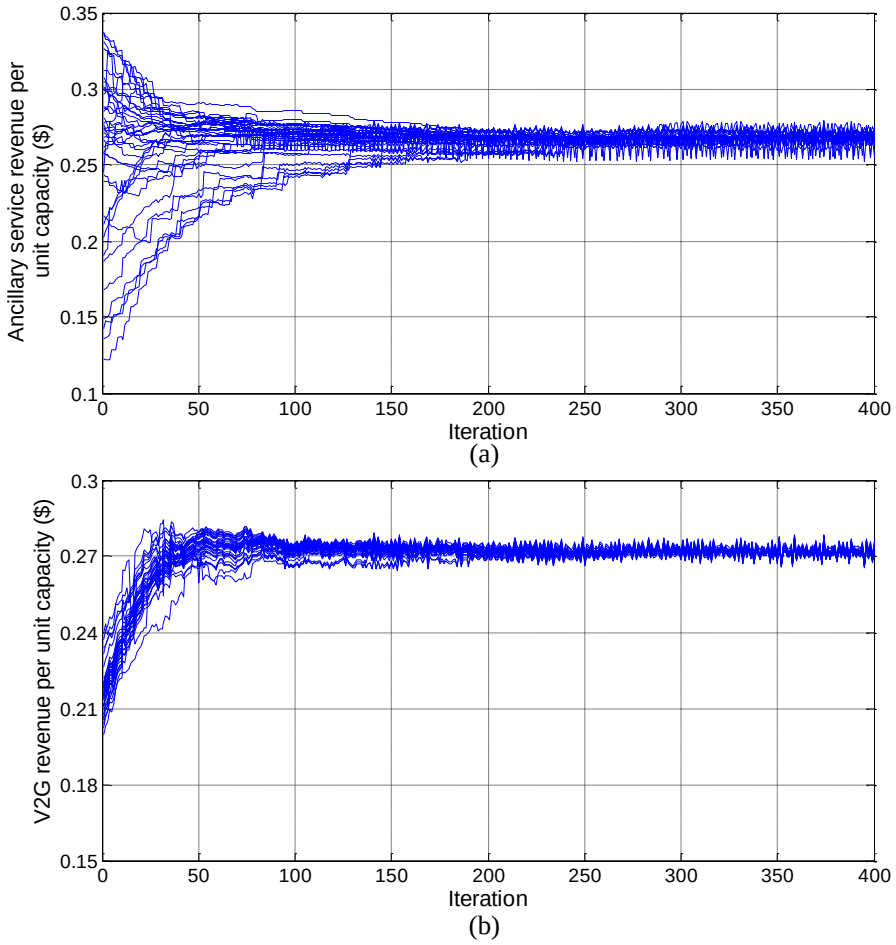

Figure 5. 6 Convergence curves of evolutionary game using algorithm 5.2. (a) Convergence curve of ancillary service revenue per unit capacity. (b) Convergence curve of V2G revenue per unit capacity.

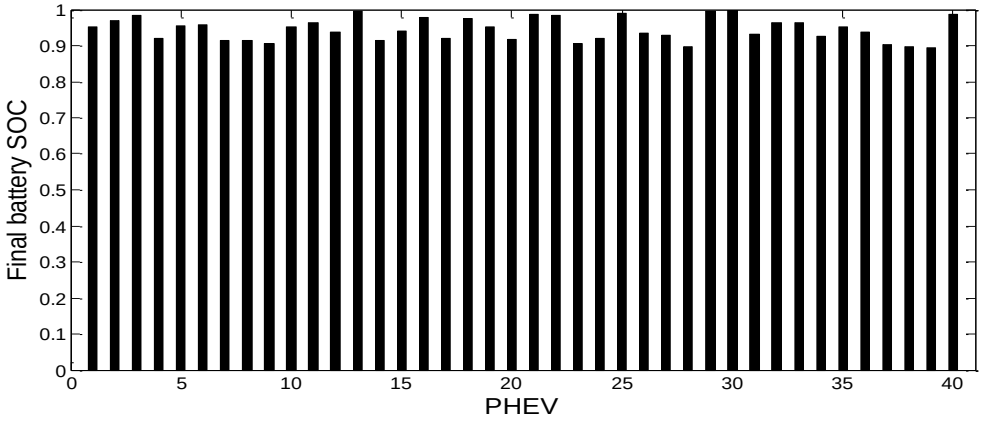

Figure 5. 7 Final battery SOCs of PHEVs with the hierarchical game approach.

5.4.3 **Economic and Power Quality Benefits of the Hierarchical Game Approach**

Fig. 5.8 shows the load demand of the system based on the three control strategies. The proposed hierarchical approach reduces the peak load, and the load demand curve becomes more flattened. Fig. 5.9 shows voltage curves of the load point 34 of the test system with different control strategies. As shown in the figure, the proposed algorithm is able to reduce the voltage deviation effectively. Table 5.1 shows the costs of all PHEVs based on different control strategies. The hierarchical game approach is capable of significantly reducing the total cost through intelligent management of the V2G capacity.

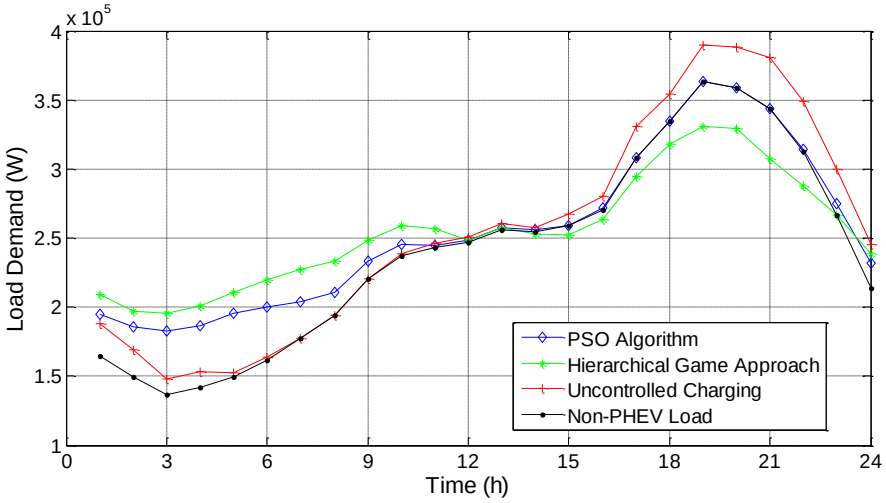

Figure 5. 8 Load demand of the system with different control strategies.

Table 5. 1 Costs of Different Control Strategies

	Chargi ng Cost ($)	Peak load Shave Earning($)	Ancillary Service Earning ($)	Total Cost ($)
Uncontrolled	150.12	N/A	24.16	125.96
PSO Algorithm	61.01	N/A	31.07	29.94
Hierarchical Game Approach	56.21	40.18	21.83	-5.80

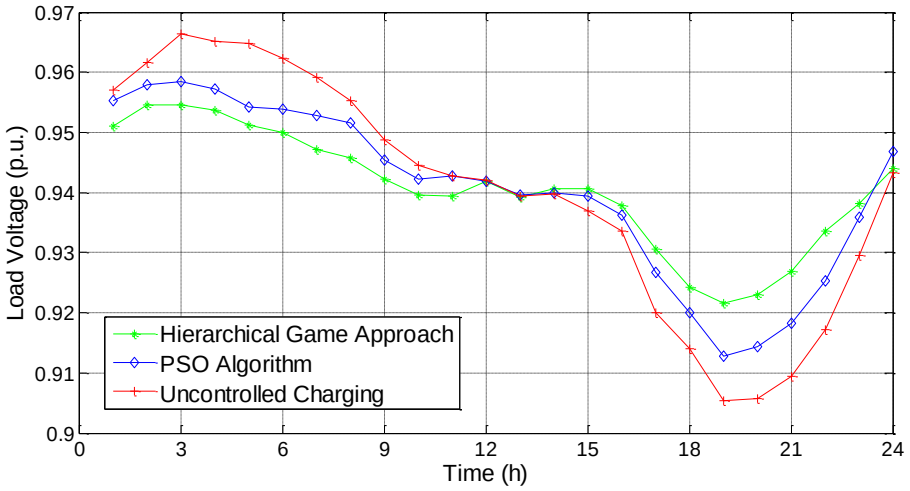

Figure 5. 9 Voltage curves of node 34 with different control strategies

5.4.4 Reliability Benefits of Reliability-Differentiated Service with the Proposed Hierarchical Game Approach

In this subsection, the reliability benefits of the reliability-differentiated service and the proposed hierarchical game approach are illustrated. Table 5.2 shows the reliability indices of the residential distribution system under different control strategies. According to the results, it can be found that the proposed hierarchical game approach has a positive impact on the reliability indices. The values of SAIFI, SAIDI and CAIDI are considerably decreased, which indicates that customers experienced less frequent interruptions and shorter outage duration each year; while the increase of ASAI implies that customers suffered from fewer time periods without power service. Fig. 5.10 shows the electricity price curves of three households with different priority indexes. It is clear that the household with higher priority index pays a higher electricity price. The values of corresponding reliability indices for these three households are shown in Table 5.3. According to the simulation results, the values of HIFI and HIDI are decreased with the increased priority index. This indicates that the household experienced less frequent interruptions and shorter outage duration each year. It can be concluded that while being responsible for

paying higher electricity prices those households with higher priority indexes received a higher quality of service.

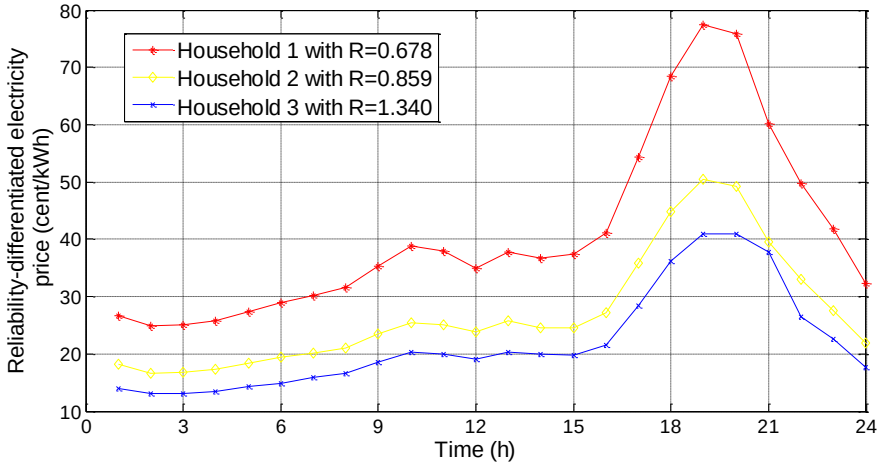

Figure 5. 10 Reliability-differentiated electricity prices for different households.

Table 5. 2 Reliability Indices for the Residential Distribution System Under Different Control Strategies

	SAIFI	SAIDI	CAIDI	ASAI
Uncontrolled	46.42	732.56	15.78	0.9163
PSO Algorithm	1.315	6.762	5.142	0.9992
Hierarchical Game Approach	1.062	5.125	4.826	0.9994

Table 5. 3 Reliability Indices for Different Households with Different Priority Indexes

	HIFI	HIDI	HIMI
Household 1 with $R_1 = 0.678$	1.457	6.963	2.4
Household 2 with $R_2 = 0.859$	1.123	5.867	2.2
Household 3 with $R_3 = 1.340$	0.698	3.156	2.0

6. Real-Time Charging Navigation of Electric Vehicles to Fast Charging Stations

6.1 Introduction

Various studies have been conducted for investigating EVs' impacts on the power system [16], [26]-[28], [63], [65] [78]-83]. Most of them assumed that EVs are charged at home, which are focused on controlling the charging process of EVs in order to shave the peak load or improve the power quality [26]-[28],[63],[65]. For the charging station, the charging duration is much shorter than the home charging. With fast charging, EVs can be charged to full SOC within half an hour [16], [78]-[79], while the home charging needs 6 to 8 hours. Thus, mitigating the negative impact of EVs on power systems through controlling the charging duration and charging rate of EVs is not applicable for the scenario of charging stations. One promising solution is to attract EVs to charge at appropriate times so as to optimize the charging load of EVCSs. In this case, the impact from the transportation system is not negligible for the management and coordination of multiple EVCSs. Reference [78] proposed a rapid charging navigation system for EVs based on the power system coupled with the traffic data accounting for the impact due to traffic flow. The power market is also a factor that should be considered in managing EVCSs. Multiple EVCSs in the same area may belong to different owners, so competitions between different EVCSs can be caused. This type of competition has been modeled by game-theoretic approaches in [16], [78], [80]-[81]. A supermodular game is proposed in [80] to study the competition among EVCSs with renewable power generators. A large fleet of EVs is studied in a mean-field game model to minimize their charging cost in [81]. Reference [82] proposed an optimal EV route model based on a learnable partheno-genetic

algorithm to minimize the total distribution costs of the EV route. A decentralized policy is studied in [83] to assign electric vehicles to a network of charging stations with the goal of minimizing the queueing time. However, little work has been done to formulate both the traffic flow and the competition of EVCSs into an integrated problem.

This chapter proposes an integrated charging navigation framework, which is made up of the power system, transportation system, navigation system, EVCSs and EVs. Based on this framework, a hierarchical game approach is proposed to optimize the strategies of both EVCSs and EVs at two levels. At the upper level of the hierarchical game, a non-cooperative game is proposed to model the competition between EVCSs and manage them in a decentralized fashion. Evolutionary games are formulated at the lower level to evolve the EVs' strategies in choosing EVCSs. To solve the non-cooperative game, a particle swarm optimization (PSO) learning based best response algorithm is developed, which is able to improve the economic benefits and reduce the peak load of the power grid at the same time.

6.2 System Modeling

6.2.1 System Architecture

To study the impacts from both the power system and transportation system in the EV charging process, we proposed an integrated EV charging navigation framework as shown in Fig. 6.1. The integrated EV charging navigation framework comprises four major parts: power system operation center (PSOC), EVCSs, electric vehicle navigation system (EVNS), and EV terminals.

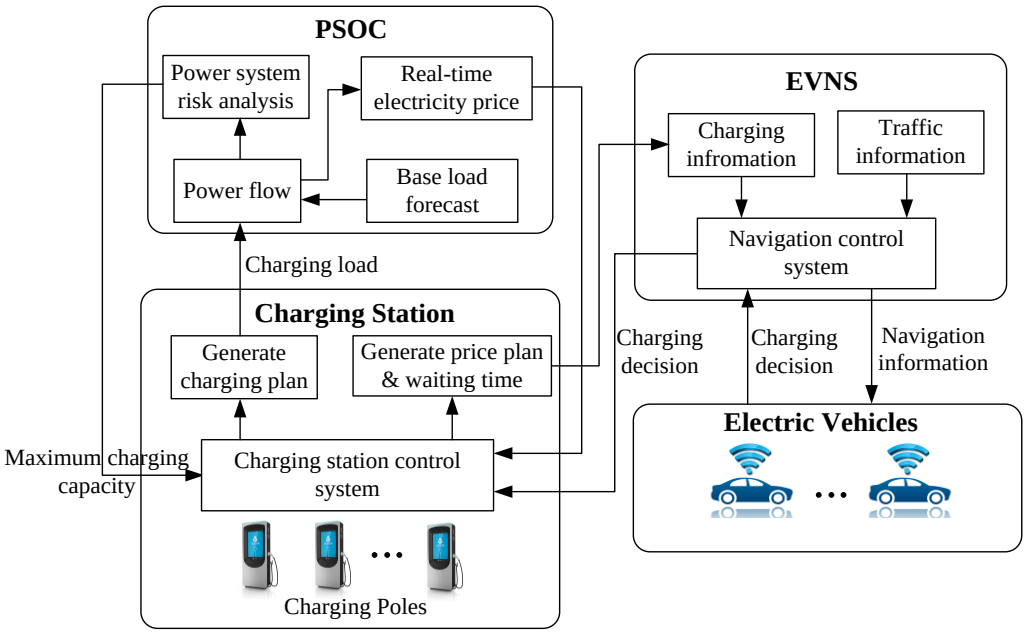

Figure 6. 1 The integrated electric vehicles charging navigation framework.

EVNS is responsible for collecting information and building connections between EVs and EVCSs. EVNS receives information from the EVCSs including the charging price and the estimated waiting time. It also collects current traffic information. Then the EVNS will broadcast the information to EVs. Upon receiving the information, EVs will decide if there is a need to charge and which EVCS should be selected (with the help of EVNS), as well as arrange the related charging activities. PSOC provides time of use (TOU) electricity prices to EVCSs based on the current load demand. Also it controls the maximum charging capacity of EVCSs to reduce the risk imposed on the power system.

6.2.2 Traffic Flow Model

The time horizon of the proposed control system is discretized into k time slots. During each time slot $t \in [k \cdot \Delta T, (k+1) \cdot \Delta T]$, (k=0, 1, 2,…, K), the traffic flow is calculated to provide necessary traffic information to the EVNS. In a destination-oriented traffic system, the EVNS needs the information on the lengths of the routes and traffic speeds to navigate vehicles.

Thus, we are focused on obtaining the traffic speeds of the lanes between neighboring traffic nodes. Three key variables in this traffic flow model are defined as follows: Traffic density $\rho_m(k)$ (veh/mile/lane) which is the number of vehicles in lane m during time slot k; traffic speed $v_m(k)$ (mile/h) which is the average speed of the vehicles in lane m during time slot k; and traffic flow $q_m(k)$ (veh/h) which is the number of vehicles leaving lane m during time slot k.

The traffic density of a lane is affected by the traffic flow as well as the start and end statuses of trips in this lane. The traffic density at time $(k+1)\Delta T$ is the sum of traffic density at time $k\Delta T$ and the increment of traffic density during time slot k. The traffic flows into the lane m can be expressed as $\sum_{\mu \in I_m} \beta_{\mu,m}(k) \cdot q_\mu(k)$ and the traffic flows out of the lane m is $\sum_{\varphi \in O_m} \beta_{m,\varphi}(k) \cdot q_\varphi(k)$, then the traffic density increment of lane m contribute by the traffic flow is $\frac{\Delta T}{L_m}\left(\sum_{\mu \in I_m} \beta_{\mu,m}(k) \cdot q_\mu(k) - \sum_{\varphi \in O_m} \beta_{m,\varphi}(k) \cdot q_\varphi(k)\right)$. The traffic density increment of lane m due to the start and end statuses of trips can be expressed as $\frac{1}{L_m}\left(N_m^s(k) - N_m^E(k)\right)$.

Thus, the traffic density can be expressed as follows:

$$\rho_m(k+1) = \rho_m(k) + \frac{\Delta T}{L_m}\left(\sum_{\mu \in I_m} \beta_{\mu,m}(k) \cdot q_\mu(k) - \sum_{\varphi \in O_m} \beta_{m,\varphi}(k) \cdot q_\varphi(k)\right) + \frac{1}{L_m}\left(N_m^s(k) - N_m^E(k)\right) \quad (6.1)$$

where I_m is the set of lanes entering lane m, $\beta_{\mu,m}$ is the turning rate of vehicles from lane μ into lane m, O_m is the set of lanes leaving lane m, L_m is the length of the lane m, $N_m^s(k)$ is the number of vehicles starting trips at lane m during time slot k, and $N_m^E(k)$ is the number of vehicles ending trips at lane m during time slot k.

The traffic speed can be calculated as follows [84]:

$$v_m(k) = v_m^f \cdot \exp\left[-\frac{1}{a_m}\left(\frac{\rho_m(k)}{\rho_{cr,m}}\right)^{a_m}\right] \quad (6.2)$$

where v_m^f is free-flow speed of lane m, $\rho_{cr,m}$ is the critical traffic density of lane m, and a_m is a statistical parameter. In the test system, we set $\rho_{cr,m} = 57.49$ (veh/mile/lane) and $a_m = 2.34$.

Based on the definition of traffic density $q_m(k)$, traffic flow $q_m(k)$ and traffic speed $v_m(k)$, the traffic flow can be naturally represented as (6.3):

$$q_m(k) = \rho_m(k) \cdot v_m(k) \tag{6.3}$$

To ensure that the traffic simulation is close to the real-world scenarios, we adopted the National Household Travel Survey (NHTS) 2009 [25] database to model the travel pattern of EVs. NHTS 2009 is the most comprehensive travel survey in US available to date. It contains trip attributes such as trip start time, trip end time and travel distance which can be used to generate the travel pattern. However, to simulate the traffic flow, spatial data should be added to the vehicle dataset. The spatial data contains the places where the vehicle starts and stops coupled with the travel route. The procedure for simulating the traffic flow can be elaborated as follows:

- Step 1: Initialize all the vehicles in the simulated traffic system. The initial start places of vehicles are set randomly to be within the simulated area.
- Step 2: Generate the start time, end time and travel distance of each trip according to NHTS.
- Step 3: Set the destination of each trip according to its travel distance and estimate the detailed driving route.
- Step 4: Randomly select some vehicles as EVs from the simulated vehicles based on the EVs penetration level.
- Step 5: Analyze the traffic flow of each lane in the transportation system using (6.1)-(6.3).

The detailed procedure for the traffic simulation of EVs is shown in Fig. 6.2. The EVs evaluate their current statuses at the beginning of each trip and make recharging decisions. If an EV finishes the charging process, it will continue the remaining trips of the day.

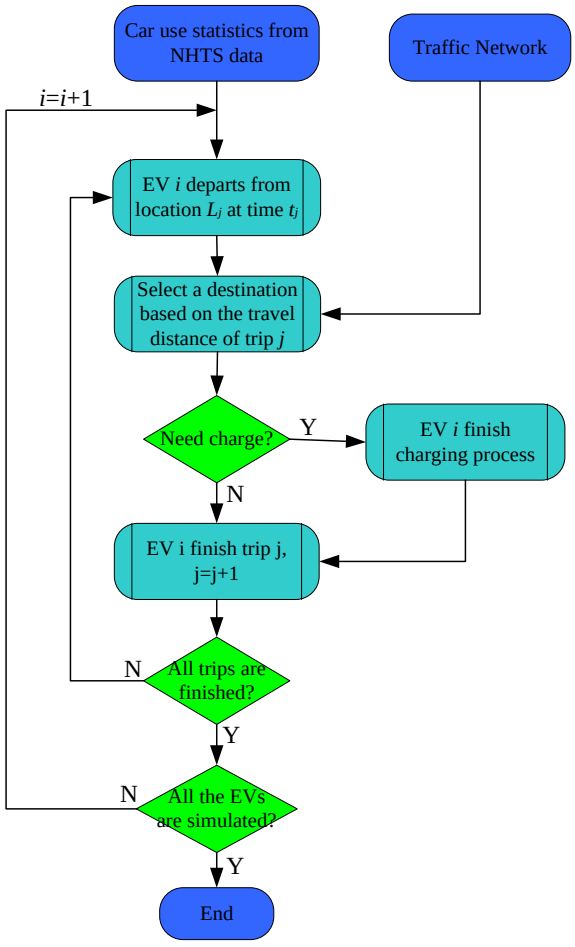

Figure 6. 2 Traffic simulation with real-time EV driving pattern.

6.2.3 Electric Vehicle Strategy

Multiple factors may affect the decisions of EVs, such as the state of charge (SOC), charging price, the distance to the charging station and the waiting time. When an EV receives the information from EVNS, it will make the decision on whether charge is needed or not. The charging probability is defined as follows:

$$p_j(k) = \begin{cases} 1, & \text{if } SOC_{j,k} < 20\% \\ \exp\left[\frac{SOC_{j,k}-20\%}{SOC_{j,k}-100\%} \cdot \frac{a_p \cdot \sum_{i=1}^{I} r_{i,k}}{I \cdot r_{max}}\right], & \text{if } 20\% \le SOC_{j,k} < 100\% \end{cases} \quad (6.4)$$

where $SOC_{j,k}$ is the SOC of EV j at time slot k, $r_{i,k}$ is the charging price of charging station i, r_{max} is the maximal limit of the charging price, I is the total number of charging stations, and a_p is vehicle charging probability parameters. We set $a_p = 0.8$ in this study.

When the SOC of an EV is less than 20%, the charging probability will be 1 to avoid the depletion of battery during travel. Otherwise, the charging probability will be affected by the current SOC and the charging prices of EVCSs. As shown in (6.4), the charging probability of an EV will increase with the decrease of SOC and the decrease of average charging price. When SOC of an EV is close to 100%, the charging probability will be approximately 0%.

EVCSs can buy electricity at a relatively lower rate compared to the rate of home charging [80]. However, as the EVCS needs to make profit, the charging price may be higher for the EV owner compared to charging at home. Thus the EVs may not be fully charged through rapid charging at EVCSs, and we propose a model to optimally determine the energy needs to be purchased for an EV based on its current SOC and the charging price. We use quadratic utility function [85]-[87] to quantify the utility that an EV receives when charging at an EVCS as it is widely used in the literature. Without loss of generality, we design the quadratic utility function as:

$$u_{j,k}(E_{j,k}) = v_j \cdot E_{j,k} - \frac{\theta_j}{2} {E_{j,k}}^2, E_{j,k\,min} \le E_{j,k} \le E_{j,k\,max} \quad (6.5)$$

where v_j and θ_j are constant parameters for each EV, $E_{j,k\,min}$ and $E_{j,k\,max}$ denote the minimal and maximal charging energy for the EV.

Clearly, the minimal and maximal charging energy of an EV is related with its current SOC and they are defined as follows:

$$E_{j,k\,min} = Max\{SOC_{j,min} \cdot Cap_j + E_{res,j} - SOC_{j,k} \cdot Cap_j, 0\} \tag{6.6}$$

$$E_{j,k\,max} = (1 - SOC_{j,k}) \cdot Cap_j \tag{6.7}$$

where $SOC_{j,min}$ is the minimal limit of the SOC of EV j, Cap_j is the battery capacity of EV j, $E_{res,j}$ is the estimated energy needed for the rest trips of EV j during the day, and $SOC_{j,k}$ is the current SOC of EV j.

As EVs need to pay for the energy purchased at the EVCSs, the welfare function of an EV when charging at an EVCS can be described as:

$$w_{j,k}(E_{j,k}) = u_{j,k}(E_{j,k}) - r_{i,k}^{j} \cdot E_{j,k} \tag{6.8}$$

where $r_{i,k}^{j}$ is the charging price.

Thus, the optimal energy purchased of an EV j charging at EVCS i can be obtained as follows:

$$E_{j,k}^{*} = \text{argmax}_{E_{j,k}} w_{j,k}(E_{j,k}) = \begin{cases} E_{j,k\,min}, & \text{if } \frac{v_j - r_{i,k}^{j}}{\theta_j} < E_{j,k\,min} \\ \frac{v_j - r_{i,k}^{j}}{\theta_j}, & \text{if } E_{j,k\,min} \le \frac{v_j - r_{i,k}^{j}}{\theta_j} \le E_{j,k\,max} \\ E_{j,k\,max}, & \text{if } E_{j,k\,max} < \frac{v_j - r_{i,k}^{j}}{\theta_j} \end{cases} \tag{6.9}$$

Once an EV responds to the charging navigation signal, it has to choose a charging station and the charging station will hold the current charging price for the EV. An EV selects an EVCS based on its economic and time costs. The economic cost comprises the charging cost and the fuel cost. The time cost consists of the travel time and the waiting time. The travel time is the time used by the EV for traveling to the charging station which is certainly affected by the traffic flow. Thus, the cost of EV j selecting EVCS i can be expressed as follows:

$$cost_{i,j} = \lambda t_{i,j}^{total} + (E_{j,k}^{*} + d_{i,j} \cdot E_{travel}) r_{i,k}^{j} \tag{6.10}$$

$$t_{i,j}^{total} = t_{i,j}^{travel} + E[W_Q] \tag{6.11}$$

where $t_{i,j}^{travel}$ is the travel time of EV j to charging station i, $E[W_Q]$ is the estimated waiting time of EV j at charging station i, $r_{i,j}$ is the charging price, $d_{i,j}$ is the travel distance from the EV to the charging station, E_{travel} is the energy consumption per miles for EV, and λ is the weighting factor of the time cost.

6.2.4 Charging Station Strategy

We assume that the charging stations belong to different owners, and their only goal is to maximize their own profits. The EVCSs will compete with each other for attracting EVs to charge at their charging poles. Each EVCS has a limited number of charging poles $s_i, i \in I$. And if the number of EVs at an EVCS is more than the available charging poles, the EVs will wait in the queue. The number of available charging poles is dependent on the current state of the power distribution system. The charging capacity of the EVCSs is limited by the PSOC at the peak load time in order to reduce the risk of the power system as shown in Fig. 6.1. The EVCSs buy power from the power grid at a lower price and sell power to EVs at a higher price in order to make profits.

In order to reduce the peak load of the system, a vTOU rate policy is developed based on the system load demand for encouraging EVCSs to attract EVs to charge at off-peak times. The electricity price is defined as:

$$\rho_k = \alpha \cdot P_{sys}^t \tag{6.12}$$

where α is price parameters, and P_{sys}^t is the load demand of the system at time slot t.

According to (6.12), the electricity price is higher at the peak-load hours. Thus, the EVCSs will offer higher charging prices and there is a lower probability for EVs to charge during these

time periods. As a result, the charge load can be shifted to off-peak hours based on this pricing policy.

EVCSs' strategies are the charging prices at each time slot which are denoted as:

$$\pi_i = [r_{i,0}, r_{i,1}, \dots, r_{i,k}, \dots, r_{i,K}], \ \forall i \in I \tag{6.13}$$

The revenue of an EVCS can be expressed as:

$$U_i = \sum_{k=1}^{K} \left(\sum_{j=1}^{N_{i,k}} E_{j,k}^{i*} \cdot r_{i,k} - P_k^i \cdot \rho_k \right) \tag{6.14}$$

where $N_{i,k}$ is the total number of EVs choosing EVCS i at time slot k, and P_k^i is the total charging load of EVCS i at time slot k.

6.2.5 EVs' Queueing Model

In the proposed integrated EV navigation system, EVs will wait in a queue if all the charging poles are occupied at an EVCS and the EVCS will announce its estimated waiting time to EVs which need to make charging decisions.

In this subsection, we model the queueing process of EVs at a charging station as an M/M/s/c queue [88], [89]. The queueing model is shown in Fig. 6.3. The proposed M/M/s/c queue is a multi-server queue with s identical servers and a maximum queueing length of c. In the queueing model, each charging pole can be viewed as a server and the customers are the EVs. As shown in the figure, the EVs are served based on a first-come-first-serve (FCFS) rule. The waiting time is estimated based on the queueing model and it is broadcasted to EVs through EVNS to help the EVs make charging decisions.

In this chapter, EVs' strategies in choosing EVCSs are affected by the pricing strategies of the charging stations. We will formulate an evolutionary game to evolve the EV's strategies in choosing EVCSs in the next Section and the arrival rate of EVs at a certain EVCS λ_k is derived

accordingly. As service rate of the charging poles is not affected by the strategies of EVCSs, it is assumed to follow an exponential distribution. At each time slot, the queue will evolve to a stable state and the waiting time can be estimated.

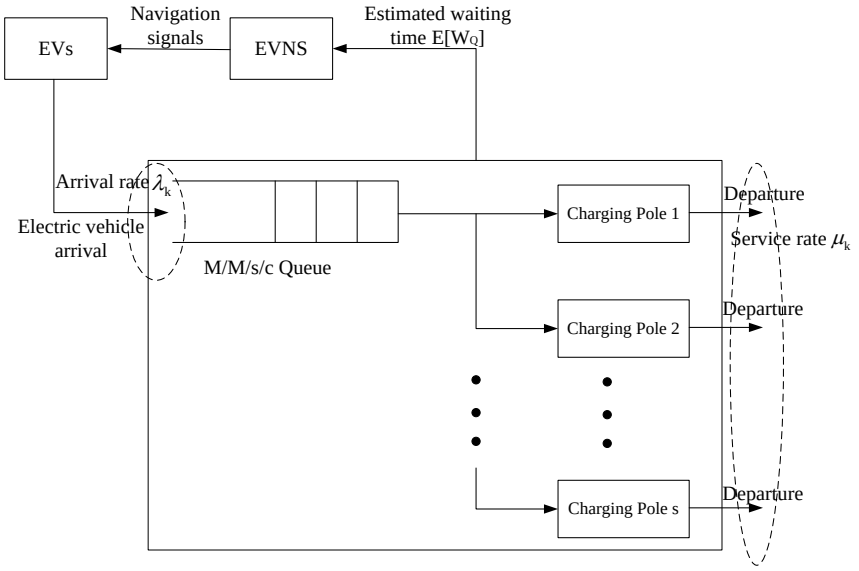

Figure 6. 3 EVs' queueing model at a charging station.

The evolving process of the proposed queueing model is based on a birth-death process and its state transition diagram is shown in Fig. 6.4. As shown in the figure, the states indicate the number of EVs in the queue. If the number of EVs in the charging station n is less than the number of charging poles s, then the departure rate of EVs is $n\mu_k$; if $s < n \leq c$, the departure rate is $s\mu_k$ as there are only s servers in the queueing system.

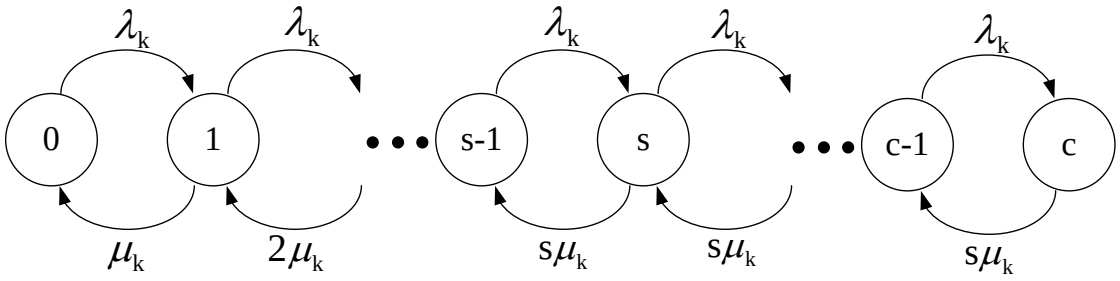

Figure 6. 4 State transition diagram of the queueing model.

The infinitesimal generator matrix of the queueing system $\mathbf{P}_k$ is shown in (6.15).

$$\mathbf{P}_k = \begin{bmatrix} -\lambda_k & \lambda_k & 0 & 0 & 0 & 0 & \cdot & \cdots & \cdot \\ \mu_k & -(\mu_k+\lambda_k) & \lambda_k & 0 & 0 & 0 & \cdot & \cdots & \cdot \\ 0 & 2\mu_k & -(2\mu_k+\lambda_k) & \lambda_k & 0 & 0 & \cdot & \cdots & \cdot \\ 0 & 0 & 3\mu_k & -(3\mu_k+\lambda_k) & \lambda_k & 0 & \cdot & \cdots & \cdot \\ \cdot & \cdots & \cdot & \ddots & \ddots & \ddots & \cdot & \cdots & \cdot \\ \cdot & \cdots & \cdot & \cdots & s\mu_k & -(s\mu_k+\lambda_k) & \lambda_k & \cdots & \cdot \\ \cdot & \cdots & \cdot & \cdots & \cdot & s\mu_k & -(s\mu_k+\lambda_k) & \lambda_k & \cdots \\ \cdot & \cdots & \cdot & \cdots & \cdot & \cdots & \ddots & \cdot & \cdots \\ \cdot & \cdots & \cdot & \cdots & \cdot & \cdots & \ldots & s\mu_k & -s\mu_k \end{bmatrix} \tag{6.15}$$

Let $\overline{\Pi} = [\Pi_1, \Pi_2, \cdots \Pi_s, \cdots]$ denote the stationary distribution vector. Then, the stationary condition of the queueing system can be expressed as:

$$\overline{\Pi} \cdot \mathrm{P_k} = 0 \tag{6.16}$$

Let $\mathrm{A} = \lambda_\mathrm{k}/\mu_\mathrm{k}$. We can obtain the following steady-state equations based on (6.16):

For state 1: $\Pi_1 = \mathrm{A}\Pi_0$.

For state 2: $\Pi_2 = \mathrm{A}\Pi_1/2 = \mathrm{A}^2\Pi_0/2!$

For state 3: $\Pi_3 = \mathrm{A}\Pi_2/3 = \mathrm{A}^3\Pi_0/3!$

For state s: $\Pi_\mathrm{s} = \mathrm{A}\Pi_{\mathrm{s}-1}/\mathrm{s} = \mathrm{A}^\mathrm{s}\Pi_0/\mathrm{s}!$

For state $\mathrm{s}+1$: $\Pi_{\mathrm{s}+1} = \mathrm{A}\Pi_\mathrm{s}/\mathrm{s} = \mathrm{A}^{\mathrm{s}+1}\Pi_0/(\mathrm{s}!\,\mathrm{s})$

For state $\mathrm{s}+2$: $\Pi_{\mathrm{s}+2} = \mathrm{A}\Pi_{\mathrm{s}+1}/\mathrm{s} = \mathrm{A}^{\mathrm{s}+2}\Pi_0/(\mathrm{s}!\,\mathrm{s}^2)$

For state c: $\Pi_\mathrm{c} = \mathrm{A}\Pi_{\mathrm{c}-1}/\mathrm{s} = \mathrm{A}^\mathrm{c}\Pi_0/(\mathrm{s}!\,\mathrm{s}^{\mathrm{c}-\mathrm{s}})$

Then we can conclude the stationary distribution as follows:

$$\Pi_\mathrm{n} = \begin{cases} \frac{\mathrm{A}^\mathrm{n}\Pi_0}{\mathrm{n}!}, & \text{if } 0 \le \mathrm{n} \le \mathrm{s} \\ \frac{\mathrm{A}^\mathrm{s}}{\mathrm{s}!}\left(\frac{\mathrm{A}}{\mathrm{s}}\right)^{\mathrm{n}-\mathrm{s}}\Pi_0, & \text{if } \mathrm{s} < \mathrm{n} \le \mathrm{c} \end{cases} \tag{6.17}$$

Consider the constraint of the stationary distribution in (6.18):

$$\sum_{\mathrm{n}=0}^{\mathrm{c}} \Pi_\mathrm{n} = 1 \tag{6.18}$$

We can obtain:

$$\Pi_0 = \left(\sum_{n=0}^{s-1} \frac{A^n}{n!} + \frac{A^s}{s!}\sum_{n=s}^{c}\left(\frac{A}{s}\right)^{n-s}\right)^{-1} \tag{6.19}$$

The mean queue length is derived as follows [18]:

$$E[N_Q] = \sum_{n=s+1}^{c}(n-s)\,\Pi_n \tag{6.20}$$

The waiting time can be derived by Little's formula [18] as:

$$E[W_Q] = \frac{E[N_Q]}{\lambda_k(1-\Pi_c)} \tag{6.21}$$

6.2.6 EVs' Impact on Distribution System Reliability

EVs can affect the reliability of a distribution system by overloading the transformers and transmission lines at peak load hours. Thus, a real-time transformer outage rate is needed to evaluate the impact of EVs on distribution system reliability. Instead of using a constant outage rate, we formulate the operational reliability of the distribution network by considering the real-time outage rate of the distribution transformer. The hybrid transformer failure probability model can be expressed as follows based on [69]:

$$P_f = 1 - (1 - P_{rand}) \times (1 - P_{af}) \tag{6.22}$$

where P_{rand} is the random failure probability and P_{af} is the transformer aging failure under various load conditions .

The current-dependent overload protection outage rate can be obtained through (6.23)-(6.25) [69]:

$$P_{pt}(I) = \begin{cases} P_{unreq}, & \text{if } I < I_{pe}(1-\varepsilon_I) \\ P_{req}\int_{I_{pe}(1-\varepsilon_I)}^{I} f(I_{pk})dI_{pk} + P_{unreq}\int_{I}^{I_{pe}(1+\varepsilon_I)} f(I_{pk})dI_{pk}, & \text{if } I_{pe}(1-\varepsilon_I) < I < I_{pe}(1+\varepsilon_I) \\ P_{req}, & \text{if } I > I_{pe}(1+\varepsilon_I) \end{cases} \tag{6.23}$$

$$f(I_{pk}) = \begin{cases} 0, & \text{if } I_{pk} < I_{pe}(1-\varepsilon_I) \text{ or } I_{pk} > I_{pe}(1+\varepsilon_I) \\ \dfrac{e^{\left(-(I_{pk}-I_{pe})^2/2\sigma^2\right)}}{\alpha_I \sigma\sqrt{2\pi}}, & \text{if } I_{pe}(1-\varepsilon_I) < I_{pk} < I_{pe}(1+\varepsilon_I) \end{cases} \quad (6.24)$$

$$\alpha_I = \phi\left(\frac{\varepsilon_I I_{pe}}{\sigma}\right) - \phi\left(\frac{-\varepsilon_I I_{pe}}{\sigma}\right) \quad (6.25)$$

where ϕ is the cumulative distribution function of the standard normal distribution, P_{unreq} is the outage rate when the overload protection is not required, P_{req} is the outage rate when the overload protection is required, I_{pk} is pick-up current for the protection relay, I_{pe} is the expected value of I_{pk}, σ is standard variance of I_{pk}, ε_I is the percentage error of current mismatch.

Thus, the real-time transformer outage rate can be built by considering both the failure rate and overload protection rate as follows:

$$P_{trans}^{t} = 1 - (1 - P_f(t)) \times (1 - P_{pt}(I_t)) \quad (6.26)$$

6.3 Hierarchical Game Formulation

The proposed hierarchical game framework consists of two levels of games. At the upper level, a non-cooperative game is formulated to coordinate the pricing strategies of EVCSs to maximize their personal profits. Based on the pricing strategies of EVCSs, multiple evolutionary games are formulated at the lower level for different groups of EVs to evolve their strategies in choosing EVCSs. During each step of the non-cooperative game, an evolutionary equilibrium will be reached for each evolutionary game at the lower level and the EVs' strategies in choosing EVCSs are optimized. Once the Nash equilibrium is reached for the non-cooperative game, the games at the two levels will both reach their equilibriums. Then the strategies for both EVs and EVCSs are optimized and the solution to the formulated problem is found.

6.3.1 Evolutionary Games of EVs

Currently, EVs are considered as price takers by researchers in the charging navigation problem as the charging decision of one EV does not have enough power to affect pricing strategies of the charging stations [80]-[82]. However, with the development of the connected vehicle technology, EVs may be able to cooperate with each other and bid charging prices as a group. Thus, EVs can work together as a group to negotiate charging prices with charging stations. In the proposed integrated charging navigation framework, EVs can cooperate with their neighboring EVs to bargain charging prices with EVCSs as a group. We assign the EVs at the same lane into one group as they have similar travel distance to different EVCSs. The strategy evolving of each EV group is guided by an evolutionary game.

Two important concepts in evolutionary games are replicator dynamics and population [57]. In the context of evolutionary games, the population refers to a set of players with the same strategy and the population share is the percentage of the population with a certain strategy. The replicator dynamics controls the reproduction speed of the population according to the payoff of the population's strategy. In the proposed evolutionary game, each EV has to choose a charging station to recharge its battery and it can gradually evolve its strategy based on the current pricing strategies of EVCSs. Thus, the population share is defined as the probability distribution of an EV choosing different EVCSs. Based on evolution strategy, we propose a replicator dynamics to guide the evolution of the population share.

Based on the traffic simulation model, we can obtain the number EVs at time slot k in lane m which is denoted as $N_{m,k}^{T}$. Then the number of players in the m_{th} evolutionary game is:

$$N_{m,k} = N_{m,k}^{T} \cdot p_j(k) \tag{6.27}$$

where $p_j(k)$ is the charging probability of EVs at time slot k.

Let $y_{m,k}^{i}$ denote the probability of an EV choosing to charge at EVCS i at time slot k, where $0 \le y_{m,k}^{i} \le 1$ and $\sum_{i=1}^{I} y_{m,k}^{i} = 1$. Thus, we can denote the population share as $Y_k = [y_{m,k}^{1}, y_{m,k}^{2}, \dots, y_{m,k}^{i}, \dots, y_{m,k}^{I}]$. Then we can define the accumulated EVs' utility choosing EVCS i as:

$$U_{i,m}^{EV} = -\sum_{j=1}^{N_{m,k}} [\lambda t_{i,j}^{total} + (E_{j,k}^{*} + d_{i,j} \cdot E_{travel}) r_{i,k}^{j}] \tag{6.28}$$

where $t_{i,j}^{total} = t_{i,j}^{travel} + E[W_{Q,i}]$.

The average utility of choosing different EVCSs is denoted as:

$$\bar{U}_{m}^{EV} = \sum_{i=1}^{I} y_{m,k}^{i} U_{i,m}^{EV} \tag{6.29}$$

Accordingly, the replicator dynamics can be defined as:

$$\frac{\partial y_{m,k}^{i}}{\partial t} = \delta y_{m,k}^{i} (U_{i,m}^{EV} - \bar{U}_{m}^{EV}), \forall i \in I \tag{6.30}$$

where δ is the learning rate of the replicator dynamics.

Note that the probability of an EV choosing EVCS i will increase when the utility for choosing EVCS i is larger than the average utility, and vice versa. Thus, the proposed replicator dynamics can maximize the utility of the EVs.

The evolutionary equilibrium is the solution of evolutionary game which is a stable condition that the strategy state stops evolving. For the formulated problem, the evolutionary equilibrium is reached when:

$$\frac{\partial y_{m,k}^{i}}{\partial t} = \dot{y}_{m,k}^{i} = 0, \forall i \in I \tag{6.31}$$

$$\Pi_{i}^{EV} = \bar{\Pi}^{EV}, \quad \forall i \in I \tag{6.32}$$

The evolutionary equilibrium is denoted by $Y_{m,k}^{*} = [y_{m,k}^{1*}, y_{m,k}^{2*}, \dots, y_{m,k}^{i*}, \dots, y_{m,k}^{I*}]$.

When the evolutionary equilibriums of all the evolutionary games are reached, the optimal strategies of all the EVs are obtained and arrival rate of EVs can be calculated.

The arrival rate of EVs at EVCS i can be expressed as:

$$\lambda_{i,k} = \sum_{m=1}^{M} N_{m,k} \cdot y_{m,k}^{i*} \tag{6.33}$$

6.3.2 Non-Cooperative Game of EVCSs

1) Non-cooperative Game Formulation

In this subsection, we formulate a price adjustment game for multiple EVCSs. To coordinate the set of $I(I = [1,2,\cdots,I])$ EVCSs, a non-cooperative EVCS interaction game $\mathbb{G}$ is defined as follows:

- Players: The set of all I EVCSs.
- Strategies: For each EVCS, choose a charging price strategy $\pi_i, \forall \pi_i \in F_i$.
- Payoffs: The i_{th} EVCS receives payment $U_i(\pi_i, \pi_{-i})$ as shown in (6.14).

The most common solution for a non-cooperative game is the Nash equilibrium which is defined as follows:

Definition 6.1: For the proposed non-cooperative game $\mathbb{G} = \{I, \{\pi_i\}_{i\in I}, \{U_i\}_{i\in I}\}$, a strategy tuple $\Psi = \{\pi_i^*\}_{i\in I}$ constitutes a Nash equilibrium when no player can improve its utility by unilaterally deviating from its current strategy. It is formulated as a set of inequalities:

$$U_i(\pi_i^*, \pi_{-i}^*) \geq U_i(\pi_i, \pi_{-i}^*), \ \forall \pi_i \in F_i, \forall i \in I \tag{6.34}$$

The existence of a unique Nash equilibrium is uncertain in a general non-cooperative game [34]. We hereby included a small positive variable ε_1 to get an approximate Nash equilibrium as described in (6.35) [90]. As the approximate Nash equilibrium results in a similar performance and it can reduce the computational time of the best response strategy [90], it can be used as the solution of the proposed non-cooperative game.

$$U_i(\pi_i^*, \pi_{-i}^*) \geq U_i(\pi_i, \pi_{-i}^*) - \varepsilon_1, \ \forall \pi_i \in F_i, \forall i \in I \tag{6.35}$$

2) The Proposed Algorithm

To find the Nash equilibrium for the proposed game $\mathbb{G}$, we applied a dynamic best response strategy which is defined as follows:

Definition 6.2: For each player $i \in \mathcal{M}$, while other players have a fixed strategy tuple π_{-i}, the best response strategy π_i' for the i_{th} player is:

$$\pi_i' = \text{argmax}_{\pi_i \in F_i}\{U_i(\pi_i, \pi_{-i})\} \tag{6.36}$$

Thus, the players will continue to update their strategies based on the strategies of other players in a sequential and iterative fashion. This dynamic response process continues until the approximated Nash equilibrium is reached.

As the payoff function of the proposed game is nonlinear, analytical methods such as dynamic programing is not applicable. The strategies described in (6.13) constitute a very large search space, so enumeration method is also not applicable. Thus, computational intelligence methods have been used by researchers to search the Nash equilibrium [91]. To solve the formulated game, we applied two artificial intelligence based algorithms, namely particle swarm optimization (PSO) [32] and evolution strategy (ES), to find the best response strategy for each player. The performances of these two algorithms are studied and compared in the simulation studies.

The reason of using PSO is because it is very suitable for this problem. In this problem, the control variable is the charging prices of the EVCSs. The charging price vector of an EVCS can be mapped into a search space and the charging prices at each time slot can be naturally viewed as different dimensions in the search space. The value of the charging price can be encoded as the coordinates in the specified dimension. Another suitable algorithm for this problem is ES, as the data structure of ES corresponds to real-valued vectors.

The proposed best response algorithm is summarized in Algorithm 6.1 as follows:

Algorithm 6.1 The best response algorithm for the non-cooperative game

---

1: Input randomly initialize strategies for all players.

2: repeat

3: for i=1,…, I do

4: The player i finds its current best response strategy π_i' based on PSO algorithm. Then the player provides other players with its current best response strategy π_i'.

5: end for

6: until the approximate Nash equilibrium (6.35) is reached.

7: Output control strategies and stop.

In Algorithm 6.1, each player is required to provide its current best response strategy to other players. Thus, it is possible that the player may cheat other players by injecting untruthful information if cheating can increase its utility. However, we will show that all the players will provide truthful information about their best response strategies in theorem 6.1.

Theorem 6.1: In the algorithm 6.1, no player can benefit by misreporting its best response strategy. That is, the players are self-enforced to provide their truthful strategy information.

Proof: see the Appendix.

6.4 Case Studies

6.4.1 Simulation Environment

Simulation studies are performed based on the transportation network of Milwaukee, Wisconsin. Fig. 6.5 shows the transportation network and its topological graph. Four EVCSs are located at traffic nodes 20, 23, 25 and 28. The free-flow traffic speed is 30 miles/h. The traffic flow simulation considers 50,000 vehicles and 5% of them are EVs. The topology of the studied distribution system is based on the IEEE 34-node test feeder [37] as shown in Fig. 6.6. Four EVCSs are connected to four load points which are labeled from EVCS1 to EVCS4 in the figure. Assume a transformer is located at node 1 and 2,500 houses are randomly located at other nodes. The load profile of a single household is shown in Fig. 6.7 and the base load in the distribution system consists of the load of 2500 households. Assume the interruption rates for the main feeder and lateral feeder are 0.1 interruptions /year and 0.2 interruptions /year respectively; the average times to repair for the main feeder and lateral feeder are 2.5 hours and 1 hour respectively. The procedure for reliability analysis is based on Monte Carlo simulation and can be found in our previous work [77]. The shortest route navigation approach is used as a benchmarking control strategy. In this strategy, EVs are guided to the nearest EVCS for recharging their batteries when their SOCs are below 40%.

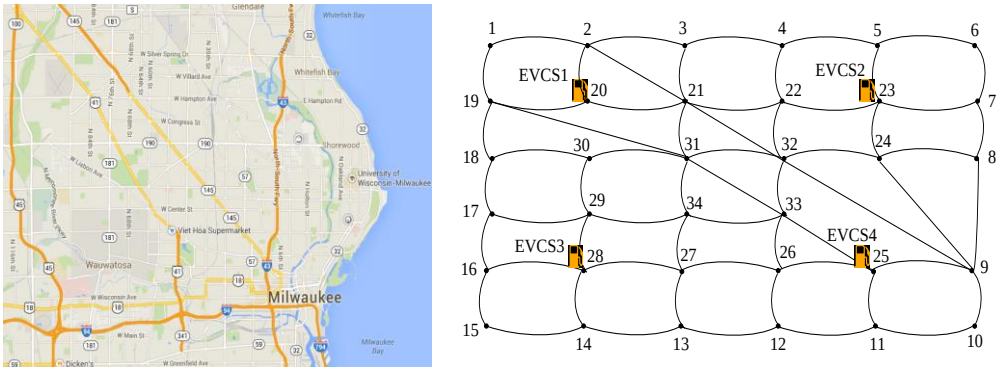

Transportation Network

Topological Graph

Figure 6. 5 Topology of the transportation network under test.

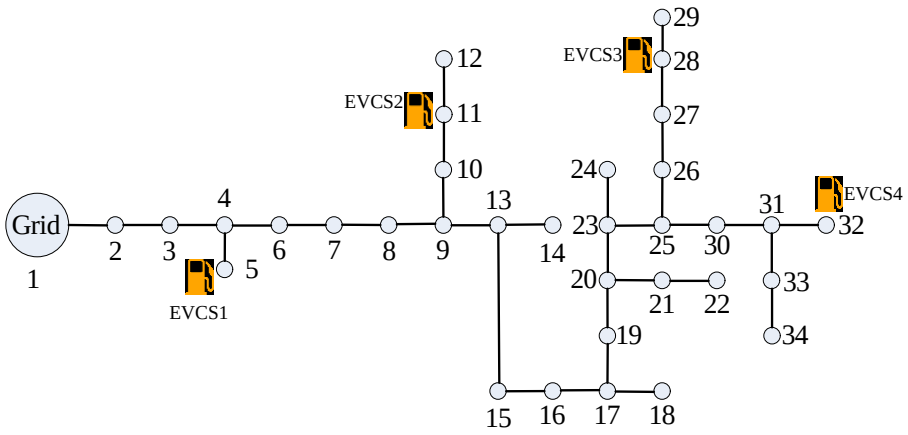

Figure 6. 6 The topology of the studied residential distribution grid.

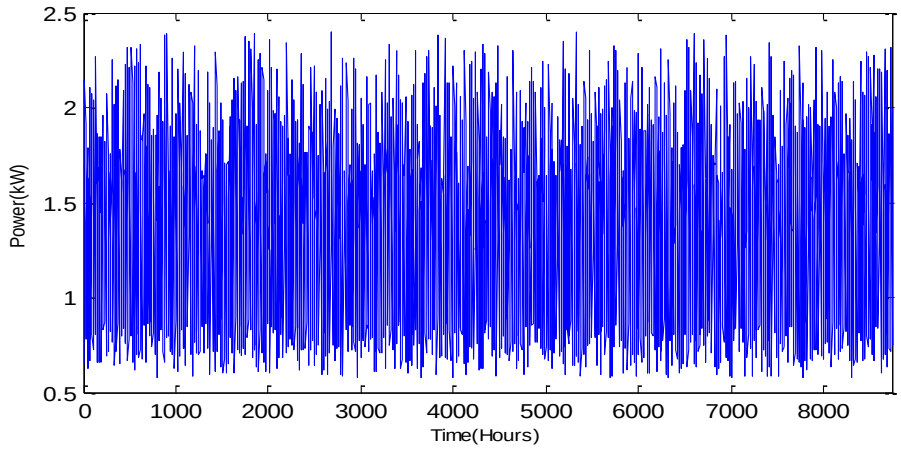

Figure 6. 7 Annual load profile for a single household

6.4.2 Simulation Results

Fig. 6.8 shows the simulation results of the average traffic speed of the transportation system during a day. The traffic conditions vary during the day time. The traffic is most congested during 8:00-10:00 and 17:00-19:00 when most people commute to/from the working places. Fig. 6.9 shows the convergence curves of the PSO algorithm and evolution strategy during an iteration of the best response algorithm. The response algorithms search the best response strategy for the player after other players choose their strategies. It ensures the effectiveness of the proposed best response algorithm in finding the Nash equilibrium. As shown

in Fig. 6.9, PSO algorithm converges faster and results in higher revenues compared with the evolution strategy.

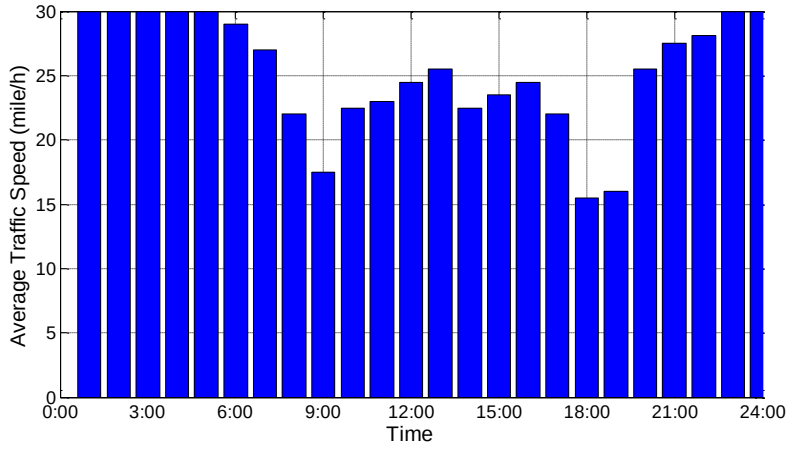

Figure 6. 8 Average traffic speed of the test system.

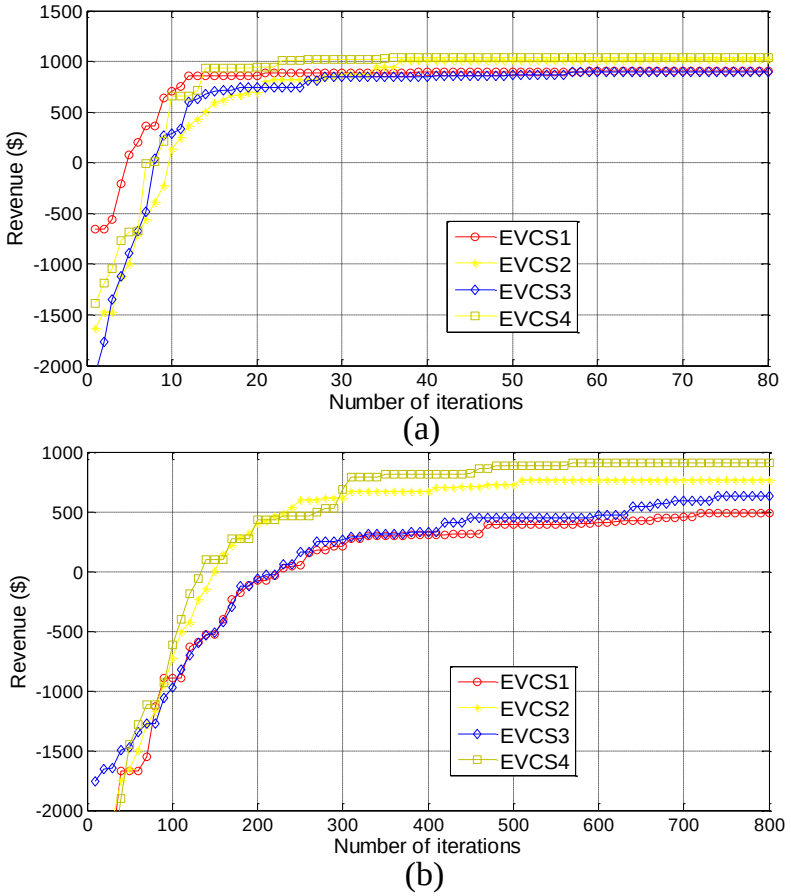

Figure 6. 9 Convergence curves of different response algorithms in a best response iteration. (a) PSO algorithm, (b) Evolution strategy.

The response time of PSO algorithm is also shorter than evolution strategy as shown in Fig. 6.10. Thus, the PSO algorithm is used for searching the best response strategies in the proposed non-cooperative game. The convergence behavior of the proposed non-cooperative game approach is shown in Fig. 6.11. As shown in the figure, the payoffs of all the players converge to a stable state after several iterations. Thus, the approximate Nash equilibrium has been reached, and the EVCSs will not deviate from their current price strategies. Their revenues reach a stable state after competing with each other

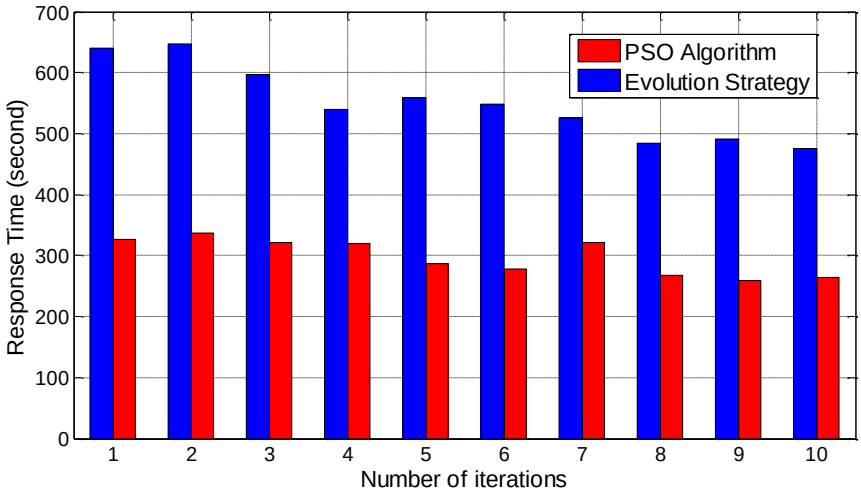

Figure 6. 10 Response time of different response algorithms during the iterations of the non-cooperative game.

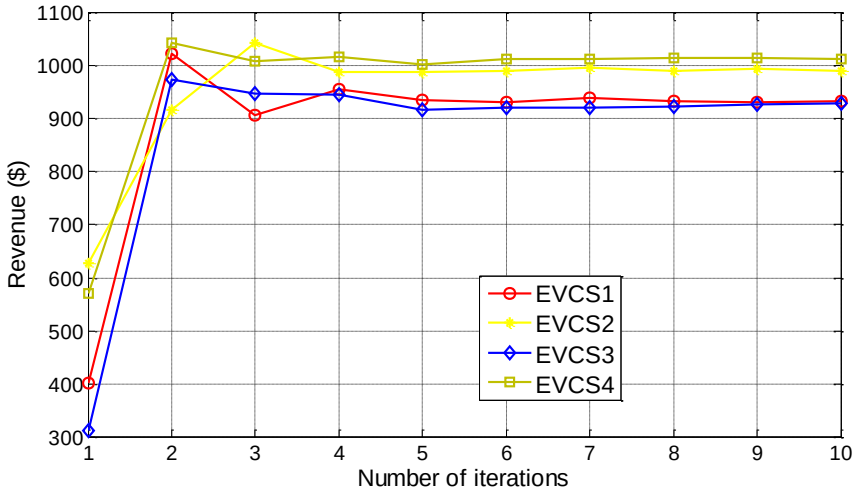

Figure 6. 11 Convergence of the non-cooperative game.

Fig. 6.12 shows the load demand of the system. The charging load incurred by EVCSs increases the peak load of the system. Compared with the shortest route navigation approach, the proposed integrated navigation approach reduced the burden of the peak load by attracting more EVs to charge at off-peak hours when the electricity price is lower. Fig. 6.13 gives the average time consumed by EVs to recharge their batteries. The time consumed by EVs comprises the travel time to EVCSs and the waiting time at the EVCSs. As shown in the figure, the proposed integrated navigation approach results in less average time consumed. As the proposed approach provides the EVs with the information on the traffic conditions and the estimated waiting time at different EVCSs, the EVs will not only save travel time by avoiding congested routes but also reduce waiting time by selecting a less crowded EVCS. The reliability indices of the residential distribution system under different navigation approaches are shown in Table 6.1. The reliability metrics used in Table 6.1 are system average interruption frequency index (SAIFI), system average interruption duration index (SAIDI), customer average interruption duration index (CAIDI), and average service availability index (ASAI) [92]. SAIFI is the average instances of interruption per customer experienced per year due to the failure of the system components. SAIDI is the average outage duration per customer suffered per year. The unit of SAIDI is hour/system customer/year. CAIDI is the average outage duration of those customer interruptions, and its unit is hour/customer interruption. ASAI is the ratio of customer hours of available service and the customer hours demanded per year and the unit is 100%. Base on the results in Table 6.1, it can be concluded that the proposed approach has a positive impact on the reliability indices. The values of SAIFI, SAIDI and CAIDI are considerably decreased compared with the shortest route approach.

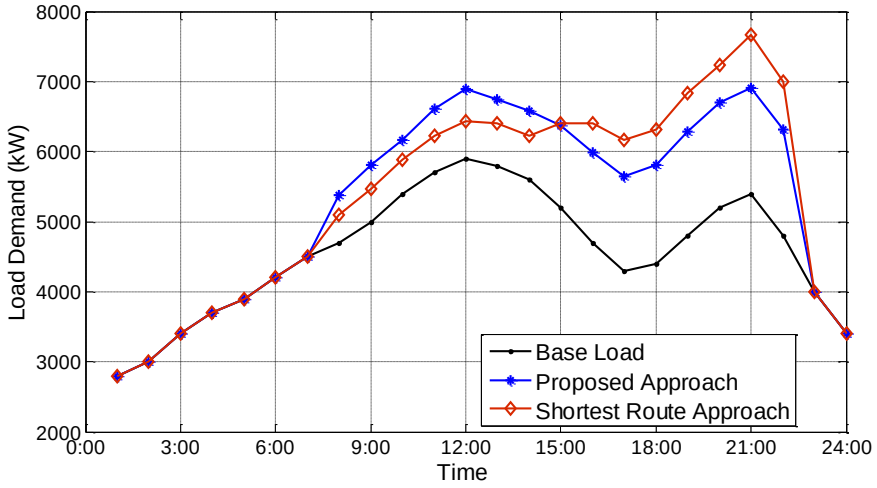

Figure 6. 12 Load demand curves of the system with different EV navigation strategies.

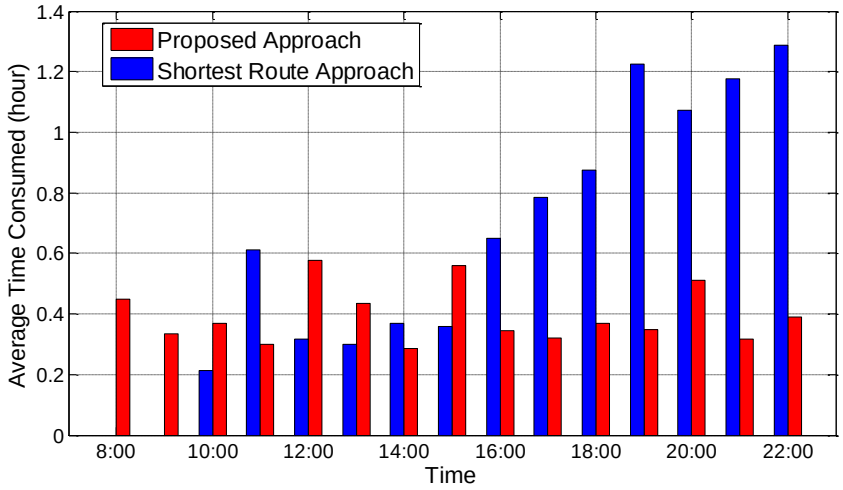

Figure 6. 13 The average time consumed by EVs with different navigation strategies at different time windows.

Table 6. 1 Reliability Indices for the Distribution System Under Different Navigation Approaches

	SAIFI	SAIDI	CAIDI	ASAI
Shortest Route Approach	51.23	808.64	15.78	0.9077
Proposed Approach	1.079	5.364	4.971	0.9994

7. Adequacy Assessment of Power Distribution Network with Large Fleets of PHEVs Considering Condition-Dependent Transformer Faults

7.1 Introduction

Plug-in hybrid electric vehicles (PHEVs) are expected to have a bright future, which are seen as a potential solution to alleviating environmental problems and energy crisis. Compared with traditional cars, PHEV has an extra electrical motor, a battery storage system, and a charging and V2G system [93]. Its battery capacity can reach up to 10 KWh or more, and it has a driving range of at least 30 miles at all electric mode [94]. The design of different driving modes makes PHEV more flexible as compared with common electric vehicles (EVs) since it is able to satisfy customer requirements with longer driving range. Therefore, PHEV is facing a great opportunity to become more popular in the near future. The proliferation of PHEVs in our society will shift the burden on environment and crude oil demand to the power grid. On the one hand, the environmental problem such as global warming and air pollution can be alleviated and crude oil demand can be reduced; on the other hand, the charging activity of PHEVs will increase the peak load demand and cause power quality problems.

In recent years, PHEV penetration level is rapidly increasing worldwide. According to the Electric Power Research Institute (EPRI) the penetration level of PHEV may increase to about 60% in U.S. by the year of 2050 [95]. In the future, high penetration level of PHEVs will pose a great challenge to the distribution grid due to their intermittent charging load. The charging load of large fleets of PHEVs may seriously increase the peak load, overloading the transformers and

transmission lines if it is not properly controlled. The high penetration of PHEVs will thus definitely affect the power system reliability and increase the system risk. On the other hand, with the development of vehicle-to-grid (V2G) technology, the PHEVs are able to serve as distributed energy storage resources. Through V2G, PHEVs can provide power to its owner's household and its neighboring households during system outages.

To date, various studies have been conducted on the optimal management of PHEVs to maximize its economic profits. For instance, smart charging algorithms have been studied in [17] to reduce the charging cost and improve the power quality. Reference [42] studied the ancillary services provided by PHEVs through the vehicle-to-grid (V2G) technology. Chang, et al. applied Markov Decision Processes (MDPs) to model the uncertainty of customers' behaviors in demand side management (DSM) [96]. Reference [66] applied the game theory to integrate PHEVs as demand side resources for DSM in the building energy control. Also there is a number of literature studying the impact of distributed generation (DG) on the reliability of distribution networks [97]-[100]. However, very limited work has been done to quantify the impact of massive PHEVs on the distribution grid reliability in a smart grid environment from the perspective of power system adequacy.

This chapter proposes a comprehensive framework for adequacy evaluation of power distribution network with large-scale PHEV penetrations. A condition-dependent outage model is used in this study to obtain the time sequential failure rate of the transformer. Also, a business model for the PHEVs is developed to incentivize the PHEV owners to charge their PHEVs in a way that could enhance the distribution system adequacy. Based on this model, a smart charging algorithm is proposed for the PHEVs to minimize their charging cost and enhance the adequacy of the distribution network at the same time.

7.2 System Model

7.2.1 Mathematical modeling of PHEVs

The PHEV driving pattern and load demand used in this chapter are obtained from Chapter 2. In this chapter, we use vectors $T = [1,\cdots,t,\cdots,T]$ and $M = [1,\cdots,d,\cdots,M]$ to indicate the charging time horizon and the numbering of PHEVs. PHEVs serve as electricity consumers, providers and holders. It is assumed that PHEV owners will provide the expected departure time and the desired SOC to the aggregator when plugged in. Then we can generate the plug-in time $t_{in,d}$, plug-out time $t_{out,d}$ and the required energy $E_{req,d}$ of each PHEV in the system. The PHEVs can be controlled at two states: charging and idle.

We use a vector k to express the charging strategy of a PHEV as follows:

$$k_d = \left[k_d^{t_{in,d}},\cdots,k_d^t,\cdots,k_d^{t_{out,d}}\right], \forall\, d\epsilon\mathbf{M} \tag{7.1}$$

The required charging energy constraint is:

$$E_{req,d} = \sum_{t=t_{in,d}}^{t_{out,d}} k_d^t \cdot P_{rate}^d \cdot \Delta t, \forall\, d\epsilon\mathbf{M} \tag{7.2}$$

where P_{rate}^d is the rated charging power of the d_{th} PHEV and Δt is time duration of each time slot.

The SOC of a PHEV at a certain time slot t_x can be expressed as:

$$SOC_d^{t_x} = SOC_d^{t_{in,d}} + \sum_{t=t_{in,d}}^{t_x} \frac{k_d^t \cdot P_{rate}^d \cdot \Delta t}{Cap_d},\ \forall d\epsilon M, t_{in,d} \le t_x \le t_{out,d} \tag{7.3}$$

where $SOC_d^{t_{in,d}}$ is the SOC of the d_{th} PHEV at its plug-in time slot $t_{in,d}$ and Cap_d is capacity of the d_{th} PHEV.

To protect the battery from early degradation, the battery SOC should be bounded as follows:

$$SOC_{min} < SOC_d^t < SOC_{max}, \forall\, d\epsilon M \tag{7.4}$$

where SOC_{min} is the minimal limit of SOC and SOC_{max} is SOC_{max} is the maximal limit of SOC.

The total charging power is calculated as:

$$P_{EV}^{t} = \sum_{d=1}^{N} k_{d}^{t} \cdot P_{rate}^{d}, \forall\, t \epsilon T \tag{7.5}$$

Thus, the average charging power of the system can be expressed as:

$$P_{avg} = \frac{1}{T}\sum_{t=1}^{T}(P_{Base}^{t} + P_{EV}^{t}) \tag{7.6}$$

where P_{Base}^{t} is the base load demand of the studied system.

In this study, the power grid motivates the PHEVs owners to participate in the proposed reliability support program by offering economic benefits. Also, this kind of program between PHEV owners and the power grid will give power grid the right to operate them as distributed generators during system interruptions. PHEV owners will receive economic compensation for providing energy capacity to improve the reliability of the system. They will also be paid by feeding the power back to the grid during the system interruptions. To ensure that the PHEVs can be charged to their desired SOCs after an interruption, only those PHEVs with extra plug-in time and high SOCs are allowed to export energy to the grid during the interruption.

If an interruption occurs at time slot t_x and the repair time is t_r, the energy needed to charge the PHEV to the desired SOC can be expressed as:

$$E_{req,d}^{t_x} = (SOC_{d}^{des} - SOC_{d}^{t_x})Cap_{d} \tag{7.7}$$

where SOC_{d}^{des} is the desired state of charge of d_{th} PHEV.

The available energy can be charged by the PHEV after the interruption is expressed as:

$$E_{avail,d}^{t_x,t_r} = (t_{out,d} - t_x - t_r)P_{rate}^{d} \tag{7.8}$$

The PHEV is allowed to supply power to the grid during the interruption only when $E_{avail,d}^{t_x,t_r} > E_{req,d}^{t_x}$. The energy can be exported to the grid during the interruption is constrained by:

$$E_{V2G,d}^{t_x,t_r} \leq \max\{E_{avail,d}^{t_x,t_r} - E_{req,d}^{t_x},\ 0\} \tag{7.9}$$

Another constraint for the V2G energy is the minimal SOC limit. That is the minimal SOC of the PHEV during the interruption, which can be expressed as:

$$E_{V2G,d}^{t_x,t_r} \leq (SOC_d^{t_x} - SOC_{min})Cap_d \tag{7.10}$$

Thus, the energy that can be exported to the grid during the interruption is calculated as:

$$E_{V2G,d}^{t_x,t_r} = \min\{\max(E_{avail,d}^{t_x,t_r} - E_{req,d}^{t_x},\ 0), (SOC_d^{t_x} - SOC_{min})Cap_d\} \tag{7.11}$$

To ensure the load recovery ability of the PHEVs, the PHEVs are encouraged to maintain a high level of SOCs at the early stage of their plug-in time duration. Thus, they are paid to maintain this kind of potential load recovery ability. As we do not know the repair time before an interruption occurs, we ignore the impact of the repair time when considering the potential load recovery ability of PHEVs. At a specific time slot t_x, the energy that can be charged by the PHEV during the remaining plug-in time is:

$$E_{rem,d}^{t_x} = (t_{out,d} - t_x)P_{rate}^{d} \tag{7.12}$$

So the potential energy that can be used for load recovery is calculated as:

$$E_{Pot,d}^{t_x} = \min\{E_{rem,d}^{t_x} - E_{req,d}^{t_x}, (SOC_d^{t_x} - SOC_{min})Cap_d\} \tag{7.13}$$

where $E_{rem,d}^{t_x} \geq E_{req,d}^{t_x}, \forall d \in M$.

Thus, the PHEVs are paid by their potential load recovery ability at each plug-in time slot as follows:

$$Earn_d^{rel} = \mu \cdot \sum_{t_{in,d}}^{t_{out,d}} E_{Pot,d}^{t_x} \tag{7.14}$$

where μ is the pricing factor for PHEVs providing reliability support.

The objective function is to minimize the total cost of the PHEV owners. The total cost consists of two parts including the charging cost, and the profit earned by providing reliability support.

The charging cost is described as:

$$\mathrm{Cos}_{\mathrm{chg}} = \sum_{t=1}^{T} P_{EV}^{t} \cdot \rho_t \tag{7.15}$$

The profit earned by providing reliability support is:

$$\mathrm{Earn}_{\mathrm{rel}} = \mu \cdot \sum_{d=1}^{M} \mathrm{Earn}_{d}^{\mathrm{rel}} = \mu \sum_{d=1}^{M} \sum_{t_{in,d}}^{t_{out,d}} E_{Pot,d}^{t_{x,d}} \tag{7.16}$$

The total cost is:

$$\mathrm{Cost} = \mathrm{Cos}_{\mathrm{chg}} - \mathrm{Earn}_{\mathrm{rel}} \tag{7.17}$$

So the objective function can be expressed as:

$$\min\{\mathrm{Cost}, \mathrm{s.t.}\,(7.2) - (7.4)\} \tag{7.18}$$

7.2.2 Smart charging algorithm

As the formulated problem has a nonlinear objective function and the strategy space is very large, analytical methods and enumerative method are both not applicable. Thus, particle swarm optimization (PSO) [32] is adopted as it is suitable for solving nonlinear problems and is rather effective when dealing with a large search space.

PSO originates from the collective behaviors exhibited in bird flocking and fish schooling. In PSO, the possible solution of a target problem is mapped into to search space and the locations of the particle in the search are the potential solutions to the problem. Solving the problem is equivalent to finding the optimal location in the search space. In this specific problem, we need to find the optimal charging strategies of PHEVs. The charging strategy vector of each PHEV

can be defined as a dimension of the search space, and the charging strategy vector can be encoded as the coordinates in the specific dimension. The particles continuously update their locations and velocities in the search space according to (7.19)-(7.21). The fitness of each potential solution is evaluated by the objective function (7.18). If an optimum value is achieved by a specific particle, the position of the particle will be stored as a personal best position pBest. And if an optimum value is achieved among all the particles, the position of this particle will be saved as a global best position gBest. When the iteration is over, the best value position gBest can be found to optimize the objective function and the best location of the particle is the optimal strategy.

$$v_{id}^{k+1} = wv_{id}^{k} + C_1 \cdot rand_1 \cdot \left(pBest_i - x_{id}^{k}\right) + C_2 \cdot rand_2 \cdot \left(gBest - x_{id}^{k}\right) \tag{7.19}$$

$$x_{id}^{k+1} = x_{id}^{k} + v_{id}^{k+1} \tag{7.20}$$

$$w = w_{max} - k \cdot \frac{w_{max} - w_{min}}{k_{max}} \tag{7.21}$$

where v_{ij} is the velocity of particle i at dimension j, x_{ij} is the position of particle i at dimension j, w is the inertia weight, k is the iteration number, and C_1 and C_2 are the learning factors.

In this specific problem, we need to find the optimal charging strategy of PHEVs. The charging strategy vector of each PHEV can be defined as a dimension of the search space, and the charging strategy vector can be encoded as the coordinates in the specific dimension.

7.3 Simulation Model Description

In a distribution system with large fleet of PHEVs, various charging loads can easily change the load profile of the system and affect the artificial operation history for components such transformers and feeders. Thus, the conventional adequacy assessment of distribution systems with statistically constant failure rates are not suitable for this application, and a more

comprehensive model is needed for the reliability evaluation of the distribution system with PHEV penetrations. A condition-dependent outage model [69], [101] for the transformer is deployed in this study to obtain its time sequential failure rate. This condition-dependent transformer failure rate is able to take the impact from the various charging strategies of PHEVs into consideration in the reliability evaluation of the distribution network, and can more truly reflect the impact of various PHEV charging patterns on the adequacy of the distribution network.

7.3.1 Condition-Dependent Transformer Failure Model

The hybrid transformer failure model considers both the random failure and the aging failure of the transformer. Random failures can be caused by multiple random events such as animal damages, human errors, lightning flashes and storms. Their failure rates can be obtained from the historical data. However, the aging failure mode is much more complicated, which is related to the actual operation conditions of the transformer. According to the model in [69], the transformer aging failure under various load conditions can be represented as follows:

$$P_{af} = 1 - e^{\frac{(\frac{T_{LOI,total}}{15000})^{\beta} - (\frac{T_{LOI,total}+\Delta t_e}{15000})^{\beta}}{ce^{\frac{\theta_0+273}{}}}} \quad (7.22)$$

where $T_{LOI,total}$ is the loss of insulation life during a time period N, C and β are constant values based on the end-of-life failure, θ_O is the reference temperature, and Δt_e is the equivalent operation time.

As the mechanisms of random failures and aging failures of transformers are different, they are independent events. Assuming the random failure probability is P_{random}, the hybrid transformer failure probability model can be expressed as follows:

$$P_{trans} = 1 - (1 - P_{random}) \times (1 - P_{af}) \quad (7.23)$$

Thus, the proposed hybrid transformer failure model is condition-dependent and the failure rate of the transformer is affected by its loading conditions.

7.3.2 Transformer Protection Outage Model

Transformer overheating is mainly caused by overload operation. Therefore, overload protection is important in preventing transformers from overheating. When transformers are overloaded, they can be disconnected by opening the current-controlled overload relays. According to IEEE C57.92 [102], uncertainties may exist when the current is close to the relay pickup current due to current mismatch. Current mismatch can be caused by multiple factors such as measurement errors and over excitation. The mathematical model for calculating the current-dependent overload protection outage rate can be obtained as follows [69]:

$$P_{protection}(I) = P_{unrequire}, \text{ if } I < I_{pe}(1-\varepsilon_I) \tag{7.24}$$

$$P_{protection}(I) = P_{require}\int_{I_{pe}(1-\varepsilon_I)}^{I} f(I_{pick})dI_{pick} + P_{unrequire}\int_{I}^{I_{pe}(1+\varepsilon_I)} f(I_{pick})dI_{pick},$$

$$\text{if } I_{pe}(1-\varepsilon_I) < I < I_{pe}(1+\varepsilon_I) \tag{7.25}$$

$$P_{protection}(I) = P_{require}(I), \text{ if } I > I_{pe}(1+\varepsilon_I) \tag{7.26}$$

where $P_{unrequire}$ is the outage rate for transformer when the overload protection is not required, $P_{require}$ is the outage rate for transformer when the overload protection is required, I_{pick} is the pick-up current value, I_{pe} is the expectation value of I_{pick}, ε_I is the percentage error of current mismatch, and $f(I_{pick})$ is the probability density function for I_{pick} which can be expressed as follows:

$$f(I_{pick}) = \begin{cases} 0, & \text{if } I_{pick} < I_{pe}(1-\varepsilon_I) \text{ or } I_{pick} > I_{pe}(1+\varepsilon_I) \\ \dfrac{e^{\left(-(I_{pick}-I_{pe})^2/2\sigma^2\right)}}{\alpha_I\sigma\sqrt{2\pi}}, & \text{if} I_{pe}(1-\varepsilon_I) < I_{pick} < I_{pe}(1+\varepsilon_I) \end{cases} \tag{7.27}$$

$$\alpha_I = \phi\left(\frac{\varepsilon_I I_{pe}}{\sigma}\right) - \phi\left(\frac{-\varepsilon_I I_{pe}}{\sigma}\right) \quad (7.28)$$

where σ^2 is the variance of I_{pick}, and ϕ is the cumulative distribution function of the standard normal distribution.

7.3.3 Feeder Protection Outage Model

A probabilistic feeder protection model [103] is adopted in this study. We assume that each feeder has a trigger value of I_{op} for overcurrent protection. The trigger value is assumed to follow a normal distribution as follows:

$$g(I_{op}) = \frac{1}{\sqrt{2\pi}\delta} \exp\left[-\frac{(I_{op}-I_{set})^2}{2\delta^2}\right] \quad (7.29)$$

where I_{op} is the trigger current for feeder overcurrent protection, I_{set} is the expected value of I_{op} and δ^2 is the variance of I_{op}.

The virtual setting value I_{set} is the expected value of I_{op}. I_{set} is defined based on the feeder properties and its values is set as the operating limits of the feeder. For a given value of the feeder current I, the protection operation probability is defined as:

$$P_{feed}(I) = Pr(I \geq I_{op}) = \int_0^I g(I_{op}) dI_{op} \quad (7.30)$$

I_{set} is set as 8 kA for main feeder and 2 kA for lateral feeder in the test system.

7.4 Adequacy Assessment of Active Residential Distribution Network with PHEVs

7.4.1 Load Restoration Mechanism

When an interruption occurs in the system, the affected load points are determined by evaluating their minimal path. The minimal path for a load point is defined as the path between the load point and the source. If the path has been taken out, the connection between the load point and the source will be lost. The V2G topology at a load point is shown in Fig. 7.1. During an interruption, PHEVs will first supply power to their own households. Those households with excess power will act as virtual power plant (VPP) and supply power to the households suffering from the power deficiency. Based on the SOCs of PHEVs and the load demand of households, the excess power and the load demand can be calculated. If the excess power cannot satisfy the load demand, load will be curtailed. In order to minimize the number of households affected by the interruption, the households with less load demand will have a higher priority in the restoration sequence.

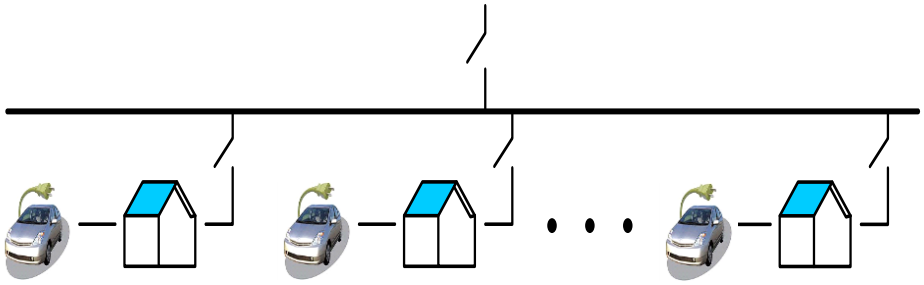

Figure 7. 1 V2G topology at a certain load point.

The restoration process can be elaborated as follows:

Step 1) Once a failure event has been detected in the system, record the time of this event as t_x.

Step 2) Check the minimal paths of all the load points and determine the blackout area.

Step 3) Calculate the available V2G energy $E_{V2G,d}^{t_x,t_r}$ for each PHEV in the blackout area.

Step 4) Based on the load demand of the households and the available V2G energy in the blackout area, determine each household is whether a customer or a VPP.

Step 5) For the households operated as customers, queueing them from the lowest load demand to the highest load demand. Those households with lower load demands will be restored first. Trim the households which have lower priority in the restoration sequence.

Step 6) Those households operated as VPPs supply power to other households operated as customers based on the restoration sequence. Update the available SOCs of the PHEVs for the next time step.

Step 7) Check if the fault has been cleared. If the fault has not been cleared, go to Step 3, otherwise go to Step 8.

Step 8) End the restoration process, and generate the loss of load duration for each household.

7.4.2 Basic Simulation Procedure Using Monte Carlo Method

Analytical approaches and Monte Carlo simulation are two basic methods for adequacy evaluation of distribution system. The load point adequacy indices and system level adequacy indices can be calculated by analytical methods [104]. While analytical methods are able to calculate the mean and average values for the system adequacy indices including SAIFI, SAIDI, CAIDI, etc., Monte Carlo simulation can be used to obtain the probability distribution of these system adequacy indices [105]. The state duration probability distributions of components can be simulated by Monte Carlo simulation and the adequacy index probability distributions can also be calculated by Monte Carlo simulation.

In Monte Carlo simulation, the artificial history can be applied to identify the occurrence of contingencies and their impact on the distribution system by generating an artificial history of faults for each component [106], [107]. The artificial history can be derived based on a two-state model. In the two-state model, the component is either in the up state or in the down state. The

up state indicates the normal condition of the component, and the down state represents the faulty condition of the component due to the failure. In a simulated up and down state history, time to failure (TTF) indicates the time during which the component remains in the up state and time to replace (TTR) means the time during which the component is in the down state. For each component n, TTF and TTR are obtain by generating random numbers between [0, 1], as shown in (7.31) and (7.32) [106]-[108].

$$\mathrm{TTF_n} = -\frac{\ln(\mathrm{U_n})}{\lambda_n} \times 8760 \tag{7.31}$$

$$\mathrm{TTR_n} = -\ln(\mathrm{U_n}) \times \mathrm{MTTR_n} \tag{7.32}$$

where $\mathrm{U_n}$ is a uniformly distributed random number between [0, 1]; λ_n is the failure rate; and $\mathrm{MTTR_n}$ is the mean time to repair.

When a component failure occurs in the system, the affected load points will be located and the impact of the failure will be analyzed. The operation/restoration history of a load point can be generated through determining the load point failures.

7.4.3 Adequacy Assessment Procedure

The detailed procedure for evaluating system adequacy using Monte Carlo simulation is described as follows:

Step 1) Generate the driving pattern of PHEVs. Determine the plug-in time, plug-out time and required energy for each PHEV.

Step 2) Determine the optimal charging sequence of each PHEV based on the smart charging algorithm.

Step 3) Generate an artificial hourly history of each component.

Step 4) Detect the failure event in the system.

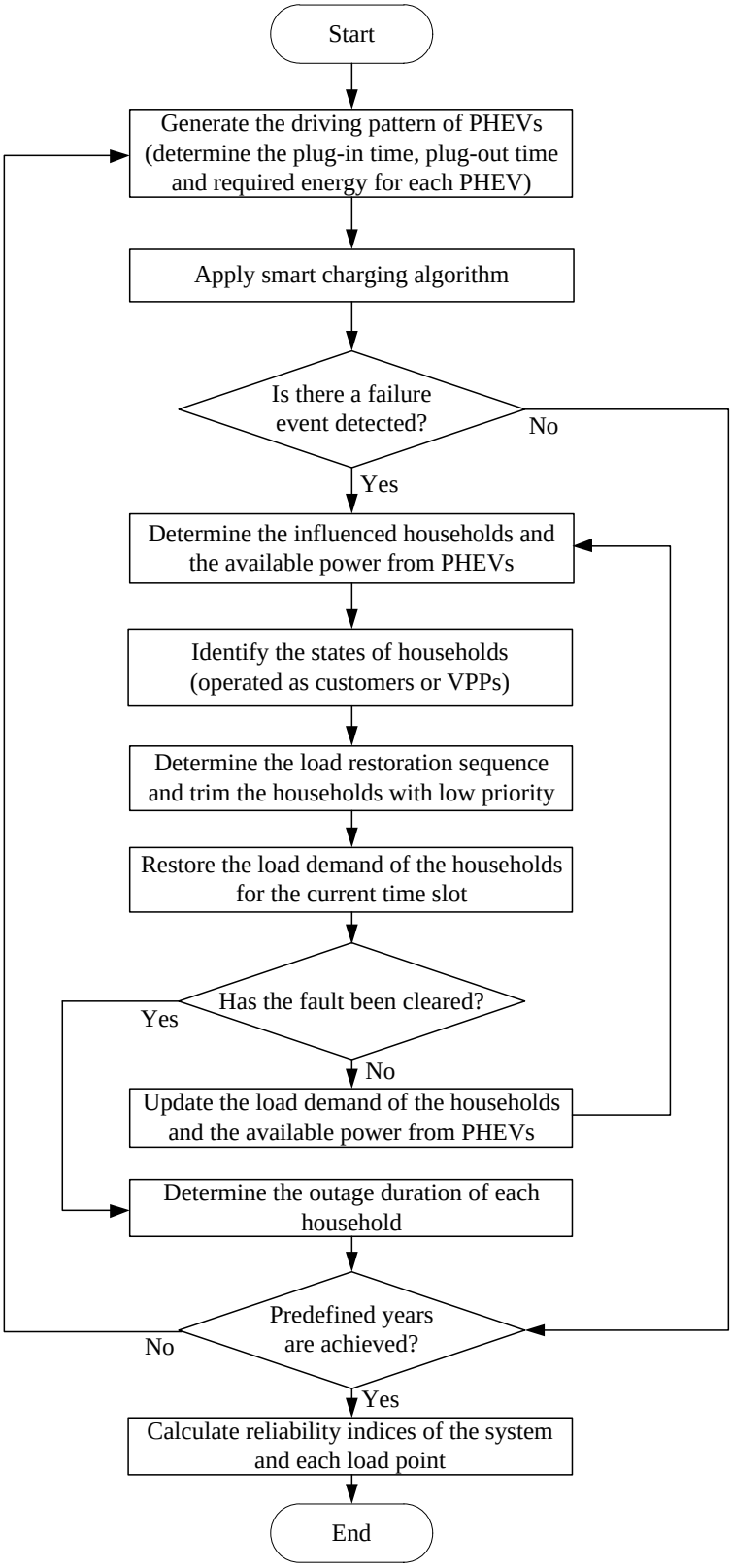

Figure 7. 2 Simulation procedures for integrated distribution and PHEV systems.

Step 5) Determine the influenced households and the available V2G energy of the PHEVs.

Step 6) Execute the load restoration procedures.

Step 7) Update the load demand of the households and available V2G energy of the PHEVs for the next time step.

Step 8) Repeat steps 5)-7) until the fault has been cleared.

Step 9) Determine the outage duration of each household.

Step 10) Repeat steps 1)-9) until the predefined number of simulation years has been achieved.

Step 11) Calculate the adequacy indices such as SAIFI and SAIDI according to the operation/restoration history of all households.

Step 12) Aggregate the adequacy indices to produce the probability distribution.

The flow chart in Fig. 7.2 illustrates the complete simulation procedure for evaluating the impact of PHEVs penetration on the distribution system reliability using Monte Carlo simulation. Notice that the TTFs for transformer and transformer protection are obtained based on (7.23) and (7.24)-(7.28), respectively.

7.5 Case Studies and Simulation Results

7.5.1 Residential Distribution Network Under Test

IEEE 34-node test feeder [37] shown in Fig. 7.3 is used as a representative residential radial network. The node number is marked in the figure. In the system, load point 1 is connected to the grid, and each of other load points has 2 households connected to each phase transformer for a total of 198 households. Assume each household has two vehicles and the penetration level of

PHEVs is defined as the percentage of PHEVs among all the vehicles in these households. For the main feeder and the lateral feeder, the interruption rates are 0.1 interruptions/year and 0.25 interruptions/year, and the average times to repair are 3 hours and 1 hour, respectively. The availability of the charging/discharging equipment also has impacts on the system adequacy.

The voltage level in this distribution system has been scaled down to 120 V for residential use. The daily load profiles for a single household in different seasons [38] are illustrated in Fig. 7.4. To add more randomness to the system, other two load profiles in each season are generated by shifting ±1 hours of Fig. 7.4. The load profile of each house is randomly chosen from the three load profiles in each season, and peak loads of the households are randomly scaled from 3 kW to 5 kW. The PHEVs are assumed to be the Chevrolet Volt with 16 kWh battery capacity. In addition, $\mathrm{SOC}_{\min}$ is set as 20% and $\mathrm{SOC}_{\max}$ is set as 90%. A 1,000 kVA transformer located between node 1 and node 2 is chosen for simulation studies based on the total demands of the customers in this residential distribution system. The charging level of PHEVs is set as AC Level 1 (1.8 kW) and the charging/discharging efficiency factor is set as $\eta = 0.92$.

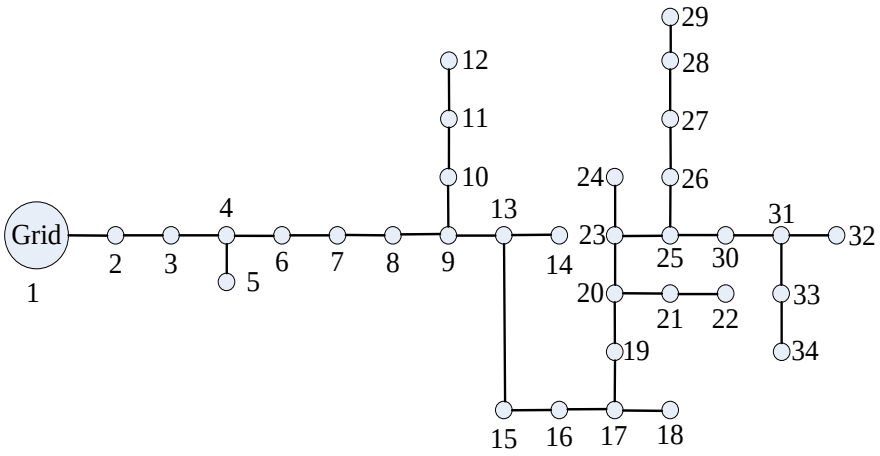

Figure 7. 3 The topology of the studied residential distribution system.

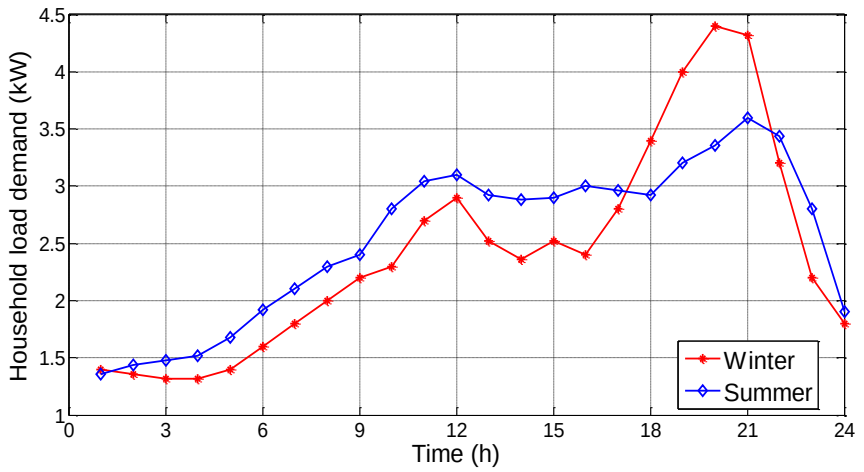

Figure 7. 4 Typical daily load profiles for a single household in different seasons.

7.5.2 The performance of the proposed smart charging algorithm

In this section, various simulations are carried out to demonstrate the effectiveness of the proposed smart charging algorithm. Uncontrolled charging is used as the benchmarking control strategy. PHEVs are assumed to start charging immediately when they arrived home when uncontrolled charging is applied. The proposed smart charging will arrange the charging sequence wisely to reduce the charging cost under the demand reponse program. Four different PHEV penetration levels of 10%, 20%, 50% and 100% are tested in this study to validate the advantages for the proposed smart charging algorithm.

The convergence curve of the PSO-based smart charging algorithm is shown in Fig. 7.5. Table 7.1 shows the peak load of the system with different control strategies and penetration levels. It shows that the smart charging can effectively reduce the peak load of the system. The charging cost in winter is shown in Table 7.2. The uncontrolled charging has a higher earning from providing reliability support as it charges the PHEVs immediately when they arrive home. Thus, PHEVs will have higher SOCs at the early stage of their plug-in duration. However, this kind of aggressive charging strategy will increase the peak load of the system dramatically and

put the system at risk. While making less earnings by providing reliability support, the proposed smart charging strategy results in lower total cost by shifting the charging load from peak load hours to off-peak load hours.

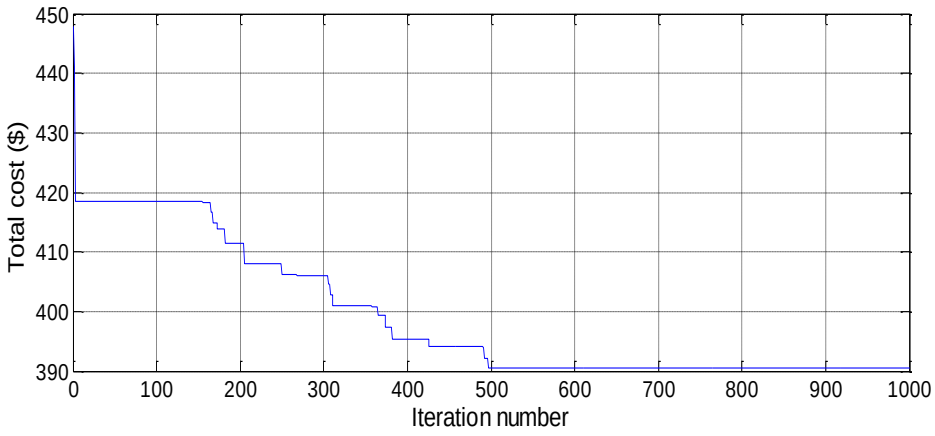

Figure 7. 5 The convergence curve of the smart charging algorithm.

Table 7. 1 Peak Load of Different Control Strategies and PHEV Penetration Levels (kW)

	10%	**20%**	**50%**	**100%**
Uncontrolled Charging	765	798	866	1041
Smart Charging	751	772	815	894

Table 7. 2 Costs of Different Control Strategies at 50% PHEV Penetration Level in Winter

	Charging Cost ($)	Reliability Support Earning($)	Total Cost ($)
Uncontrolled	699.39	97.45	601.94
Smart Charging	465.88	75.31	390.57

7.5.3 Adequacy Evaluation

The adequacy metrics used in this chapter are system average interruption frequency index (SAIFI), system average interruption duration index (SAIDI), customer average interruption duration index (CAIDI), average service availability index (ASAI) and expected energy not supplied (EENS) [92]. SAIFI is the average instances of interruption per customer experienced per year due to the failure of the system components. The unit of SAIFI is interruptions/system customer/year. SAIDI is the average outage duration per customer suffered per year. The unit of SAIDI is hour/system customer/year. CAIDI is the average outage duration of those customer interruptions, and its unit is hour/customer interruption. ASAI is the ratio of customer hours of available service and the customer hours demanded per year.

In this section, the impact of charging behavior of PHEVs on the overall system adequacy is investigated. The adequacy of the integrated residential distribution and PHEVs system are assessed at different PHEV penetration levels. The adequacy evaluation takes the impact from different seasons into consideration. The daily load demand profiles for the households are generated based on the two load profiles from the summer and winter at different seasons. Also, the ambient temperature for the transformer is set differently for summer and winter. The simulation is carried out using different household demand profiles and the ambient temperatures in different seasons.

Given an interruption occurs at the main feeder (repair time is 3-h) between load point 1 and load point 2 at a given hour, the recovered load demand is shown in Fig. 7.6. As shown in the figure, the V2G energy capacity from PHEVs varies during the day. The low V2G energy capacity period is from 7 am to 3 pm as most of the PHEVs are on the road. The V2G energy capacity reaches its peak at 7 pm to 11 pm as most PHEVs are arrived home and start charging.

It can also be found from Fig. 7.6 that the uncontrolled charging reaches a higher V2G energy capacity as it charges the PHEVs immediately when they arrive home. This uncontrolled charging strategy also puts the system at risk as it increases the system peak load.

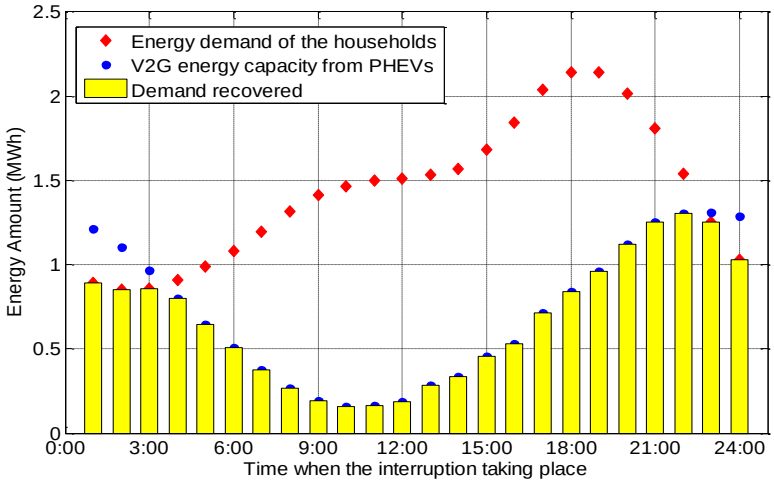

(a) Smart charging

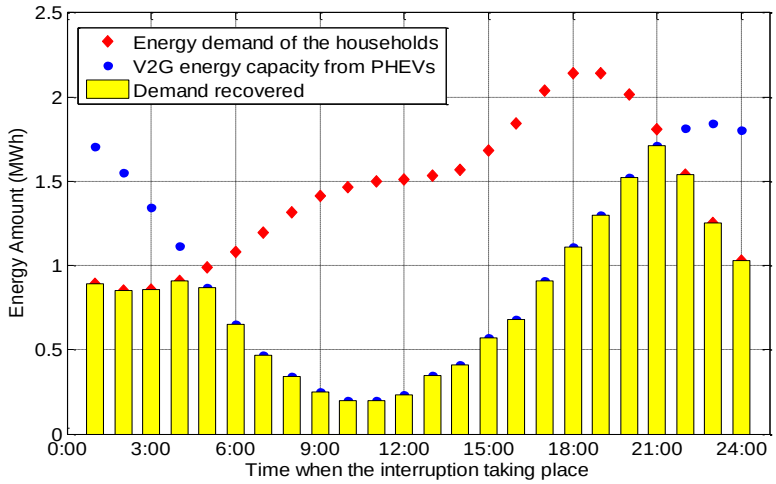

(a) Uncontrolled charging

Figure 7. 6 Demand recovered for the system in winter during an interruption at 50% PHEV penetration level.

The transformer parameters used in this case study are obtained from [18] and [21]. Table 7.3 and Table 7.4 show the simulation results of reliability indices under the uncontrolled charging strategy and smart charging strategy, respectively. According to the results, it can be found that the adequacy indices have been significantly impacted in a negative manner if a high penetration level of PHEVs is integrated into the distribution system for charging without proper

control. The values of SAIFI, SAIDI and CAIDI are considerably increased, which indicates that customers experienced more frequent interruptions and longer outage durations each year; while the decrease of ASAI implies that customers suffered from more time periods without power service.

Table 7. 3 Adequacy indices of the distribution system with uncontrolled charging.

Indices / Penetration	SAIFI	SAIDI	CAIDI	ASAI	EENS (MWh/year)
10% PHEVs	1.2809	5.1927	4.0538	0.9954	0.9684
20% PHEVs	1.2596	5.0089	3.9767	0.9934	0.6256
50% PHEVs	6.0358	79.826	13.225	0.9849	14.367
100% PHEVs	324.31	5030.6	15.511	0.4237	1253.3

Table 7. 4 Adequacy indices of the distribution system with smart charging.

Indices / Penetration	SAIFI	SAIDI	CAIDI	ASAI	EENS (MWh/year)
10% PHEVs	1.2436	6.1499	4.9451	0.9918	1.1239
20% PHEVs	1.2731	7.1469	5.6136	0.9957	0.8249
50% PHEVs	1.2381	5.5182	4.4570	0.9934	4.7991
100% PHEVs	12.918	187.35	14.503	0.9746	43.540

Comparing different penetration levels of PHEVs, it can be found that for a very low penetration level of PHEV (less than 20%), the increase of PHEV penetration level will benefit the system adequacy as more V2G energy capacity can be used in the system. However, as the PHEV penetration level increases to a very high level, the charging demand of PHEVs will increase the peak load of the system. Its negative impact on the system adequacy will overweigh its benefits in providing load restoration service. This is because a higher penetration level of

PHEVs inevitably increases the load demand. The increased load has a higher probability of producing large currents which may trigger the transformer protection more frequently, causing more failure periods in the distribution grid operations.

It can be observed that most negative impacts can be eliminated at a lower PHEVs penetration level through the proposed smart charging method. This validates the effectiveness of the proposed smart charging scheme from the perspective of maintaining system adequacy. However, if the PHEV penetration grows too high (100% penetration level), the negative impacts can only be reduced to some extent but cannot be eliminated after applying the proposed smart charging scheme. This is because a high penetration level of PHEVs incurs a very large load that cannot be handled. The proposed smart charging is able to reduce the pick-up current for the transformer, which is however still much larger than the expected one because of the large PHEV charging load.

7.5.4 Sensitivity Studies

Two kinds of sensitivity studies are carried out in this section to quantify the impacts of the PHEV penetration level, the transformer capacity, PHEV charging level and battery capacity on the power system adequacy.

1) The impact of PHEV penetration level on the distribution system adequacy

As we have analyzed in Table 7.3-7.4, the penetration level of PHEVs has a significant impact on the adequacy indices. The high penetration level of PHEV has a negative impact on the system adequacy. Thus, the penetration level of PHEV cannot exceed a certain limit to ensure the system adequacy. The main focus of this case study is to identify the maximum number of PHEVs that can be connected to the system without affecting the system adequacy. Fig. 7.7 shows the system EENS with different control strategies at different PHEV penetration

levels. It can be seen from the figure that the EENS increases dramatically with the increase of PHEV penetration level for both control strategies. For a requirement of EENS being less than 10 MWh/year, the maximum PHEV penetration levels for the smart charging and uncontrolled charging are 71% and 44%, respectively. Compared with the uncontrolled charging strategy, the proposed smart charging strategy can increase the penetration level of PHEVs by 27%.

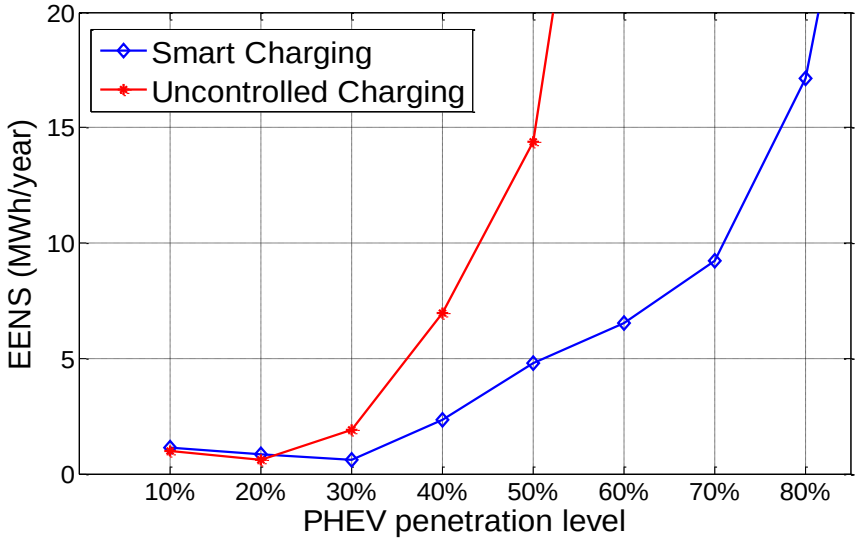

Figure 7. 7 EENS of the system with different control strategies at different PHEV penetration levels

2) The impact of transformer capacity factor, PHEV's charging level and battery capacity on the distribution system adequacy

It is clear from the analysis in Section 7.3 that the increase of transformer capacity will have a positive impact on the system adequacy. Also the PHEV's charging level and battery capacity will affect its ability in load restoration during an interruption. To analyze their impacts on the system adequacy, we build three scenarios in this case study.

- Scenario 1: The base case. It is the same as the system setup in Section 7.5.1.
- Scenario 2: Increasing the transformer capacity from 1000 kVA to 1200 kVA.
- Scenario 3: Increasing the charging level from AC level I (1.8 kW) to AC level II (3.6 kW). Also increasing the battery capacity from 16 kWh to 24 kWh.

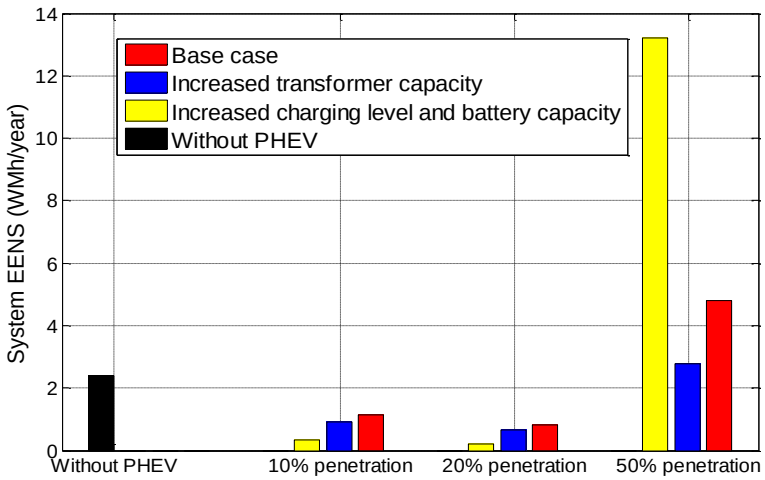

Figure 7. 8 Comparison of the impacts of different scenarios on the system EENS.

Fig. 7.8 compares the impacts of different scenarios on the system's EENS. It can be seen from the figure that increasing the charging level and battery capacity results in a better performance than increasing the transformer capacity in reducing the EENS at low PHEV penetration levels. However, with high PHEV penetration levels, the increase of the charging level and battery capacity has a negative impact on the EENS as it inevitably increases the charging load demand of the PHEVs and overloads the transformer. The increase of transformer capacity can effectively reduce the EENS with high penetration levels of PHEVs.

8. Conclusions and Outlook

This chapter draws the conclusions of this dissertation. Also, the possible future research directions in this research field will be presented.

8.1 Conclusions

This dissertation studies various aspects of the integration of PHEVs into power distribution systems. The detailed summaries of the research conducted in this dissertation are listed as follows:

- Chapter 2 proposes a load profile modeling framework (LPMF) for PHEVs, which takes both the characteristics of driving pattern and vehicle parameters into consideration. Moreover, to analyze the relationship between the arrival time, departure time and daily mileage of PHEVs, the author proposes a Stochastic Fuzzy Model to synthetize the driving pattern.
- A two-layer intelligent optimization algorithm to optimize the charging process of PHEVs is presented in Chapter 3. The proposed algorithm is able to achieve four goals by flattening the load demand, improving power quality, providing frequency regulation service, and minimizing the total charging cost.
- Chapter 4 designs an LFC system with PHEVs and proposes a hierarchical game framework for PHEVs to optimize their charging process and participate in frequency regulation simultaneously. In the proposed game framework, a non-cooperative game is proposed to guide the frequency regulation capacity bids of aggregators in the upper level and a Markov game is adopted at the lower level to coordinate the charging of PHEVs based on the regulation price from the upper level game. The games at the two levels cooperate with one

another, and will finally evolve to an optimal state where the performance for both the frequency regulation and the charging process are optimized.

- A reliability-differentiated framework to enable reliability-differentiated service in a residential distribution network with PHEVs has been proposed in Chapter 5. Thus, the customers can be served at different reliability levels. This chapter also develops a reliability-differentiated pricing mechanism which is able to improve the reliability of the residential distribution system as well as provide differentiated power prices to the customers according to their different requirements on reliability. Finally, a hierarchical game approach will be proposed in this chapter to coordinate the charging process of PHEVs. While traditional non-cooperative game may have multiple Nash equilibriums, the proposed hierarchical game gives a refined solution which will not end with suboptimal solutions.
- Chapter 6 proposes an integrated charging navigation framework will be proposed. This charging navigation framework is made up of the power system, transportation system, navigation system, electric vehicle charging stations (EVCSs) and EVs. Based on this framework, a hierarchical game approach is proposed to optimize the strategies of both EVCSs and EVs at two levels. At the upper level of the hierarchical game, a non-cooperative game is proposed to model the competition between EVCSs and manage them in a decentralized fashion. Evolutionary games are formulated at the lower level to evolve the EVs' strategies in choosing EVCSs.
- Chapter 7 systematically investigated the impact of large scale penetration of PHEVs on power distribution system adequacy. An integrated, stochastic adequacy model is developed by combining the stochastic factors in both the PHEVs penetration part and distribution network part. A detailed hybrid transformer failure model has been presented, which is able

to more truly reflect the changing failure rate due to increased loads by PHEVs charging. Monte Carlo simulation has been applied to obtain the adequacy indices. Simulation results confirmed that the proposed smart charging strategy is able to effectively reduce the negative impacts of PHEVs on system adequacy at the high penetration level of PHEVs

8.2 Outlook

To extend the research work presented in this dissertation, the possible research directions may include:

- Charging station planning for integrated power distribution and transportation system. The placement of charging stations in a city area may have impacts on both the traffic flow and power system reliability. Future study may consider both the optimal location and optimal control strategies of charging stations to make it an integrated problem. Currently, the research on charging station planning is not mature. Many detailed models are still needed to be incorporated in the planning of charging stations such as the EV navigation model, the charging station operational model and the interconnections between the power distribution network and transportation network. The planning of charging stations should consider the impacts from both the power distribution network and transportation network such as the layout of the city traffic network, the power distribution network topology, the EV travel pattern, the electricity market, power system reliability, EV owners' convenience and the traffic flow efficiency, etc. Inappropriate placement of charging stations could lead to negative effects on both the power system and transportation system. Without considering the operational model of charging station in the electricity market and the business model for EV charging navigation, the planning results will not be accurate, leading to uninformed decisions. Thus, it is of great importance to build an integrative, comprehensive charging

station planning model, which considers the planning and operation of the charging stations as an integrated problem.

- Consider the impact of renewable resources' impact on the control strategies of the charging stations. Charging stations can have their own renewable resources such as wind turbines and solar panels. It is beneficial for both the power grid and charging stations to integrate renewable resources in charging stations. On the one hand, the charging load of the charging stations could buffer the intermittency of the renewable resources and enable higher penetration of the renewable energy in the power grid. On the other hand, the charging stations can earn revenues by selling the power generated by the renewable resources to the EVs or the power grid.
- Cooperative game based EV charging navigation. Currently, most studies treat EVs as price takers in the electricity market as a single EV has a very small charging demand, which does not have enough effect on the charging stations' pricing strategies. However, with the evolving concept of connected vehicles, EVs will be able to communicate with each other when choosing their charging stations. For instance, several EVs may cooperate with each other and form a group to compete with other EVs in choosing charging stations. Different from the centralized optimization, game theory gives a more reasonable business model by maximizing the utility of each player instead of the total utility of all the players. In game theory, we assume that the players are rational and selfish profit making entities which is true in the real-world market. However, the non-cooperative game may reach a smaller total utility as it lacks the mechanism of cooperation. This motivates us to apply the cooperative game model for the EVs. The utilities of EVs may not always conflict with each other, and some of the EVs can make more profits by cooperating with other EVs to bid a more

favorable charging price. The charging stations may also be willing to lower its charging price for attracting large groups of EVs.

REFERENCES

[1] C. Pang, P. Dutta, and M. Kezunovic, "BEVs/PHEVs as Dispersed Energy Storage for V2B Uses in the Smart Grid," *IEEE Transactions on Smart Grid*, vol. 3, no. 1, pp 473-482, March 2012

[2] C. Pang, P. Dutta, S. Kim, M. Kezunovic, and I. Damnjanovic, "PHEVs as Dynamically Configurable Dispersed Energy Storage for V2B Uses in the Smart Grid," *The 7th Mediterranean Conference and Exhibition on Power Generation, Transmission and Distribution,* Agia Napa, Cyprus, Nov. 2010.

[3] Y. G. Rebours, D. S. Kirschen, M. Trotignon, and S. Rossignol, "A survey of frequency and voltage control ancillary services-Part II: Economic features," *IEEE Trans. Power Systems*, vol. 22, no. 1, pp. 358-366, Feb. 2007.

[4] N. Ullah, T. Thiringer, and D. Karlsson, "Temporary primary frequency control support by variable speed wind turbines-Potential and applications", *IEEE Trans. Power Systems*, vol. 23, pp. 601-612, May 2008.

[5] H. Bevrani and T. Hiyama, "On load frequency regulation with time delays: design and real-time implementation", *IEEE Trans. on Energy Conversion*, vol. 24, pp. 292-300, Mar. 2009.

[6] H. Bevrani, A. Ghosh, and G. Ledwich, "Renewable energy sources and frequency regulation: survey and new perspectives", *IET Renewable Power Generation*, vol. 4, pp. 438-457, Sep. 2010.

[7] H. Bevrani and P. Daneshmand, "Fuzzy Logic-Based Load Frequency Control Concerning High Penetration of Wind Turbines", *IEEE Systems Journal*, vol. 6, pp. 173-180, Mar. 2012.

[8] P. Mercier, R. Cherkaoui, A. Oudalov, "Optimizing a Battery Energy Storage System for Frequency Control Application in an Isolated Power System", *IEEE Trans. Power Systems*, vol. 24, pp. 1469-1477, Aug. 2009.

[9] C. Quinn, D. Zimmerle, and T. H. Bradley, "The effect of communication architecture on the availability, reliability, and economics of plug-in hybrid electric vehicle-to-grid ancillary services," *J. Power Sources*, vol. 195, no. 5, pp. 1500-1509, Mar. 2010.

[10] N. Rau and Y. Hegazy, *Reliability Differentiated Pricing of Electricity Service*, NRRI series, 90–5. National Regulatory Research Institute, Columbus, 1990.

[11] N. Siddiqi and L. Baughman, "Reliability differentiated real-time pricing of electricity," *IEEE Transactions on Power Systems*, vol.8, no.2, pp.548-554, May 1993.

[12] N. Siddiqi and L. Baughman, "Reliability differentiated pricing of spinning reserve," *IEEE Transactions on Power Systems*, vol.10, no.3, pp.1211-1218, Aug 1995.

[13] Y. Hegazy and M. Guldmann, “Reliability pricing of electric power service: a probabilistic production cost modeling approach”, *Energy* 21(2):87–97, 1996.

[14] A. Klementavicius and V. Radziukynas, "Differentiated Reliability Pricing Model for Customers of Distribution Grids." *Handbook of Networks in Power Systems* I. Berlin Heidelberg: Springer, 2012, pp. 213-239.

[15] M. Glachant and F. Leveque, Electricity Reform in Europe: *Towards a Single Energy Market,* Edward Elgar Publishing, Cheltenham, 2009.

[16] W. Lee, L. Xiang, R. Schober and V.W.S. Wong, "Analysis of the behavior of electric vehicle charging stations with renewable generations," *in Proc. 2013 IEEE Smart Grid Communications Conf.,* pp.145-150.

[17] K. Clement, E. Haesen, and J. Driesen, “The Impact of Charging Plug-In Hybrid Electric Vehicles on a Residential Distribution Grid,” *IEEE Trans. Power Systems,* vol. 25, pp. 371-380, Feb. 2010.

[18] P. Zhang, K. Qian, C. Zhou, B. Stewart, and D. Hepburn, “A Methodology for Optimization of Power Systems Demand Due to Electric Vehicle Charging Load,” *IEEE Trans. Power Systems,* vol. 27, pp. 1628-1636, Aug. 2012.

[19] Z. Darabi and M. Ferdowsi, “Aggregated Impact of Plug-in Hybrid Electric Vehicles on Electricity Demand Profile,” *IEEE Trans. Sustainable Energy,* vol. 2, pp. 501-508, Oct. 2011.

[20] S. Shafiee, M. Firuzabad, and M. Rastegar, “Investigating the Impacts of Plug-in Hybrid Electric Vehicles on Power Distribution Systems,” *IEEE Trans. Smart Grid,* vol. 4, no. 3, pp. 1351-1360, Sep. 2013.

[21] W. Su and M. Chow, “Performance Evaluation of an EDA-Based Large-Scale Plug-In Hybrid Electric Vehicle Charging Algorithm,” *IEEE Trans. Smart Grid,* vol. 3, pp. 308-315, Mar. 2012.

[22] A. Lojowska, D. Kurowicka, G. Papaehthymiou, and L. Sluis, “Stochastic Modeling of Power Demand Due to EVs Using Copula,” *IEEE Trans. Power Systems,* vol. 27, pp. 1960-1968, Nov. 2012.

[23] T. Lee, B. Adornato, and Z. Filipi, “Synthesis of Real-World Driving Cycles and Their Use for Estimating PHEV Energy Consumption and Charging Opportunities: Case Study for Midwest/U.S.,” *IEEE Trans. Vehicular Technology,* vol. 60, pp. 4153-4163, Nov. 2011.

[24] T. Lee, B. Adornato, and Z. Filipi, “Stochastic Modeling for Studies of Real-World PHEV Usage: Driving Schedule and Daily Temporal Distributions,” *IEEE Trans. Vehicular Technology,* vol. 61, pp. 4193-1502, May. 2012.

[25] National Household Travel Survey, 2009. [online]. Available: http:// nhts.ornl.gov.

[26] E. Sortomme, M. Hindi, and S. Macpherson, “Coordinated Charging of Plug-In Hybrid Electric Vehicles to Minimize Distribution System Losses,” *IEEE Trans. Smart Grid*, vol. 2, pp. 198-205, Mar. 2011.

[27] H. Sekyung, H. Soohee, and K. Sezaki, “Development of an Optimal Vehicle-to-Grid Aggregator for Frequency Regulation,” *IEEE Trans. Smart Grid,* vol. 1, pp. 65-72, Jun. 2010.

[28] B. Geng, J. Mills, and D. Sun, "Two-Stage Charging Strategy for Plug-In Electric Vehicles at the Residential Transformer Level," *IEEE Transactions on Smart Grid*, vol.4, no.3, pp.1442-1452, Sept. 2013.

[29] H. Liang, B. Choi, W. Zhuang, and X. Shen, "Towards optimal energy store-carry-and-deliver for PHEVs via V2G system," *in Proceedings of IEEE INFOCOM*, pp.1674-1682, March 2012.

[30] B. Lunz, H. Walz, and D. U. Sauer, "Optimizing vehicle-to-grid charging strategies using genetic algorithms under the consideration of battery aging," *IEEE Vehicle Power and Propulsion Conference (VPPC),* pp.1-7, Sept. 2011.

[31] S. Han, S. Han, and K. Sezaki, "Economic assessment on V2G frequency regulation regarding the battery degradation," *IEEE PES Innovative Smart Grid Technologies (ISGT),* pp.1-6, Jan. 2012.

[32] J. Kennedy and R. C. Eberhart, “Particle Swarm Optimization,” *IEEE International Conference on Neutral Networks,* Australia, 1995, pp. 1942-1948.

[33] L. Fenandez, T. Roman, R. Cossent, C. Domingo, P. Frias, “Assessment of the impact of plug-in electric vehicles on distribution network,” *IEEE Trans. Power System,* vol. 26, no. 1, pp. 206-213, Feb. 2011.

[34] S. Hadley, “Impact of plug-in hybrid vehicles on the electric grid,” Oak Ridge National Laboratory, TN, USA, Tech. Rep. ORNL/TM-2006/554, 2006.

[35] W. Su, H. Eichi, W. Zeng, and M. Chow, "A survey on the electrification of transportation in a smart grid environment," *IEEE Transactions on Industrial Informatics,* vol. 8, no.1, pp. 1-10, Feb. 2012.

[36] W. Kempton and J. Tomic, “Vehicle-to-grid power fundamentals: Calculation capacity and net revenue,” *J. Power Source*, vol. 144, pp. 268-279, 2005.

[37] W. H Kersting, “Radial distribution test feeders,” *in Proc. IEEE Power Eng. Soc. Winter Meeting,* Jan. 2001. [online]. Available: http://ewh.ieee.org/soc/pes /dsacom/.

[38] J. A. Jardini, C. M. Tahan, and M. R. Gouvea, “Daily load profiles for residential, commercial and industrial low voltage consumers,” *IEEE Trans. Power Delivery,* vol. 15, pp. 375-380, Jan. 2000.

[39] W. Kersting, *Distribution System Modeling and Analysis,* Boca Raton, FL: CRC, 2002.

[40] Y. Mu, J. Wu, J. Ekanayake, N. Jenkins, and H. Jia, "Primary Frequency Response From Electric Vehicles in the Great Britain Power System", *IEEE Trans. Smart Grid,* vol. 4, pp. 1142-1150, Jun. 2013.

[41] T. Masuta and A. Yokoyama, "Supplementary Load Frequency Control by Use of a Number of Both Electric Vehicles and Heat Pump Water Heaters", *IEEE Trans. Smart Grid,* vol. 3, pp. 1253-1262, Sep. 2012.

[42] M. Galus, S. Koch, and G. Anderson, "Provision of Load Frequency control by PHEVs, Controllable Loads, and a Cogeneration Unit", *IEEE Trans. Industrial Electronics,* vol. 58, pp. 4568-4582. Oct. 2011.

[43] K. Shimizu, T. Masuta, Y. Ota, and A. Yokoyama, "A new load frequency control method in power system using vehicle to grid system considering users' convenience", *in Proc. 2011 17th Power Syst. Compute. Conf.*, pp. 1-7, Stockholm, Sweden, Aug. 2011.

[44] S. Vachirasricirikul and I. Ngamroo, "Robust LFC in a Smart Grid with Wind Power Penetration by Coordinated V2G Control and Frequency Controller," *IEEE Trans. Smart Grid,* vol. 5, pp. 308-315, Jan. 2014.

[45] J. Pahasa and I. Ngamroo, "Coordinated Control of Wind Turbine Blade Pitch Angle and PHEVs Using MPCs for Load Frequency Control of Microgrid," *IEEE Systems Journal,* vol. 10, no. 1, pp. 97-105, Mar. 2016.

[46] M. Datta and T. Senjyu, "Fuzzy Control of Distributed PV Inverters/ Energy Storage/ Electric Vehicles for Frequency Regulation in a Large Power System," *IEEE Trans. Smart Grid,* vol. 4, pp. 479-488, Mar. 2013.

[47] M. Ansari, A. Al-Awami, E. Sortomme, and M. Abido, "Coordinated Bidding of Ancillary Services for Vehicle-to-Grid Using Fuzzy Optimization," *IEEE Trans. Smart Grid,* vol. 6, pp. 261-270, Jan. 2015.

[48] J. Donadee and M. Ilic, "Stochastic Optimization of Grid to Vehicle Frequency Regulation Capacity Bids," *IEEE Trans. Smart Grid,* vol. 5, pp. 1061-1069, Mar. 2014.

[49] H. Chen, R. He, and X. Wang, "Cooperative Control of Power System Load and Frequency by Using Differential Game," *IEEE Trans. Control System Technology,* vol. 23, pp. 882-897, May 2015.

[50] P. Kundur, *Power System Stability and Control,* Englewood Cliffs, NJ: McGraw-Hill, 1994

[51] H. Bevrani, *Robust power system frequency control*, Springer, New York, 2009.

[52] N. Jaleeli, D. N. Ewart, L. H. Fink, and A. G. Hoffmann, "Understanding automatic generation control," *IEEE Trans. Power Systems*, vol. 7, pp. 1106-1122, Aug. 1992.

[53] L. Shapley, “Stochastic games,” *Proc. 1953 Nat. Acad. Sci.,* vol. 39, no. 10, pp. 1095-1100.

[54] J. B. Rosen, “Existence and uniqueness of equilibrium points for concave N-person games,” *Econometrica,* vol. 33, no. 3, pp. 520–534, 1965.

[55] D. Fudenberg and J. Tirole, *Game Theory*, Cambridge, MA: MIT Press, 1991.

[56] J. Filar and K. Vrieze, *Competitive Markov Decision Processes,* New York: Springer-Verlag, 1997.

[57] T. Vincent, *Evolutionary Game Theory,* National Selection, and Darwinian Dynamics, Cambridge University Press, 2005.

[58] H. Bevrani and A. G. Tikdari, “An ANN-based power system emergency control scheme in the presence of high wind power penetration,” *in Wind Power Systems: Applications of Computational Intelligence, ser. Springer Book Series on Green Energy and Technology*, Edited by L. Wang, C. Singh, and A. Kusiak, Berlin Heidelberg, Springer-Verlag, pp. 215-254, 2010.

[59] A. Mohamed, V. Salehi, T. Ma and O. Mohammed, "Real-Time Energy Management Algorithm for Plug-In Hybrid Electric Vehicle Charging Parks Involving Sustainable Energy," *IEEE Trans. Sustainable Energy*, vol.5, no.2, pp.577-586, April 2014.

[60] S. Chakraborty, T. Ito, T. Senjyu, and A.Y. Saber, "Intelligent Economic Operation of Smart-Grid Facilitating Fuzzy Advanced Quantum Evolutionary Method," *IEEE Trans. Sustainable Energy*, vol.4, no.4, pp.905-916, Oct. 2013.

[61] J. Tan, L. Wang, Z. Wang, and R. Yang, “Optimization of PHEV charging strategy to improve power quality in a residential distribution grid”, *in Proc. 2013 IEEE Power & Energy Society General Meeting*, pp. 1-5.

[62] J. Tan and L. Wang, “A Two-Layer Evolution Strategy Particle Swarm Optimization Algorithm for Plug-in Hybrid Electric Vehicles at Residential Distribution Grid”, *in Proc. IEEE 2014 Power & Energy Society General Meeting,* National Harbor, MD, July 2014.

[63] J. Tan and L. Wang, “Integration of Plug-in Hybrid Electric Vehicles into Residential Distribution Grid Based on Two-Layer Intelligent Optimization” *IEEE Trans. Smart Grid,* vol. 5, no. 4, pp. 1774-1784, July 2014.

[64] J. Tan and L. Wang, “Real-Time Coordinated Management of PHEVs at Residential Level via MDPs and Game Theory”, *in Proc. IEEE Power & Energy Society General Meeting,* National Harbor, MD, July 2014.

[65] H. Nguyen and J. Song, "Optimal charging and discharging for multiple PHEVs with demand side management in vehicle-to-building," *J. Communications and Networks,* vol.14, no.6, pp. 662-671, Dec. 2012.

[66] C. Wu, H. Mohsenian-Rad, and J. Huang, "Vehicle-to-Aggregator Interaction Game," *IEEE Transactions on Smart Grid*, vol.3, no.1, pp.434-442, March 2012.

[67] J. Hofbauer and K. Sigmund, "Evolutionary game dynamics," *Bul. Amer. Math. Soc.*, vol. 40, no. 4, pp. 479-519, July 2003.

[68] A. S. Chuang, "Demand-side Integration for System Reliability," *IEEE Power Tech., Lausanne*, pp.1617-1622, July 2007.

[69] J. He, Y. Sun, P. Wang, and L. Cheng, "A hybrid conditions-dependent outage model of transformer in reliability evaluation," *IEEE Trans. Power Delivery*, vol.24, no.4, pp.2025-2033, Oct. 2009.

[70] S. de la Torre, J. Contreras, and A. J. Conejo, "Finding multiperiod Nash equilibrium in pool-based electricity markets," *IEEE Trans. Power Syst.*, vol. 24, no. 2, pp. 878-888, May 2009.

[71] T. Dai and W. Qiao, "Trading Wind Power in a Competitive Electricity Market Using Stochastic Programing and Game Theory," *IEEE Trans. Sustainable Energy*, vol.4, no.3, pp.805-815, July 2013.

[72] A. X. Jiang, and K. Leyton-Brown. "A Tutorial on the Proof of the Existence of Nash Equilibria," University of British Columbia Technical Report TR-2007-25, 2009.

[73] D. Niyato and E. Hossain, "Dynamics of network selection in heterogeneous wireless networks: An evolutionary game approach," *IEEE Trans. Vehicular Technology*, vol. 58, no. 4, pp. 2008-2017, 2009.

[74] K. Zhu, E. Hossain, and D. Niyato, "Pricing, Spectrum Sharing, and Service Selection in Two-Tier Small Cell Networks: A Hierarchical Dynamic Game Approach," *IEEE Trans. Mobile Computing*, no.99, pp.1-8, July 2013.

[75] B. Chai, J. Chen, Z. Yang and Y. Zhang, "Demand Response Management With Multiple Utility Companies: A Two-Level Game Approach," *IEEE Trans. Smart Grid*, vol.5, no.2, pp.722-731, Mar. 2014.

[76] J. E. Slotine and W. Li, Applied Nonlinear Control. Englewood Cliffs, NJ, USA: Prentice Hall, 2000.

[77] Z. Wang, R. Yang, L. Wang, and J. Tan, "Reliability assessment of integrated residential distribution and PHEV systems using Monte Carlo simulation," *in Proc. 2013 IEEE Power & Energy Society General Meeting*, Vancouver, Canada, pp. 1-5.

[78] J. Escudero-Garzas, and G. Seco-Granados, "Charging station selection optimization for plug-in electric vehicles: An oligopolistic game-theoretic framework," *in Proc. 2012 IEEE PES Innovative Smart Grid Technologies (ISGT) Conf.*, pp.1-8.

[79] Q. Guo, S. Xin, H. Sun, Z. Li, and B. Zhang, "Rapid-Charging Navigation of Electric Vehicles Based on Real-Time Power Systems and Traffic Data," *IEEE Trans. Smart Grid*, vol.5, no.4, pp.1969-1979, Jul. 2014.

[80] W. Lee, L. Xiang, R. Schober, and V. W. S. Wong, " Electric Vehicle Charging Stations with Renewable Power Generators: A Game Theoretical Analysis," *IEEE Trans. Smart Grid*, vol. 6, no. 2, pp. 608-617, Mar. 2015.

[81] R. Couillet, S. M. Perlaza, H. Tembine, and M. Debbah, "Electrical vehicles in the smart grid: a mean field game analysis," *IEEE J. Selected Areas in Communications*, vol. 30, no. 6, pp. 1086-1096, Jul. 2012.

[82] H. Yang, S. Yang, Y. Xu, E. Cao. M. Lai, and Z. Dong, "Electric Vehicle Route Optimization Considering Time-of-Use Electricity Price by Learnable Partheno-Genetic Algorithm," *IEEE Trans. Smart Grid*, vol. 6, no. 2, pp. 657-666, Mar. 2015.

[83] E. Yudovina and G. Michailidis, "Socially Optimal Charging Strategies for Electric Vehicles," *IEEE Trans. Automatic Control*, vol. 60, no. 3, pp. 837-842, Mar. 2015.

[84] A. Kotsialos, M. Papageorgiou, C. Diakaki, Y. Pavlis, and F. Middelham "Traffic flow modeling of large-scale motorway networks using the macroscopic modeling tool METANET," *IEEE Trans. Intelligent Transportation Systems*, vol.3, no. 4, pp. 282-292, Dec. 2002.

[85] A. Mohsenian-Rad, V. M. S. Wong, J. Jatskevichi, R. Schober, and A. Leon-Garcia, "Autonomous demand-side management based on game theoretic energy consumption scheduling for the future smart grid," *IEEE Trans. Smart Grid*, vol. 1, no. 3, pp. 320–331, Dec. 2010.

[86] P. Samadi, A. Mohsenian-Rad, R. Schober, V. W. S. Wong, and J. Jatskevich, "Optimal real-time pricing algorithm based on utility maximization for smart grid," *in Proc. 2010 IEEE Smart Grid Communications Conf.*, pp. 415–420.

[87] L. Chen, N. Li, S. H. Low, and J. C. Doyle, "Two market models for demand response in power networks," *in Proc. 2010 IEEE Smart Grid Communications Conf.*, pp. 397–402.

[88] R. Nelson, Probability, Stochastic Processes, and Queueing Theory, Springer-Verlag, New York, ISBN 0-387-94452-4, 1995.

[89] H. M. Taylor and S. Karlin, *An Introduction to Stochastic Modeling*, Academic Press, Third Edition, ISBN 0-12-684887-4, 1998.

[90] S. Hemon, M. Rougemont, and M. Santha, "Approximate Nash Equilibria for Multi-player Games," *Algorithmic Game Theory*, Lecture Notes in Computer Science 4997, 267–278, 2008.

[91] N. G. Pavlidis, K. E. Parsopoulos, and M. N. Vrahatis, “Computing Nash equilibria through computational intelligence methods,” *J. Computational and Applied Mathematics,* vol. 175, pp. 113-136, Mar. 2005.

[92] R. Billinton, and W. Li, *Reliability Assessment of Electric Power System Using Monte Carlo Methods*, Plenum Press, New York, 1994

[93] A. K. Srivastava, B. Annabathina, and S. Kamalasadan, “The challenges and policy options for integrating plug-in hybrid electric vehicle into the electric grid,” *Electr. J.*, vol. 23, no. 3, pp. 83-91, 2010.

[94] T. H. Bradleya and A. A. Frankb, “Design, demonstrations and sustain-ability impact assessments for plug-in hybrid electric vehicle,” *Renew-able Sustainable Energy Rev.,* vol. 13, no. 1, pp. 115-128, Jan. 2009.

[95] M. Duvall and E. Knipping, “Environmental assessment of plug-in hybrid electric vehicles,” EPRI Jul. 2007 [online]. Available: http://mydocs.epri.com.docs/ CorporateDocumnet/SectorPages/Portfolio/PDM/PHEV-ExecSum-voll.pdf

[96] T.-H. Chang, M. Alizadeh, and A. Scaglione, "Real-time power balancing via decentralized coordinated home energy scheduling," *IEEE Transactions on Smart Grid,* vol.4, no.3, pp. 1490-1504, Sept. 2013.

[97] Y. Ding, M. Xie, Q. Wu, and J. Østergaard, "Development of energy and reserve pre-dispatch and re-dispatch models for real-time price risk and reliability assessment," *IET Generation, Transmission & Distribution,* vol. 8, no. 7, pp. 1338-1345, Jul. 2014.

[98] K. Zou, A. P. Agalgaonkar, K. M. Muttaqi, and S. Perera, "An Analytical Approach for Reliability Evaluation of Distribution Systems Containing Dispatchable and Nondispatchable Renewable DG Units," *IEEE Trans. Smart Grid,* vol. 5, no. 6, pp. 2657-2665, Nov. 2014.

[99] L. Goel, Q. Wu, and P. Wang, "Reliability enhancement of a deregulated power system considering demand response," *in Proc. of IEEE Power Engineering Society General Meeting*, Montreal, Que., Canada, pp. 1-6, 2006.

[100] C. Chen, W. Wu, B. Zhang, and C. Singh, "An Analytical Adequacy Evaluation Method for Distribution Networks Considering Protection Strategies and Distributed Generators," *IEEE Trans. Power Delivery*, vol. 30, no. 3, pp. 1392-1400, Jun. 2015.

[101] C. Farmer, P. Hines, J. Dowds, and S. Blumsack, “Modeling the impact of increasing PHEV loads on the distribution infrastructure,” *in Proc. of IEEE 43rd Hawaii International Conference on System Science*, Jan. 2010, pp. 1-10.

[102] Available [online]: http://standards.ieee.org/findstds/standard/C57.92-1981. html

[103] X. Xu, J. Mitra, T. Wang, and L. Mu, “An Evaluation Strategy for Microgrid Reliability Considering the Effects of Protection System,” *IEEE Transactions on Power Delivery*, vol. 31, no. 5, pp. 1989-1997, Oct. 2016.

[104] R. Billinton and R.N. Allan, *Reliability Evaluation of Energy Systems: Concepts and Techniques,* Plenum, New York, 1983.

[105] R. Billinton and E. Wojczynski, "Distributional variation of distribution system reliability indices," *IEEE Transactions on Power Apparatus and Systems*, vol. 104, pp.3152-3160, 1985.

[106] R. Billinton and P. Wang, "Teaching distribution system reliability evaluation using Monte Carlo simulation," *IEEE Transactions on Power System*, vo.14, pp.397-403, 1999.

[107] W. Liu, M. Zhang, B. Zeng, L. Wu and J. Zhang, "Analyzing the impacts of electric vehicle charging on distribution system reliability," *in proc. of IEEE Innovative Smart Grid Technologies - Asia (ISGT Asia)*, Tianjin, China, May 2012, pp. 1-6.

[108] F. Li and N. Sabir, "Monte Carlo simulation to evaluate the reliability improvement with DG connected to distribution systems," *in Proc. of the 8th WSEAS International Conference on Electric Power Systems*, High Voltages, Electric Machines (Power'08), Venice, Italy, Nov. 2008, pp. 177-182.

[109] M. Feldman, and T. Tamir, "Convergence of best-response dynamics in games with conflicting congestion effects," *in Internet and Network Economics (Lecture Notes in Computer Science)*, vol. 7695, P. Goldberg, Ed. Berlin, Germany: Springer-Verlag, pp. 496–503, 2012.

Appendix: Proof of the Theorems

Proof of Theorem 4.1

Proof: To prove it is more cost effective to let PHEVs charge at the rated charging power, we need to find out the cost of a PHEV during the plug-in time horizon, including the charging cost, the earning from peak load shaving and the earning from frequency regulation.

For a baseline charging power $P_{EV,h}$ and a frequency regulation capacity C_h at a specific time slot h, the instantaneous charging power $P_{EV,t}$ is constrained by:

$$P_{EV,h} - C_h \leq P_{EV,t} \leq P_{EV,h} + C_h \tag{A.1}$$

Also, the charging and discharging power of the PHEV is constrained by its rated charging and discharging power P_{rate}. Thus, during the plug-in time span $h \in [h_{in}\ h_{out}]$, its frequency regulation capacity is dynamic according to the charging power as follows:

$$C_h = \begin{cases} P_{rate} - P_{EV,h}\,, if\ P_{EV,h} > 0 \\ P_{rate} + P_{EV,h}\,, if\ P_{EV,h} < 0 \end{cases} \tag{A.2}$$

The required charging energy constraint is:

$$E_{req} = \sum_{h=h_{in}}^{h_{out}} P_{EV,h} \cdot \Delta h \tag{A.3}$$

where Δh is the duration of the time step.

The total V2G energy capacity of the PHEV can be expressed as:

$$Vcap = (h_{out} - h_{in})P_{rate} - E_{req} \tag{A.4}$$

Define the V2G strategy κ as the percentage of V2G capacity used for frequency regulation as follows:

$$\kappa = \frac{Vcap - 2E_{dis}}{Vcap} \tag{A.5}$$

where E_{dis} is the discharged energy of the PHEV for peak load shaving during the plug-in time span.

To satisfy the required charging energy constraint, the charged energy is:

$$E_{chg} = E_{req} + E_{dis} \tag{A.6}$$

To prove Theorem 4.1, it is equivalent to proving that for any V2G strategy κ, it is more cost effective to let the PHEV charge and discharge at its rated power.

For a certain V2G strategy κ, the total frequency regulation capacity over the plug-in time span is:

$$C_{tot} = \sum_{h=h_{in}}^{h_{out}} C_h = N \cdot \Delta h \cdot P_{rate} - (E_{chg} + 2E_{dis}) = N \cdot \Delta h \cdot P_{rate} - (E_{req} + 2E_{dis}) \tag{A.7}$$

Thus, for a certain V2G strategy κ, the total frequency regulation capacity is a constant value.

The frequency regulation earning for the PHEV can be expressed as:

$$Earn_{reg} = \sum_{h=h_{in}}^{h_{out}} C_h \cdot r_h^{reg} = C_{tot} \cdot r_{avg}^{reg} \tag{A.8}$$

where r_h^{reg} is the frequency regulation price at time slot h and r_{avg}^{reg} is the average frequency regulation price.

As proved in Section 4.3.3, when the optimal frequency regulation price has been reached, we have the contracted regulation capacity as $C_{con,h}^j = \frac{(\alpha+\beta)p_{Ar,h}^j - \beta R_j}{2\alpha^2}$. As we have:

$$C_{con,h}^{j*} = argmax_{C_{con,h}^j}\left(U_{TSO,h}^j\right) = C_{ev,h}^j + \frac{R_j - p_{Ar,h}^j}{2\alpha} \tag{A.9}$$

Then we have

$$p_{Ar,h}^j = \frac{2\alpha^2 C_{ev,h}^j + (\alpha+\beta)R_j}{2\alpha+\beta} \tag{A.10}$$

As $\frac{\partial p_{Ar,h}^j}{\partial C_{ev,h}^j} = \frac{2\alpha^2}{2\alpha+\beta} > 0$, the frequency regulation price increases with the regulation capacity. The total regulation capacity for the aggregator will increase at certain hours if charging power is

increased. Then the average frequency regulation price r_{avg}^{reg} will increase. So $Earn_{reg}$ increases with the increasing charging power.

Notice that the Markov game will automatically assign the discharging time slots to peak price hours and charging time slots to off-peak price hours to maximize the PHEV's revenue. The charging cost considering the peak load shaving can be expressed as:

$$\Theta = r_{\kappa}^{chg}(x)E_{dis} - r_{\kappa}^{dis}(x)E_{chg} \tag{A.11}$$

where $r_{\kappa}^{dis}(x)$ is the average discharging price, $r_{\kappa}^{chg}(x)$ is the average charging price, and $x = P_{EV}/P_{rate}$.

Clearly, for any value of x the peak price hours are used for discharging and off-peak price hours are used for charging. If the value of x increases, more power can be discharged at higher electricity rates and also more power can be charged at lower electricity rates. Thus, r_{κ}^{dis} increases with the increase of x and r_{κ}^{chg} decreases with the increase of x. As E_{dis} is constant for a certain V2G strategy κ, Θ will also decrease with the increase of x. Thus, the charging cost will be minimized if the PHEV is charged at its rated power.

Thus, the cost of the PHEV $Cost = \Theta - Earn_{reg}$ will be minimized if the PHEV charges and discharges at its rated power. Therefore, it is the more cost effect to let PHEVs charge at their rated charging power. □

Proof of Theorem 5.1

Proof: Notice that the proposed non-cooperative game has a finite number of players and action profiles. According to Lemma 5.1, at least one Nash equilibrium exist in the game. It is clear that every best response dynamics converges to a pure Nash equilibrium if the number of iterations is infinitely great [109]. The proposed approximate Nash equilibrium can guarantee a

reasonable convergence time by appropriately setting the parameter ε_1 [90]. Finally, the possible missing Nash equilibrium will be captured in the approximated Nash equilibrium [71]. Therefore, the proposed non-cooperative game will converge to the approximated Nash equilibrium (5.32) under best response strategy. □

Proof of Theorem 5.2

Proof: According to the definition of $\mathrm{Earn}_{\mathrm{anci}}^{\mathrm{d}}$, we have $\frac{\partial \mathrm{Earn}_{\mathrm{anci}}^{\mathrm{d}}(\mathrm{y_d})}{\partial \mathrm{y_d}} = \mathrm{VCap_d}(\mathrm{reg_t} + \mathrm{MSR_t}(\mathrm{y_d}))$. According to (5.23), the ancillary services capacity of the system $\mathrm{P}_{\mathrm{Anci}}^{\mathrm{t}}$ will increase with $\mathrm{y_d}$. Based on (5.7) and (5.10), the marginal spinning reserve price $\mathrm{MSR_t}(\mathrm{y_d})$will decrease with the increase of $\mathrm{P}_{\mathrm{Anci}}^{\mathrm{t}}$. As $\mathrm{VCap_d}$ and $\mathrm{reg_t}$ are constants, so $\frac{\partial \mathrm{Earn}_{\mathrm{anci}}^{\mathrm{d}}(\mathrm{y_d})}{\partial \mathrm{y_d}}$ will decrease with the increase of $\mathrm{y_d}$ and $\frac{\partial \mathrm{Earn}_{\mathrm{anci}}^{\mathrm{d}}(\mathrm{y_d}+\Delta \mathrm{y_d})}{\partial \mathrm{y_d}} < \frac{\partial \mathrm{Earn}_{\mathrm{anci}}^{\mathrm{d}}(\mathrm{y_d})}{\partial \mathrm{y_d}}$ when $\Delta \mathrm{y_d} > 0$. So we can obtain $\frac{\partial^2 \mathrm{Earn}_{\mathrm{anci}}^{\mathrm{d}}(\mathrm{y_d})}{\partial {\mathrm{y_d}}^2} = \lim_{\Delta \mathrm{y_d} \to 0} \frac{\frac{\partial \mathrm{Earn}_{\mathrm{anci}}^{\mathrm{d}}(\mathrm{y_d}+\Delta \mathrm{y_d})}{\partial \mathrm{y_d}} - \frac{\partial \mathrm{Earn}_{\mathrm{anci}}^{\mathrm{d}}(\mathrm{y_d})}{\partial \mathrm{y_d}}}{\Delta \mathrm{y_d}} < 0$.

Notice that the best response strategy in the non-cooperative game will automatically assign the discharging time slots to peak price hours and charging time slots to off-peak price hours to maximize the revenue. Based on the definition of dominant solution matrix in Section 5.2.2, we have $\frac{\partial \mathrm{Earn}_{\mathrm{pls}}^{\mathrm{d}}(\mathrm{y_d})}{\partial \mathrm{y_d}} = -\mathrm{VCap_d}\left(\Delta \mathrm{r}_{\mathrm{d}}^{\mathrm{pls}}(\mathrm{y_d}) - \frac{\mathrm{c_b}.\mathrm{Cap_d}+\mathrm{c_L}}{\mathrm{L_C}\cdot\mathrm{Cap_d}\cdot\mathrm{DOD}}\right)$, where $\Delta \mathrm{r}_{\mathrm{d}}^{\mathrm{pls}}(\mathrm{y_d}) = \mathrm{r}_{\mathrm{d}}^{\mathrm{dis}}(\mathrm{y_d}) - \mathrm{r}_{\mathrm{d}}^{\mathrm{chg}}(\mathrm{y_d})$ is the discharging and charging price difference for using the V2G capacity for peak load shaving at $\mathrm{y_d}$. Clearly, for any value of $\mathrm{y_d}$, the peak price hours are used for discharging and off-peak price hours are used for charging. If the value of $\mathrm{y_d}$ increases, the peak load shaving capacity decreases and the remaining discharging and charging time slots will be allocated to peak price and off-peak price hours respectively. Therefore, the discharging capacity at relatively

lower peak price hour and the charging capacity at the relatively higher off-peak price hour are used for ancillary service, which indicates $r_d^{dis}(y_d + \Delta y_d) > r_d^{dis}(y_d)$ and $r_d^{chg}(y_d + \Delta y_d) < r_d^{chg}(y_d)$ when $\Delta y_d > 0$. Thus, $\Delta r_d^{pls}(y_d + \Delta y_d) > \Delta r_d^{pls}(y_d)$. Therefore, $\frac{\partial Earn_{pls}^{d}(y_d)}{\partial y_d}$ will decrease with the increase of y_d and $\frac{\partial Earn_{pls}^{d}(y_d+\Delta y_d)}{\partial y_d} < \frac{\partial Earn_{pls}^{d}(y_d)}{\partial y_d}$ when $\Delta y_d > 0$. So we can draw the conclusion that $\frac{\partial^2 Earn_{pls}^{d}(y_d)}{\partial {y_d}^2} = \lim_{\Delta y_d \to 0} \frac{\frac{\partial Earn_{pls}^{d}(y_d+\Delta y_d)}{\partial y_d} - \frac{\partial Earn_{pls}^{d}(y_d)}{\partial y_d}}{\Delta y_d} < 0.$

Therefore, we have $\frac{\partial^2 Earn_{V2G}^{d}}{\partial {y_d}^2} = \frac{\partial^2 Earn_{anci}^{d}}{\partial {y_d}^2} + \frac{\partial^2 Earn_{pls}^{d}}{\partial {y_d}^2} < 0$. So $Earn_{V2G}^{d}$ is a concave function of y_d and there exists a y_d^* for maximizing the value of $\pi_d^{V2G} = \frac{Earn_{V2G}^{d}}{VCap_d}$.

□

Proof of Theorem 5.3

Proof: Define a tracking error function $e_d = y_d^* - y_d$ and a Lyapunov function $V_d(t) = (e_d)^2$. Since $V_d(t) \geq 0$, the Lyapunov function is positive definite. $V_d(t) \to \infty$ when $t \to \infty$.

The first order derivative of $V_d(t)$can be expressed as:

$$\dot{V}_d(t) = \frac{\partial (e_d)^2}{\partial t} = 2e_d \frac{\partial e_d}{\partial t} = -2e_d \frac{\partial y_d}{\partial t} = -2\delta y_d (y_d^* - y_d)\left(\pi_d^{anci} - \overline{\pi}_{V2G}\right) \qquad (A.12)$$

Notice that $\frac{\partial Earn_{anci}^{d}(y_d)}{\partial y_d}$ is a decreasing function of y_d. So the ancillary service earning for per unit capacity decreases with the increase of y_d, which indicates the per unit ancillary service revenue $\pi_d^{anci} = \frac{Earn_{anci}^{d}}{y_d \cdot VCap_d}$ is a decreasing function of y_d. If $\pi_d^{anci} > \overline{\pi}_{V2G}$, according to (5.37), we can obtain $\frac{\partial y_d}{\partial t} > 0$. Clearly, we have $y_d^* > y_d$. Therefore $\dot{V}_d(t) < 0$. Similarly, if $\pi_d^{anci} < \overline{\pi}_{V2G}$,

we have $y_d^* < y_d$ and $\dot{V}_d(t) < 0$. According to Lemma 5.3, the system is stable and the evolutionary game will converge to the proposed evolutionary equilibrium. □

Proof of Theorem 6.1

Proof: To prove the theorem, it suffices to show that a player's best choice is to provide its true strategy information when other players reveal their true strategy information.

Let $\pi_1^*, .., \pi_i^*, ..., \pi_I^*$ denote the Nash equilibrium of the non-cooperative game when all the players provide truthful information. Denote $\pi_1^*, .., \bar{\pi}_i, ..., \pi_I^*$ as the Nash equilibrium reached when player i provides untruthful information about its strategy $\bar{\pi}_i$. We denote the utility of player i when providing truthful and untruthful information as U_i^* and $\bar{U}_i$ respectively.

Based on the definition of best response strategy we have $\pi_i^* = \pi_i' = \text{argmax}_{\pi_i \in F_i}\{U_i(\pi_i, \pi_{-i}^*)\}$ which means $\forall \pi_i \in F_i,\ \forall i \in I, U_i^* \geq \bar{U}_i$. That is, the player i cannot benefit by misreporting its best response strategy. Therefore, we can conclude that all the players in algorithm 6.1 will provide their truthful best response strategy. □

CURRICULUM VITAE

JUN TAN

EDUCATION

Ph.D., University of Wisconsin-Milwaukee, Milwaukee, WI, May 2017

M.S., Huazhong University of Science & Technology, Wuhan, China, Mar. 2012

B.S., Huazhong University of Science & Technology, Wuhan, China, Jun. 2009

DISSERTATION TITLE

INTEGRATION OF MASSIVE PLUG-IN HYBRID ELECTRIC VEHICLES INTO POWER DISTRIBUTION SYSTEMS: MODELING, OPTIMIZATION, AND IMPACT ANALYSIS

RESEARCH INTEREST

Complex system modeling, simulation, analysis and optimization; Intelligent computing and game-theoretic analysis; PHEV integration; Renewable energy integration; Smart grid, micro grid, operation and planning in competitive electricity markets.

RESEARCH EXPERIENCES

EECS Department, College of Engineering & Applied Science, University of Wisconsin-Milwaukee, WI

EV Integration, Charging Station Operation and Planning, Green Buildings, Aug. 2014 – May. 2017

- Grid integration of large fleet of plug-in hybrid electrical vehicles.
- Modeling and control of electrical vehicle charging stations in a smart grid environment.

- Renewable energy integration in power systems.
- Electricity market modeling in smart grid environment.
- Smart building automation and control.
- Reliability differentiated service in power distribution systems.
- Develop Multi-agent Building Automation and Control Simulator (MATLAB GUI based)
- Develop a Tool for Probabilistic Reliability Evaluation of Water Distribution Networks (Visual C++ based)

EECS Department, College of Engineering, The University of Toledo, Toledo, OH

EV Integration, EV Driving Pattern Development, Power System Reliability, Aug. 2012 – Aug. 2014

- Analyzed the impact of plug-in hybrid electrical vehicles on power system reliability.
- Developed intelligent algorithms to integrate PHEVs into smart grid.
- Develop Reliability Assessment Tool for Distribution Systems with PHEVs Penetration (MATLAB GUI based).

EECS Department, College of Engineering, Huazhong University of Science and Technology, Wuhan, China

Power Electronics, Dynamic Voltage Restorer, Renewable Energy Integration, Sep. 2009– Mar. 2012

- Student research group leader for the project of designing a 200kVA Dynamic Voltage Restorer.
- Core member in research of the control technology of inverter in photovoltaic system.

TEACHING EXPERIENCES

- Lab Instructor, Electronics II, *University of Wisconsin-Milwaukee*, Spring 2015

- Lab Instructor, Introduction to Control Systems, *University of Wisconsin-Milwaukee*, Fall 2014
- Teaching Assistant, Electric Circuits, The University of Toledo, Spring 2014
- Teaching Assistant, Power System Analysis, The University of Toledo, Spring 2014
- Teaching Assistant, Electronic Energy Processing, The University of Toledo, Fall 2013
- Teaching Assistant, Case study for undergraduate students, The University of Toledo, Fall 2013
- Teaching Assistant, Electronics I, The University of Toledo, Spring 2013
- Teaching Assistant, Control Systems Design, The University of Toledo, Fall 2012

FELLOWSHIPS AND AWARDS

- Distinguished Dissertation Fellowship Award, University of Wisconsin-Milwaukee, 2016-17 Academic year.
- Distinguished Graduate Student Fellowship Award, University of Wisconsin-Milwaukee, 2015-16 Academic year.
- Journal of Modern Power Systems and Clean Energy Excellent Reviewer Award, 2016.
- IEEE Transactions on Smart Grid Best Reviewer Award, 2015.
- Chancellor's Graduate Student Award, University of Wisconsin-Milwaukee, Spring 2015.
- Excellent Student in Graduate School of HUST, Huazhong University of Science & Technology, 2011.
- State Scholarship, Huazhong University of Science & Technology, 2006.

PROFESSIONAL ACTIVITIES

- Active member of IEEE and IEEE Power & Energy Society.

- Active member of ASHRAE.
- Exhibitor at the 2016 Sustainability Summit & Exposition, Milwaukee, WI, April 13-14, 2016.
- Designer of the Mulit-agent Building Automation and Control Simulator which has been exhibited in Rockwell Automation Fair, Chicago, Nov.16-19, 2015.
- Organizer and Lab Demonstrator for the Engineer for a Day and College of Engineering Open House at the University of Toledo, Mar. 2013 and Mar. 2014.
- Volunteer for International Conference on Renewable Energy Research and Applications, Milwaukee, WI, Oct. 19-22, 2014.
- Served as the IEEE International Conference on Smart Grid Communications 2015 technical review committee.
- Conference presentation:

➢ *"Coordinated Optimization of PHEVs for Frequency Regulation Capacity Bids Using Hierarchical Game", IEEE Power & Energy Society General Meeting, Denver, Colorado, July 2015.*

➢ *"Real-Time Charging Navigation of Electric Vehicles: A Non-cooperative Game Approach", IEEE Power & Energy Society General Meeting, Denver, Colorado, July 2015.*

➢ *"Leveraging Reliability-Differentiated Pricing for Integrating PHEVs into Residential Distribution Grid", IEEE Power & Energy Society Conference on Innovative Smart Grid Technologies, Washington, D.C., 2015.*

➢ *"Real-time coordinated management of PHEVs at residential level via MDPs and game theory", IEEE Power & Energy Society General Meeting, National Harbor, MD, July 2014.*

➢ *"A Two-Layer Evolution Strategy Particle Swarm Optimization Algorithm for Plug-in Hybrid Electric Vehicles at Residential Distribution Grid", IEEE Power & Energy Society*

General Meeting, National Harbor, MD, July 2014.

- *"Assessing the impact of PHEVs on load frequency control with high penetration of wind power", IEEE PES Transmission & Distribution Conference and Exposition, Chicago, IL, April 2014.*
- *"Stochastic modeling of load demand of plug-in hybrid electric vehicles using fuzzy logic", IEEE PES Transmission & Distribution Conference and Exposition, Chicago, IL, April 2014.*
- *"Optimization of PHEV Charging Strategy to Improve Power Quality in a Residential Distribution Grid", IEEE Power & Energy Society General Meeting, Vancouver, BC, Canada, July 21-25, 2013.*

- Reviewer for top-ranking journals including
  - IEEE Transactions on Smart Grid
  - IEEE Transactions on Power Systems
  - IEEE Power Engineering Letters
  - Journal of Modern Power Systems and Clean Energy
  - Sustainable Energy Technologies and Assessments
  - Intelligent Industrial Systems

PEER-REVIEWED PUBLICATIONS

Peer-reviewed Journal Publications:

[1] **J. Tan** and L. Wang, "Integration of Plug-in Hybrid Electric Vehicles into Residential Distribution Grid Based on Two-Layer Intelligent Optimization", *IEEE Transactions on Smart Grid*, vol. 5, no. 4, pp. 1774-1784, Jul. 2014.

[2] **J. Tan** and L. Wang "Enabling Reliability-Differentiated Service in Residential Distribution Networks with PHEVs: A Hierarchical Game Approach", *IEEE Transactions on Smart Grid*, vol. 7, no. 2, pp. 684-694, Mar. 2016

[3] **J. Tan** and L. Wang "Real-Time Charging Navigation of Electric Vehicles to Fast Charging Stations: A Hierarchical Game Approach", *IEEE Transactions on Smart Grid*, vol. 8, no. 2,

pp. 846-856, Mar. 2017.

[4] **J. Tan** and L. Wang, "Adequacy Assessment of Power Distribution Network with Large Fleets of PHEVs Considering Condition-Dependent Transformer Faults", *IEEE Transactions on Smart Grid,* vol. 8, no. 2, pp. 598-608, Mar. 2017.

[5] **J. Tan** and L. Wang, "A Game-theoretic Framework for Vehicle-to-Grid Frequency Regulation Considering Smart Charging Mechanism", *IEEE Transactions on Smart Grid,* In press.

Conference Publications:

[6] **J. Tan** and L. Wang, "Coordinated Optimization of PHEVs for Frequency Regulation Capacity Bids Using Hierarchical Game", *IEEE Power & Energy Society General Meeting,* Denver, Colorado, July 2015.

[7] **J. Tan** and L. Wang, "Real-Time Charging Navigation of Electric Vehicles: A Non-cooperative Game Approach", *IEEE Power & Energy Society General Meeting*, Denver, Colorado, July 2015.

[8] **J. Tan** and L. Wang, "Leveraging Reliability-Differentiated Pricing for Integrating PHEVs into Residential Distribution Grid", *IEEE Power & Energy Society Conference on Innovative Smart Grid Technologies,* Washington, D.C., 2015.

[9] **J. Tan** and L. Wang, "Real-time coordinated management of PHEVs at residential level via MDPs and game theory", *IEEE Power & Energy Society General Meeting*, National Harbor, MD, July 2014.

[10] **J. Tan** and L. Wang, "A Two-Layer Evolution Strategy Particle Swarm Optimization Algorithm for Plug-in Hybrid Electric Vehicles at Residential Distribution Grid", *IEEE Power & Energy Society General Meeting,* National Harbor, MD, July 2014.

[11] **J. Tan** and L. Wang, “Assessing the impact of PHEVs on load frequency control with high penetration of wind power”, *IEEE PES Transmission & Distribution Conference and Exposition*, Chicago, IL, April 2014.

[12] **J. Tan** and L. Wang, “Stochastic modeling of load demand of plug-in hybrid electric vehicles using fuzzy logic”, *IEEE PES Transmission & Distribution Conference and Exposition*, Chicago, IL, April 2014.

[13] Y. Xiang, **J. Tan**, and L. Wang, “A particle swarm optimization based control strategy for plug-in hybrid electric vehicles at residential networks level”, *IEEE PES Transmission & Distribution Conference and Exposition*, Chicago, IL, April 2014.

[14] **J. Tan**, L. Wang, Z. Wang, and R. Yang, “Optimization of PHEV Charging Strategy to Improve Power Quality in a Residential Distribution Grid”, *IEEE Power & Energy Society General Meeting*, Vancouver, BC, Canada, July 21-25, 2013.

[15] **J. Tan** and L. Wang, “A Stochastic Model for Quantifying the Impact of PHEVs on a Residential Distribution Grid,” *in Proc. of IEEE International Conference on CYBER Technology*, Nanjing, China, May 26-29, 2013.

[16] Z. Wang, R. Yang, **J. Tan**, and L. Wang, “Reliability assessment of integrated residential distribution and PHEV systems using Monte Carlo simulation”, *IEEE Power & Energy Society General Meeting*, Vancouver, BC, Canada, July 21-25, 2013.

[17] H. Li, L. Wang, Y. Xiang, **J. Tan**, R. Xiao, K. Xie, and Y. Xia, "Reliability evaluation of active distribution systems considering energy storage and real-time electricity pricing," *International Conference on Probabilistic Methods Applied to Power Systems (PMAPS)*, Beijing, 2016.